INVESTIGATION OF ATMOSPHERIC TURBULENCE

Thesis by

Paul B. MacCready, Jr.

In Partial Fulfillment of the Requirements

For the Degree of

Doctor of Philosophy

California Institute of Technology

Pasadena, California

1952

ACKNOWLEDGEMENTS

The author wishes first to thank the United States Weather Bureau for its cooperation and sponsorship of this project.

Grateful acknowledgement is made of the help extended by numerous staff members and students of the California Institute of Technology, especially Dr. H. J. Stewart who originated the project and acted as its supervisor. Mr. Bart Locanthi deserves special credit for his assistance during design of the equipment, Mr. Robert Madden and Mr. William Averre for their work on the equipment, measurements, and analysis, and Dr. Liepmann and Anatol Roshko for their helpful discussions during the analysis phase of the project.

Considerable cooperation was also received from outside the Institute, notably from Mr. John Vehrencamp of U. C. L. A., who contributed many worthwhile ideas and provided some of the measuring equipment, and from members of the Navy Electronics Laboratory, Point Loma, California, who gave technical help and loaned the balloon which was used on the project.

ABSTRACT

Satisfactory measurement techniques were developed which overcame the four principal experimental problems arising in the investigation of atmospheric turbulence.

1) The data are made reproducible for statistical analyses by recording them on a portable magnetic tape recorder.

2) Measurements at elevations up to several hundred meters are made feasible by the use of a multi-cable tethering system for a balloon which supports the measuring devices.

3) and 4) The problems of measuring wind velocity fluctuations over broad ranges (frequencies between 0 and 50 cycles per second, and magnitudes between 1/4 and 20 meters per second) are solved by using hot wire anemometers together with non-linear amplifiers.

The statistical analysis of recordings made under various meteorological conditions indicates that Kolmogoroff's similarity hypothesis, concerning the isotropy of turbulence in a certain inertial sub-range of eddy sizes, is directly applicable to eddies of sizes ranging from under 10 cm. to dimensions larger than the elevation of measurement. Over this range the "2/3 law" holds for the autocorrelation coefficient and the "-5/3 law" holds for the energy spectrum, within the accuracy of the measurements. The large eddy limit of the range of the "2/3 law" appears to be considerably extended by strong thermal instability. Heat flux measurements from the correlation between temperature and vertical velocity agree reasonably with the heat flux measured with heat meters. At 70 cm. under moderate wind conditions over half the heat flux is due to eddies of periods less than two seconds. Momentum flux measurements from velocity correlations were inconclusive.

TABLE OF CONTENTS

TABLE OF CONTENTS (Cont'd)

TABLE OF CONTENTS (Cont'd)

LIST OF FIGURES

LIST OF FIGURES (Cont'd)

LIST OF FIGURES (Cont'd)

NOMENCLATURE

Any "barred" quantity ($\overline{\varphi}$, etc.) denotes the mean value, averaged over the measurement interval.

M	time constant of response (seconds)
x, y, z	axes of coordinate system. x along mean wind, y horizontal, perpendicular to mean wind, z vertical, perpendicular to mean wind, measured above ground surface
$T_1 = \overline{T} + T$	temperature ($^{\circ}$ C)
$U = \overline{U} + u$	wind velocity in x direction. (cm/sec. or meters per sec.) Also used to denote the longitudinal wind measured by the hot wires.
$V = \overline{V} + v$	wind velocity in y direction
$W = \overline{W} + w$	wind velocity in z direction
$U_H = \sqrt{U^2 + V^2}$	wind velocity in horizontal plane
$\sigma_u = \sqrt{\overline{u^2}}$	
$\sigma_v = \sqrt{\overline{v^2}}$	
$\sigma_w = \sqrt{\overline{w^2}}$	
τ	a time interval (seconds)
n	frequency (cycles per second)
ω	angular frequency (radians per second)
r	length or eddy size (cm., meters)
r_c	largest eddy following "2/3 law"
k	number of waves per unit length (cm^{-1})
	Interrelationships between τ, n, ω, r, and k: $nr = \overline{U}$, $\omega = 2\pi n$, $k = \frac{n}{\overline{U}} = \frac{1}{r}$, $\overline{U}\tau = r$
f(r)	autocorrelation coefficient for U (f(r) implies f(τ), f(n), f(ω), or f(k))
g(r)	autocorrelation coefficient for V or W
L	characteristic length = $\int_0^\infty f(r)dr$ (cm., meters)

NOMENCLATURE (Cont'd)

z_o	surface roughness coefficient (cm.)
P	shear stress across a plane (dynes cm^{-2})
P_o	surface shear stress
ϵ	energy dissipation per unit mass = $-\frac{d}{dt}(\frac{3}{2}\ \overline{u}^2)$ (in $cm^2 sec^{-3}$)
Q	heat flux across a plane (cal. $cm^{-2} sec^{-1}$)
D(i)	probability density function for "i". Distribution in time of the quantity "i".
α_i	skewness of D(i)
E(n)	energy density. Energy per unit mass cycle per second ($cm^2 sec^{-2} gm^{-1} (c.p.s.)^{-1}$) (E(n) implies $E(\omega)$, E(r), etc. $E(n) = E(k)\ \frac{1}{U}$, etc.)
$I\ \overline{u}^2(n)$	Integrated energy. Energy integrated over all frequencies greater than n. ($cm^2\ sec^{-2}$)
A	reading of vibration analyzer. (Meter units)
ρ	density of air ($gm\ cm^{-3}$)
C_p	specific heat of air at constant pressure
Ki, Ci, B, a, etc.	Various constants

I. INTRODUCTION AND SUMMARY

On 1 May, 1949, a research project in the field of atmospheric turbulence was initiated at the California Institute of Technology under Contract No. Cwb-8118 with the United States Weather Bureau. A "Progress Report on Investigation of Atmospheric Turbulence" was submitted in October, 1950, in fulfillment of this contract. The report described preliminary investigations into the experimental methods that were developed for the research. This thesis also describes these preliminary investigations, plus the changes of technique that were later found necessary, the field measurements themselves, their subsequent analysis, and the results. The content of this thesis is substantially the same as the content of the "Report on Atmospheric Turbulence" submitted to the Weather Bureau in May, 1952, in fulfillment of Contract No. Cwb-8125 which supplemented the funds of the first contract.

This research program was instituted "for the purpose of making measurements of the turbulent fluctuations in the atmosphere within 300 meters of the ground." It is felt that the most fruitful method of approach to the problems connected with the transport of energy, momentum, and particles in the atmosphere is one wherein the detailed physical processes are investigated. More adequate mathematical treatment of the subject can eventually be built on concepts utilizing data of the fluctuations themselves, rather than on data dealing with mean or integrated quantities.

Valuable experimental techniques for the statistical study of turbulent fluctuations have already been developed for the turbulence in wind tunnels, and it was planned that the present project apply these to the atmospheric case. This was in fact done, but the wind tunnel experimental methods had to be so altered for the new job that the only resemblance between the new and old methods is in the fundamental idea of measuring velocities with hot wire anemometers.

The theoretical concepts concerning turbulence in wind tunnels and in the atmosphere are generally similar, although accenting different parts of the theory. If airflow with a very thick turbulent boundary layer is desired, the atmosphere can sometimes prove to be a better "wind tunnel" than can a conventional tunnel. The range between large eddies, having dimensions similar to the sizes of the devices producing them, and tiny eddies, wherein viscosity is a large factor, is much greater in the atmosphere than in a wind tunnel--and this range is most important in certain phases of isotropic turbulence. It appears that various of the ideas concerning turbulence in the atmospheric boundary layer may also be useful at elevations and eddy sizes where the turbulence is important for aircraft stability and structural problems.

The measurement difficulties proved to be such a problem that the major portion of this research had to be devoted to the development of specialized measuring equipment and techniques, and a far lesser part, say 20^{o}/o, devoted to the actual making and analyzing of measurements.

The results demonstrate that the equipment and techniques that were evolved do work satisfactorily. The accuracies are greater than had been expected at the start of the project. The methods, however, are not simple enough to be widely applied without alteration. For example, the field equipment is made "portable", and yet moving it from laboratory to trailer requires two or more men for over half a day; the 30 foot trailer is overloaded by the large amount of equipment; setting up completely in the field takes three hours; and managing the tethered balloon correctly necessitates a crew of six men.

Although many labor-saving techniques were employed to lighten the load of the statistical analysis, the work was very tedious. With a small amount of additional equipment it will be possible in the future to reduce such analysis work considerably.

The present report first describes the problems which arise in the measurement and analysis of atmospheric turbulence, and the methods used to overcome them. It next deals with the actual making of the measurements. In the final section are discussed the analysis of the data together with interpretations of the results.

The measurement technique involved the use of two hot wire anemometers and a temperature wire resistance element which were mounted on a post or held in the air by a tethered balloon. The electrical outputs of Wheatstone Bridges from the sensing elements were brought to the ground by wires, there used to modulate separate carriers, and the carriers then amplified by

adjustable non-linear analog amplifiers and recorded on a magnetic tape recorder. The tape recorder played back the signals in the laboratory, where the carriers were separated by filters. After amplification and demodulation the signals were properly superimposed so as to give finally continuous voltages proportional to the temperature and to each of two components of velocity. The three voltages were then statistically analyzed by various integration techniques to yield the desired data.

Five magnetic tape reels ("Runs") were recorded on four separate days representative of a variety of meteorological conditions. The data collected consisted of either the horizontal wind alone, or the temperature, the longitudinal wind, and the transverse wind (vertical or horizontal). The altitude of investigation was varied from 7.5 cm. to 146 meters, with most of the records being for heights of 15, 70, and 240 cm. Mean wind velocities were between 2 and 8 meters per second. Two runs were made when the air was quite unstable, one with the air very slightly unstable, and two during neutral or slightly stable conditions.

Autocorrelation coefficients were calculated for the total horizontal wind velocity at elevations from 7.5 cm. to 146 meters, with the aid of an IBM calculator. Energy spectrum curves were found for two runs for the turbulent energy in each of the three directions. The frequencies examined were 2.5, 10, and 40 cycles per second. The convective heat flux was measured first with two heatmeters, and secondly by correlating instantaneous temperature and vertical velocity signals by a simple graphical method. In one

instance a low pass filter was employed to remove the high frequency components of the heat flux and show how much of the flux was due to the lower frequency components alone. An attempt was made to calculate the momentum flux by a correlation technique similar to that used for heat flux, but in this case the method proved too inexact to be useful.

The shape of the autocorrelation function curves, the shape of the energy spectra, and the directional distribution of the turbulent energy all agree with the results predicted for an "inertial sub-range" of eddies exhibiting isotropy by Kolmogoroff's similarity hypothesis. The isotropy exists for eddies with wavelengths as great as the height of measurement, and the range is shown to be much greater during very unstable conditions. It is felt this indicated isotropic turbulence range may in some cases exist for eddy sizes which are important for aircraft structural and control considerations.

The heat flux measurements made by the two different methods agree reasonably well. The measured flux shows a definite increase with altitude which may perhaps be explained as being due to nonhomogeneities of the local surrounding surface. It is shown that about half of the heat flux at 70 cm. elevation under the conditions of one run can be attributed to the eddies with periods less than 2 seconds. The viscous dissipation of turbulent energy was calculated and demonstrates the expected strong decrease with elevation.

II. INSTRUMENTATION AND FIELD EQUIPMENT

A. General Problems

The attempt to apply wind tunnel techniques to the problem of measuring atmospheric turbulence has introduced many new difficulties, noted in the following table.

	Wind Tunnel Turbulence	Atmospheric Turbulence
A) Frequency range-lower limit	About 20 cps	0 cps
B) Velocity Range	Mean velocity $\pm$ 5%/o	Mean velocity $\pm$ 50%/o
C) Approx. maximum direction variation	$\pm$ 4°	$\pm$ 30°
D) Repeatability (and portability)	Tunnel at fixed location, and conditions readily reproducible	Equipment must be portable and conditions are transient and irreproducible, so data must be recorded for later analysis

The major portion of the work on this research project has involved the design and construction of the specialized equipment needed to overcome these difficulties. In short, the large wind velocity variation requires the use of a non-linear electric element to counteract the non-linear hot wire response to velocity; the portability requirement has been met by using the tethered balloon; the tape recorder is substituted for the wind tunnel as a device for reproducing desired signals, and the need to pass zero frequency signals and amplify them has forced the use of a carrier wave for each electric signal.

B) Frequency Range (Velocity and Temperature Elements)

In order to design equipment, it was first necessary to ascertain

what frequencies of fluctuation were important. A hot wire anemometer has a characteristic response lag, due to its thermal inertia, and therefore greatly attenuates signals above a certain frequency range. If a hot wire has a time constant M and is recording a frequency of $\frac{\omega}{2\pi}$ cycles per second, its frequency response is diminished by a factor $\frac{1}{\sqrt{1+M^2\omega^2}}$. The response is cut one half at a frequency of $\frac{.275}{M}$ cps or a period of approximately 3.6 M seconds (1, pg. 8).

To get a rough estimate of the high end of the frequency spectrum, a hot wire anemometer of the following description was used: 1) Hot wire 0.000127 cm in diameter, $M_{(measured)} = 0.00015$ sec. sufficient for measuring frequencies up to 2000 cps; 2) Hot wire 1.2 cm in length, sufficient in a 3-1/2 mps wind to measure frequencies up to 300 cps with negligible attenuation; 3) Amplifier, linear to 10,000 cps. Therefore, this equipment gave accurate readings up to 300 cps, and attenuation was not serious until over 400 cps. Figure 1 shows the data gathered with this equipment under various atmospheric test conditions. The hot wire voltage signal was amplified, and put into a wave analyzer set to receive a 60 cycle band width. The points on Figure 1 are averages estimated very roughly from watching the wave analyzer output needle as it moved about. It illustrates that only a very small proportion of atmospheric turbulence lies above 150 cps, and even at 75 cps there is little energy when compared to the amounts at lower frequencies. Therefore 75 cps was selected as the absolute upper frequency to be considered in the equipment design.

Recent measurements not yet formally reported of atmospheric temperature fluctuations, performed by the Meteorology Laboratory of

the Navy Electronics Laboratory, San Diego, California, also indicate that frequencies above 100 cps comprise but a very small proportion of the energy spectrum. With these conclusions in mind, .00129 cm. diameter platinum wire was decided upon as the final wire to be used. Originally .00076 cm. diameter tungsten wire was tried, but even when operated at quite a low temperature its electric characteristics would change with use far too much to permit it to be considered. Platinum wire, after being annealed at red heat for a minute or so, does not have this property of becoming slowly oxidized and hence changing its characteristics, and is thus suitable for this experiment. Although more fragile than tungsten, it has another advantage in being easy to solder without first being plated electrolytically at the ends. Calculating the time constant M from the formula $M = 4.2\rho_1 A^2 s(\overline{T}-T_o)$ seconds, where

A = area of wire cross section in cm^2

ρ_1 = wire density in gm/c. c.

s = specific heat of wire material in calories/gram

$\overline{T}$ = operating temperature of wire in degrees C.

T_o = temperature of the unheated surrounding air in degrees C

i = current through the wire in amperes

r_s = resistivity of wire material in ohm-cm

(1, pg. 8), one finds M = .0083 seconds for very low wind velocities (for $T = T_o = 300^oC$), and M = approximately 0.0025 seconds at the average larger wind velocities measured. Assuming M = 0.0025 seconds at a typical operating condition, it follows that the hot wire response is reduced to $78^o/o$ at 40 cycles per second. Should it ever be desirable, the frequency response can easily be improved by using

a smaller diameter wire; the choice of 0.00127 cm. diameter wire was based largely on availability at the laboratory. Figure 2 shows the characteristics of such a wire. The points circled are the operating conditions finally decided upon for the hot wire when in still air.

The wire length was determined principally by the voltage available, and turned out to be 1.1 cm.

For temperature and heat flux measurements, the simplest solution appeared at first to be the use of a D 170575 Westinghouse thermistor, with its 4000 ohm resistance and a large $-4^{o}/o$ temperature coefficient of resistance. It has a time constant M of about 0.25 seconds (2), meaning that its response will drop to one half at 1.1 c.p.s. However, since little was known concerning the frequencies of gusts contributing to heat flux, it was deemed advisable to design a temperature sensitive device with much more rapid response. The resulting temperature probe simply consists of a 0.00127 cm. diameter tungsten wire, approximately 1 meter long, wrapped around four ceramic spacers in such a way as to keep the wire separated but still all contained within a 1 cm. cube. The small diameter gives rapid response, the long wire length gives adequate sensitivity, and the small final dimensions permit it effectively to measure "point" characteristics. The tungsten is first copper-plated at the ends, then wrapped on the spacers, and soft soldered to the conductors. Figs. 3A and 3B show the temperature probe mounted several cm. above and slightly ahead of the hot wires. Fig. 4A gives a detailed view of the probe.

The time constant of this resistance wire was not calculated, but it should be of the same order of magnitude as M for the hot wires,

say 0.003 seconds. As used, the wire carries the rather high current of 1 milliampere, and so one might worry about its heating due to this current. Tests in a wind tunnel and others made by moving the probe rapidly through the air showed that the heating effect was negligible at velocities greater than 1 m.p.s. (for at such speeds the air cools the wire to very nearly the air temperature). Another worry is that the radiant heating due to the sun might give an error to the temperature reading. When the wire was alternately shaded and unshaded, no variation in its resistance was detectable, implying that the radiant heating effect with a wire of such small size is negligible.

One problem avoided in the study of wind tunnel turbulence but present in the atmospheric case is the need to have equipment which will work even at zero frequency. This requires that all amplification and recording take place while the signal is on a carrier, since A.C. amplification is simpler than D.C. amplification. The signals from the sensing elements, particularly the temperature unit, are small and require large amplifications.

C) Velocity Range

A velocity range of 1/4 to 20 mps was assumed adequate for the airflows under consideration. The relationship between current (i) through a hot wire, or the voltage across it, to the velocity of the wind is very non-linear for the large velocity range in atmospheric turbulence. For example, King's formula (1, page 6) representing hot wire response when operated under constant temperature (constant resistance) conditions is $i^2 - a = b\sqrt{\rho U}$, where a and b are constants for a given hot wire and temperature, and ρ is the density of the air. For wind tunnel work, with its small turbulence level, the hot wire is

always operated in a small range along its characteristic curve, and the curve can be assumed linear in this region ($\frac{di}{dU}$ = constant). This simplification is not possible in the atmospheric case, where the only solution seems to be the use of a non-linear electrical circuit element to counteract the non-linearity of the hot wire response.

Smooth non-linear tube characteristics have been tried in the role of electrical analogs to the hot wire curve (3), but they are difficult to adjust and to keep in adjustment, particularly when dealing with the large amount of non-linearity present in this case. Therefore, a biased rectifier analog was decided upon, wherein 6AL5 rectifiers are used as the non-linear elements. At first IN34 crystal rectifiers were employed, but their characteristics are so dependent upon temperature as to render them useless for a precise job.

In practice the hot wire is put into a Wheatstone Bridge as one of the four resistance elements, and the bridge balanced at U = 0. This makes the output versus velocity curve pass through the origin, permitting a simpler analog circuit. In addition, the non-linearity of the bridge response in a small part cancels some of the non-linearity of the wire response. In a bridge, with constant voltage across the bridge, the wire is not operated under constant resistance, current, or voltage. The output is simply plotted versus velocity, and the analog adjusted to give the corresponding curve. For a typical experimental bridge response curve, see Figure 5.

In the biased rectifier analog circuit, the biased rectifiers, and their corresponding resistors serve to act as a variable resistance element whose resistance depends on the voltage across it. The wiring diagram for such an analog circuit is shown in Figure 6.

Assuming zero input impedance and perfect rectifiers, if the input voltage E_i is small and if $R_1 \gg R$, the value of $\frac{dE_i}{dE_o} \cong \frac{R_1}{R}$. Similarly if R_3 is much smaller than any of the other resistances and if E_i is large, $\frac{dE_i}{dE_o} \cong 1$. Thus the ratio of $\frac{dE_i}{dE_o}$ for small voltages to its value for large voltages ir roughly $\frac{R_1}{R}$.

If E_i into the analog is proportional to the voltage on Figure 3, then we wish E_o to be proportional to the velocity of that figure. Note that the ratio of

$$\frac{\text{initial slope of the curve}}{\text{final slope of the curve}} \cong 25$$

For the analog to be correct, therefore, $R_1 = 25\ R$. However, the forward resistance of a 6AL5 is not zero, the input impedance into the analog is not zero, and the output impedance into which the analog works is not infinite--all these contribute to the requirement that actually R_1 must be considerably larger than 25R.

The zero current point of a 6AL5 does not correspond to zero volts across it. This effect is canceled by adjustment of the bias resistors.

A small direct current flows continually in the back direction through various types of rectifiers. This is not a problem because only A. C. is used in this particular analog.

When such an analog is operated at low voltages (say E_i maximum less than 2 volts) the rectifiers operate on a portion of their characteristic curves that is quite rounded. Thus, instead of producing an analog which approximates the desired curve by a series of straight lines, the lines become bent and their corners rounded. If one is trying to approximate a smooth curve this is quite an advantage. If desired, the rectifiers may be grouped in pairs in order to

decrease the voltage across any one, and hence promote rounded corners in the analog curve. So successful is this method for the hot wire curve that, with only 3 biased elements, it is possible to make an analog that is exceedingly close to the desired curve. See Figure 5 for a comparison of the analog curve with the desired curve.

Approximate adjustment of the analog circuit is effected by putting the E_i on the y axis of a scope, and the E_o on the x axis. The scope then depicts the analog curve, and immediately shows the effect of each variable resistance on the slope or bias of the various line segments.

For the final adjustment of the analog, voltage into the varistor and modulator is plotted vs. voltage out of the analog. Thus the analog corrects for any non-linearity in the varistor and amplifier and transformers while at the same time correcting for the non-linearity of the hot wire response. The trial and error method must be used to make the final analog adjustments.

Due to the rectifiers, the analog circuit itself acts as a rectifier.

D. Wind Direction Change

The turbulence to be measured is assumed to be under $50^{o}/o$ i. e., in direction always within 30^{o} of the mean wind. Since the results are analyzed statistically, and it can be assumed that the numbers of times the wind veers beyond 30^{o} are relatively few, errors so induced can be neglected in the final analysis.

In wind tunnel turbulence, with its small turbulence level, linearized approximations permit quite accurate measurement of

components perpendicular to the mean flow. With the large variations in direction in the atmospheric case, first order approximations can no longer be used.

For simplicity in the following discussion, the symbols will differ from those in use throughout the rest of the report.

V = magnitude of wind velocity

$\underline{V}$ = vector representing wind velocity

V_x, V_y, V_z = components of wind velocity

$\underline{V} = \underline{i}V_x + \underline{j}V_y + \underline{h}V_z$ where $\underline{i}$, $\underline{j}$, $\underline{h}$ represent the coordinate unit vectors.

$\underline{s}$ = unit vector along hot wire

V_1, V_2, V_3 = velocities measured by hot wires 1, 2, 3

θ = angle between $\underline{s}$ and $\underline{V}$

Since V_x, V_y, V_z measurements were wanted using a minimum number of hot wires, various methods were analyzed to find out if the desired results were within the practical reach of hot wire equipment.

The first problem which presented itself was that of the response of one hot wire to wind direction changes. It was known that a hot wire responds principally to the component of wind perpendicular to it; however, for any practical mathematical approach to the design of a probe, it was necessary to see if this relation could be considered exact without introducing excessive errors. Fortunately, the assumption that "all the cooling of the wire is due to the component of the wind perpendicular to the wire" turned out to be experimentally verified within the accuracy needed for the experiment, and the formula

$$\text{Measured velocity} = V_{measured} = |\underline{V} \times \underline{s}|$$

could be used for design of a hot wire probe.

At velocities over 25 mps there is evidence that this relation

is quite exact, especially for relatively long wires (1, pg. 6). Several tests were run at medium and low velocities, and $V_{measured} = |\underline{V} \times \underline{s}|$ proved reasonably correct, for angles $\theta > 10^{o}$. (See Figure 7).

Since the calibration tunnel will not run below 2.5 mps, and since at low speeds the velocity is very difficult to read (the manometer pressure is proportional to V^2), there is an "unmeasurable region" below velocities of about 3 mps. Thus it was not possible to check the $V_{measured} = |\underline{V} \times \underline{s}|$ formula at very low speeds. However, since it was shown to be reasonably valid at 25 mps and 3.5 mps, it seems logical to extrapolate the region of validity to some lower speeds. If for a very thin wire we plot King's Formula $i^2 - a = b\sqrt{V}$ for $V \sin\theta$ instead of V when the wire direction is changed, the points at the high velocities and the point at V = 0 all lie on a straight line, so it is reasonable to extrapolate this line through the "unmeasurable region". With the 0.00127 cm. diameter wire carrying about .095 amperes that was finally selected for this project, the V = 0 reading must be off the extrapolated line because convection cuased by the wire's heating actually makes the velocity of the air around the wire finite. However, as soon as the velocity is of the order of 1/3 meter per second, this self convection effect is negligible. This was checked roughly by shutting off the mouth of the tunnel enough to lower the velocity to this amount, then reading bridge output when the wire was rotated from a horizontal to a vertical position. There was no voltage change, although there had been a large change when this was done for zero velocity.

For low speed calibration of a hot wire it is therefore satisfactory to turn the wire 60^{o} from its position perpendicular to the

flow velocity. In a later stage of this research a wind tunnel and accurate manometer were utilized which permitted quantitative readings at velocities as low as 1 meter per second. They agreed rather well with those readings obtained at higher velocities with the wire angled.

The following probe designs were considered mathematically, using the $V_{measured} = |\underline{V} \times \underline{s}|$ relation. The intention was to find a probe design which would yield V_x, V_y, and V_z accurately with a minimum amount of electronics. By a proper analog circuit for each hot wire it was assumed that a voltage proportional to the velocity perpendicular to the wire could be obtained.

Probe A. The two-dimensional flow case, with wires set as shown in Figure 8A. For this case,

$$V_x = \frac{1}{\sqrt{2}} (V_1 + V_2)$$

$$V_y = \frac{1}{\sqrt{2}} (V_1 - V_2)$$

where V_1 and V_2 are the velocities measured by wires 1 and 2 respectively.

If such a probe is to be used in a three-dimensional case, it must be pivoted on a vertical axis with a small direction vane on behind to keep it pointed into the horizontal component of the wind. Probe A is the probe actually used in this project. Figure 4B is a closeup view of the probe, while Fig. 3B shows it mounted. Flexible flat platinum wire, 0.015 cm. by 0.00025 cm., electrically connects the moving hot wire ends to the fixed conductors. Light construction of the balsa vane permits it to respond rapidly to wind direction changes. No measurements of the response time were

made, but it is estimated that the vane can accurately follow wind direction changes of even 5 cycles per second. When the probe is set with the wires in the x-z plane, it measures

$$V_z = \frac{1}{\sqrt{2}}(V_1 - V_2) \text{ and } V_{\text{horizontal}} = \sqrt{V_x^2 + V_y^2} = \frac{1}{\sqrt{2}}(V_1 + V_2)$$

The error in these terms due to the vane not being aligned with the horizontal component of wind is on the order of a cosine error, and hence negligible for small misalignments.

As regards the vertical transport of various atmospheric properties, V_z is the most important velocity component. This probe is the simplest one for finding V_z accurately and therefore is the one actually used.

Probe B. It was hoped that by means of 4 hot wires, oriented as shown in Figure 8B, that V_x, V_y, and V_z could be found with sufficient accuracy by linear combination of the measured velocities. The response of hot wire "i" to V_x, V_y, and V_z components is

$$V_i^2 = V_x^2 (c_i^2 + b_i^2) + V_y^2 (a_i^2 + c_i^2) + V_z^2 (b_i + a_i^2)$$

$$- 2V_y V_z b_i c_i - 2V_z V_x a_i c_i - 2V_x V_y b_i a_i$$

where a_i, b_i, c_i are the direction cosines of wire "i". Therefore $V_1^2 = \frac{1}{2} V_x^2 + \frac{1}{2} V_y^2 + V_z^2 - V_x V_y$ and the equations for V_2^2, V_3^2 and V_4^2 have similar forms. The crossproduct terms such as $V_x V_y$ eliminate the possibility of getting a linear relation between V_x (or V_x^2) and V_1, V_2, V_3, V_4. Therefore various linear combinations were tried, valid for small magnitudes of V_y and V_z. The

best obtainable seemed to be

$$V_x = \frac{1}{2\sqrt{2}}(V_1 \mp V_2 + V_3 \mp V_4) - \frac{|V_2 - V_1|}{10\sqrt{2}} - \frac{|V_4 - V_3|}{10\sqrt{2}}$$

$$V_y = \frac{1}{\sqrt{2}}(V_1 - V_2)$$

$$V_z = \frac{1}{\sqrt{2}}(V_3 - V_4)$$

Note the absolute value signs in the V_x equations. These are obtained electrically by getting voltage V_2-V_1 and voltage V_1-V_2, and then using a rectifier in each circuit so only the positive value of the two is utilized.

Figure 8C shows the errors in the measured values of V_x and V_y. The magnitudes of the V_z errors are the same as the V_y errors.

The formula for V_x is sufficiently accurate; the one for V_y is not. The V_y formula can be improved by the proper addition of $|V_3-V_4|$, but not enough to make it really useful. Linear terms are insufficient for giving V_y and V_z accurately enough. Probe B is considered unsatisfactory--it requires an extra hot wire, and still lacks accuracy.

Probe C. A linearized method similar to that used for Probe B was tried for the case of 3 symmetrically distributed wires--giving even less satisfactory results than with Probe B.

Probe D. A hot wire wound into a jumble with no preferred direction would measure only the magnitude of the wind. Such a wire, in conjunection with two straight wires at various angles to the wind, was considered as another probe possibility, but analysis

showed there was no hope for a solution involving linear summations of voltages.

The trick of kinking each wire so it would measure and average the wind components perpendicular to two directions was considered. This method was discarded, since it would require different cooling rates along the same wire, and therefore a single analog circuit would not be valid for more than one wind direction and velocity.

Probe E. It was assumed that an analog circuit could be built up for each wire giving a voltage proportional to V_i^2 rather than proportional to V_i. In that case, consider the probe shown in Figure 9A with three wires along the X', Y', Z' axes. (Each axis is at the same angle, $54^o40'$, to the mean wind direction.) Physically this is the same probe as Probe C, but it is connected to a different electrical analyzer. For this case

$$V_1^2 = V_y'^2 + V_z'^2$$

$$V_2^2 = V_x'^2 + V_z'^2$$

$$V_3^2 = V_x'^2 + V_y'^2$$

Therefore

$$V_x'^2 = \frac{1}{2}(-V_1^2+V_2^2+V_3^2)$$

$$V_y'^2 = \frac{1}{2}(V_1^2-V_2^2+V_3^2)$$

$$V_z'^2 = \frac{1}{2}(V_1^2+V_2^2+V_3^2)$$

Note that, with the wind direction as indicated, V_x', V_y', and V_z' are all positive. Now consider a biased rectifier analog circuit

which is the approximate analog of $E_o = \sqrt{E_{in}}$. Such an analog device is even simpler to make than the one described earlier. Since the square root curve has opposite curvature to the one for which the analog in Figure 6 was designed, the present analog must have E_{out} taken across D-G rather than across H-G (see Figure 6). As before, variable slopes permit an accuracy better than 99°/o. Using the square root analog devices V_x', V_y', V_z' from $V_x'^2$, $V_y'^2$ and $V_z'^2$ are obtained. These velocities are now transformed to the conventional X, Y, Z coordinate system, by the electrical analog to the linear formulae:

$$V_x = l_1 V_x' + m_1 V_y' + n_1 V_z'$$

$$V_y = l_2 V_x' + m_2 V_y' + n_2 V_z'$$

$$V_z = l_3 V_x' + m_3 V_y' + n_3 V_z'$$

where the l_i, m_i, and n_i are the appropriate direction cosines.

This method requires 3 extra non-linear analog circuits, but the added effort may be justified since the solution is exact. Probe E has promise, but was not used in the present work because of its complexity.

E. Portability - Balloon Tethering

In order to obtain a permanent record of the velocity and temperature fluctuation signals a relatively small portable magnetic tape recorder is used. Its application will be covered later in this report. The other principal factor permitting portable operation is the use of a tethered balloon to support the velocity and temperature sensitive

elements at a predetermined height and location. The only weak point in using a tethered balloon as a base for absolute velocity measurements is the possible movement of the anemometers relative to the ground. Therefore, in February 1949 a preliminary experiment was conducted to determine the motion of such a balloon supported hot wire station.

The preliminary experiment consisted of a test arrangement on about half the scale of the final proposed setup. The Los Angeles office of the Weather Bureau supplied a standard meteorological sounding balloon giving a net lift of 5 pounds, which was used to support a tripod with the junction point at a height of 110 meters. The balloon was tethered to the junction point with 120 meters of line. A sketch of the test layout is shown in Figure 9B.

This test showed quantitatively that the motions of junction point (Point J) were much less than the motions of the balloon (Point B) and so demonstrated the feasibility of the tethering technique. The motions of the junction point and of the balloon were observed by a single theodolite. The observed angular motions of the balloon and its equivalent lateral and vertical motions are shown in Figure 10. The observations for Point J are shown to an enlarged scale in Figure 11*. The wind during these measurements was very turbulent. Its mean velocity was about 6 m.p.s.

Briefly, the results and conclusions of this preliminary test were as follows:

---

*Figures 10 and 11 are taken from a memorandum dated 11 March 1949 which describes this preliminary test in complete detail and was submitted to the Weather Bureau with the proposal for the present research.

1. The stability of the junction point J was very good. There were several isolated large displacements when the wind yawed to wide angles. The stability may thus be improved by increasing the horizontal angle between the two upwind legs of the tripod from 60° to 90°.

2. The use of light steel wires to form the tripod which are less elastic and have less wind drag than the rayon line which was used in the preliminary test will further decrease the motion of the junction point.

With these points in mind, the features of the final setup were determined (see Fig. 9B) and are given below. The configuration was designed to permit J to be at 300 meters, except during very light winds when there is no aerodynamic lift to help lift the weight of the cables. Actual measurements were only made with J at 146 meters, although the equipment seems perfectly satisfactory for measurements at higher elevations. In the following discussion, forces and weights are given in lbs., and some of the dimensions in feet and inches wherever that turns out to be more consistent with the usual data given to specify the quantities.

(1) The balloon employed during the final field measurements is a Seyfang S-600 type (see Fig. 12A), 22 feet long, streamlined, with stabilizing fins, and giving a free lift of 12 lbs. When tethered by several pounds of cable it blows back at less than a 30° angle in winds up to 11 m.p.s. Reference 4 provides more details on the practical operation of a balloon of this type. It is interesting to note that the drag coefficient for such a balloon has an abrupt decrease of value

at a velocity in the range of 2 m.p.s. because there the laminar boundary changes to a more turbulent one which delays separation of the boundary layer from the balloon surface. At around 2 m.p.s. the balloon blows back at a 30^{o} angle. As the wind increases, the total drag actually decreases and the balloon moves forward. An additional favorable effect comes from the increased aerodynamic lift of the upward inclined balloon. It is only at velocities of over 11 m.p.s. that the balloon blows back as far as it does at 2 m.p.s.

(2) Cables E and F are No. 8 (0.020" dia.) piano wire, of 100 lbs. strength, weighing 1 lb. per 917 feet. No. 8 wire was originally also used for cable C, but after an early test with the balloon in a strong wind this was changed to No. 16 (0.037" dia.), of over 300 lbs. strength, weighing 1 lb. for 274 ft. Wire C is the one taking the strain during the balloon raising and lowering operations and so should be stronger than E and F even though these latter take most of the strain once the balloon is in position. Also it is wise to give one of the three wires extra strength as a safety precaution in case one of the other wires breaks. The end fastenings of the wires are conventional "dog-leash" clips, tested to over 100 lbs. pull. Rust, end fastenings, and possible kinks so decrease the true strength of the cables that the strength of the clips is in line with that of the cables.

These steel cables have a modulus of elasticity 60 times greater than that of rayon line, and therefore stretch much less. This means that forces parallel to A, which are transmitted directly to J, will have very little effect on J's position. The steel cables support more tension than the cables in the test case, and are much thinner than the rayon lines; thus cable sag due to wind and gravity is reduced

to negligible amounts. Cable C is maintained vertical.

(3) Cable C has a Litzendraht wire* (magnet wire, 30 strands of No. 36 copper enameled wire, single silk covered) paralleling it, blowing free downwind between J and the ground, conducting the electrical signals from the probes to the ground recording equipment. It is wound on a different winder (Fig. 12B) from that on which the steel Cable C is wound. The voltages are conducted from the winder by sliprings. The conducting Litzendraht cable and the tension-carrying piano wire cable must always be kept separate and wound on different reels to prevent the conductors from becoming shorted. The Litzendraht wire weighs 2 lbs. per 1000 feet.

(4) Cable A is 170 lb. test nylon, weighing about 1.5 lbs. for the 250 meter length. The fact that it is strong and the fact that it does not kink are valuable safety features. The long length of A puts the balloon up into smoother air, away from the turbulent gusts which are passing by J.

(5) In case the balloon breaks loose, a pressure operated plug in the balloon throat drops out and releases the helium at a predetermined altitude, permitting the balloon to be recaptured. This device is pictured in Figure 12C. The cylindrical part goes inside the throat, and the part with bellows is held on immediately outside the throat by an elastic which it releases at the special altitude. The balloon never broke loose, and so the device was never field tested.

(6) The angle between E and F, when viewed from above, is

---

*Purchased from Wheeler Insulated Wire Co., Waterbury, Connecticut.

90^{o} instead of 60^{o} as in the preliminary case.

(7) At J, a 1 meter steel tube pyramid structure provides a base for the probes, Wheatstone Bridges, and batteries. Fig. 13A shows this pyramid with the batteries omitted. The probes are fastened to the tube which hangs down along cable C. At first a balsa pyramid was made and used, but it was not suitable for the forces occurring with strong winds.

(8) At J = 300 meters, the balloon is lifting 10.6 lbs. of equipment. This will not work at low speeds because the lift of the balloon, 12 lbs., is too low to keep the wires taut when the balloon is in a downcurrent. At J = 150 meters, the balloon need lift only 7.2 lbs. of equipment, leaving it with enough excess lift to act against a normal downcurrent. At high wind velocities the balloon lift increases and cable and equipment weight is no longer a problem.

(9) Cables F and E are each wound on hand reels (Fig. 13B) equipped with locking latches. Piano wire C is wound on a heavy, hand operated, surplus reel (center winder, Fig. 13B) originally made for reeling in sounding equipment from ships. A dial on it records the length of line paid out, in fathoms. It has an excellent brake operated by the handle at its top. The metal reel in it is strong enough to withstand the terrific load of 600 meters of wire and 250 meters of nylon wound under 50 lbs. tension.

It was necessary to make many of the measurements within a few meters of the ground, and for this a guyed post provides the simplest steady platform. Figs. 3A and 3B show the final version of this post, an aluminum pole, and also show the way the probe-bridge-battery unit may be transferred without alteration from the pole to the balloon supported pyramid.

F. Measuring Equipment

(1) General Considerations.

Fig. 14 shows block diagrams of the field and laboratory equipment. In the field, the V_1, V_2 and T bridges and their associated sensing elements are supported by post or balloon at the desired position and the Litzendraht cable conducts their outputs to the modulator units. The modulators put the signals on different carriers after which the carriers are amplified, filtered, added together and put into the tape recorder. The V_1 and V_2 carriers are put through non-linear analog stages (which counteract the non-linear response of the individual hot wires) between the amplifier and filter stages. In the earlier stages it was felt that the complexity of the analog circuit would require it to be a laboratory device, for use only following the tape recorder in the laboratory. Fortunately, the analog circuit turned out to be so simple and easy to adjust that it could be taken into the field and used on the signal before the signal was put on the tape. This has the important advantage that the tape recorder affects only a linear function of velocity. A $2^{o}/o$ tape recorder error only causes a $2^{o}/o$ error in velocity measurement. If the analog came after the tape recorder, a $2^{o}/o$ tape recorder error might result in a $10^{o}/o$ or greater error in velocity measurement.

(2) Tape Recorder

The magnetic tape recorder is the critical electronic device on which this entire research project hinged, and so it will be discussed first. It has now proven itself to be an invaluable tool for such measurements as were made here. Modern improvements

(multi channel, less noise and wow) assure that magnetic tape recorders will be utilized much more extensively in future research.

A full-track Concertone tape recorder is used, with 10.5 inch diameter reels of Scotch plastic tape. This gives 1 hour of recording at a tape speed of 7.5 inches per second (for handling frequencies to 7,500 c.p.s.). A tape recorder will not record D.C., so all low frequency signals must be impressed on carrier waves.

Voltage amplitude errors on the order of $\pm 5^{o}/o$ are caused by the mechanical workings of the recorder at the 15 inches per second speed, and therefore this speed was avoided. At 7.5 inches per second the error is only about $\pm 1.5^{o}/o$ of the largest voltage the recorder would handle linearly. The particular machine employed here was thoroughly adjusted and repaired several times at the factory, and hence gave accuracies that could not be expected from stock models of such inexpensive recorders.

Fig. 15 shows the result of a complete recording-playback cycle. It depicts the initial wind velocity which cooled the hot wire versus the corresponding final voltage put out by the tape recorder in the laboratory, and thus includes all the possible errors of measurement except those which might be introduced by the final laboratory amplifier and demodulator. The linearity can be seen to be exceedingly good.

A 40 R.M.S. millivolt input signal is the largest that can be linearly handled by the recorder when the record level is set between 7 and 8. This is just enough signal to move each side of the "cat's eye" fan about 1/16 inch, and is considerably smaller

than the maximum signal which can be recorded.

On some, but not all, recordings there appears a steady oscillation at approximately 2.23 c.p.s. which presumably was put on the tape by the recorder itself (it occurs even when reproducing a perfectly constant calibration signal). It has its largest amplitude during the last quarter of the tape. It caused trouble during analysis work because the frequency is close to one being measured sometimes. A rarer but still troublesome oscillation at 1/4 c.p.s. appears on some temperature signals (carrier frequency 1750 c.p.s.) but not on velocity signals (frequencies 3000 and 5000 cps) recorded simultaneously. Some 60 c.p.s. waves are invariably present, but it is felt these are not caused by the tape recorder.

The recorder has adjustments which can be varied to minimize the noise recorded and played back. These are important and must be set after the recorder is fully warmed up.

In February 1951, a wind velocity recording was made, and several weeks later it was transcribed onto paper by a Brush Pen Recorder. In February 1952, the same tape was run and the signal again transcribed onto paper. Comparison of the papers showed that the signal now contained a large amount of noise of all frequencies, although recently recorded tapes were devoid of such noise. It must be inferred that the magnetic orientation at a point in the tape was altered during the year by the close proximity of other adjacent magnetized layers of tape. Thus tape, stored in reels, is not satisfactory as a method of keeping signals over a long period of time. This provides an interesting example of the loss of information by the increase of randomness of

molecular alignment; it can be termed an increase of entropy.

Fig. 16E shows six pen records of a typical turbulence signal played back by the tape recorder. It can be seen that the recorder reproduces the identical signal each time to a high degree of accuracy. Any error should be random and hence of no great worry in a statistical analysis.

The recorder will introduce a frequency error during the record-playback cycle that is of the same order as the frequency variation in the 60 c.p.s. line and one order smaller than the amplitude error of the line voltage. Since the equipment design utilizes carriers which must be separated by narrow filters, the voltage source to the recorder must be a good one; it is this requirement which dictated the choice of the site at the closed Lancaster Airport, where a 60 c.p.s. line is available at the sewage disposal plant of the Devel Vocational Institute. Previously a 5 K.W. motor generator had been procured, but its frequency stability was only marginal.

(3) Sensing Elements and Wheatstone Bridges

Fig. 17 is the wiring diagram for the three Wheatstone Bridges which deliver the V_1, V_2 and T signals to the field modulators. Fig. 3B shows the bridges. One branch of each bridge is formed by the resistance which is the sensing element for temperature or velocity. Each bridge is built up of wire wound precision resistors and wire wound variable resistors, and incorporates a 5 screw terminal plate for use in connecting the bridge to the sensing probe element, battery, etc. Power is supplied by two 2 volt Willard miniature wet cells (1 pound each) type ER-6-2B. At the current drain of one velocity bridge circuit (about 150 mils), tests showed an average battery voltage drop

of 0.25°/o per hour. During a typical run with all units the voltage would therefore drop about 0.5°/o. All the sensing elements were put through bridge circuits to simplify calibration by providing a zero point of voltage into the modulator.

Five strands of No. 36 copper wire comprise each 300 meter long conductor from a bridge to its modulator. Each conductor therefore has a resistance of about 80 ohms. A common return for all bridges cannot be used because it causes the bridges to interact. Since the modulator impedance is approximately 300 ohms, the voltage entering the modulator from a velocity bridge is only about 2/3 of the voltage put out by the bridge. The impedance of the modulator for the temperature signal was increased to 1000 ohms so as to prevent the relatively high impedance temperature bridge from having its output voltage reduced too much.

There is a strong potential gradient in the atmosphere, causing current to flow in vertically hung grounded conductors, and sometimes making sparks if the ground end of the wire is insulated and then permitted to come near ground. This causes no problem in clear air in the present case where the impedances are low, since the atmosphere-gradient-induced current is minute. It may be a worry during storm conditions when the gradient is much greater.

4) Electronic Equipment

The general components of the electronic field equipment have already been described. Since the conventional units follow typical electronic techniques, only the less usual features will be discussed here.

Consider the V_1 recording unit, Fig. 18. The signal from the V_1 bridge reaches the modulator through an M-derived low pass filter with infinite attenuation at the 3000 c.p.s. carrier frequency. This filter was installed in an effort to eliminate interaction between the V_1, V_2 and T units (the varistor modulator sends an AC signal from the oscillator out along the Litzendraht cable). The interaction was later shown to be due principally to an incorrect calibration technique, but the filters were left on and may conceivably provide some help.

The IN40 varistor modulator has the effect of cutting the peaks off the carrier from the oscillator at a voltage equal to $\pm$ the voltage of the input signal. Even with the variable resistances as shown, some IN40's could not be closely balanced. It is wise to purchase several varistors and select the best ones.

The 3000 c.p.s. band pass filter (with a $\pm$ 100 c.p.s. pass band) was set on a removable plug and later transferred to the laboratory unit where it was needed to help separate the carriers when the tape was played back.

Fig. 6 shows the mixing analog circuit, which simply adds the carriers and puts the voltage $\frac{V_1+V_2+T}{3}$ into the tape recorder. The maximum V_1, V_2 or T signal into this analog is 80 milliamperes.

The V_2 unit, Fig. 19, is identical to the V_1 unit except that it utilizes a carrier signal of 5000 c.p.s. Each of the velocity units has its own 6 volt storage battery to provide bias voltage for its analog circuit. A common battery cannot be applied to the two units because it correlates the V_1 and V_2 signals.

The T unit, also shown on Fig. 19, is similar to the V_1 unit except that it operates at 1750 c.p.s., needs no analog circuit, has

more amplification, and has a varistor presenting a larger impedance to the input signals. It puts out approximately 2 millivolts per ^{o}C temperature change.

It is very crucial when an analog circuit is involved that the amplification factors of the various amplifiers in the units stay constant at the prescribed level. A very stable 300 volt power supply, Fig. 20, was built, and as a further precaution its input was regulated against voltage fluctuations by a Sola transformer. It was not possible to detect an output voltage change with a conventional meter when the load was altered from 0 to 150 milliamperes. The 300 volt supply had under 2 millivolts of ripple in it. The filament supply was not regulated against load, and so it was very important to have all units operating all the time so the filament load would be constant. The same power supply served for both field and laboratory electronic units.

5) Calibration Equipment

The earliest hot wire calibrations were conducted in a low turbulence level-low velocity wind tunnel with a 3 foot square working section. Figs. 21A and 21B are pictures of a hot wire test probe holder in this tunnel. The probe holder was designed to permit a hot wire or probe with several hot wires to be rotated about a vertical axis in 10^{o} increments, and also rotated about a horizontal axis in similar increments.

Later calibrations of the wires actually used in the field were performed in the GALCIT 20-inch tunnel, described in Reference 5.

All calibrations, field and laboratory, were based on a Simpson Model 260 volt-ohm-ammeter. The voltages across the velocity bridges were adjusted to 2 volts on its scale, the analog bias voltages

were similarly set at 5.4 volts, and all bridge outputs and the simulated voltages used for analog calibration depended on the Model 260. A calibrating box (Fig. 22) was built to be used in conjunction with the meter. When the selection switch on the box is at position C, the box serves as a variable calibrated D.C. voltage source which can put a given voltage (corresponding roughly to a specified velocity) into the modulator of a velocity unit. At position A the box, which contains a galvanometer, provides a null indicator for balancing the bridge circuit for zero velocity. This is done while the Simpson meter is used to show the voltage across the hot wire. At position B the box and Simpson meter become a potentiometer which measures the bridge output vs. velocity while the hot wire from the bridge is set in the calibration tunnel.

In practice, the bridge is always set to identical operating characteristics at zero wind velocity with the null indicator and voltmeter. It is not connected to the modulator during this adjustment. Then the output curve is found by setting the wire in a wind tunnel, turning on all the equipment to simulate field operations, and observing the voltage out of the bridge with the potentiometer. For calibrating the analog circuit, the voltage corresponding to any velocity can be duplicated by the box as a voltage source (rather than running the tunnel again), and this method was used at first before it was discovered that the slight difference in impedance between the bridge circuit and the simulated voltage source introduced errors in the analog. This was corrected by building the "Wind Velocity and Temperature Simulator Box" (Fig. 22). In this box, variable resistances

take the place of the resistances used in the sensing elements of the bridges, and the variable resistances are adjusted to cause the bridges to have any desired output voltage. In this manner the bridges themselves act as voltage simulators and there is no worry about differing impedances while calibrating the analogs, or while putting a steady calibration signal into the tape recorder.

Inasmuch as it is difficult to set the tape recorder or laboratory amplifiers to any absolute figure, steady calibration signals, corresponding to a given velocity measured by each hot wire, are put on the tape at the start of each run and in the laboratory the final amplifiers are adjusted to yield the desired corresponding voltages.

There was a lack of agreement between different calibration curves of the same platinum wire which turned out to be caused by improper balancing of the bridge at zero velocity. Zero velocity was "assured" by placing a test tube around the wire--but it was finally discovered that the position of the wire in the tube had a large effect on the magnitude of the convection caused by the wire, and hence the bridge output. A standard test tube was then made wherein the hot wire is held exactly centered. The tube should be held horizontally, with the wire horizontal inside it, to obtain a minimum of convective flow. For the probe having two wires set at angles the above precautions cannot be followed in detail, but sufficient accuracy is obtained if the wires and tube are aligned before the field test and the laboratory calibration in the exact same manner.

The Shorting Switchbox, Fig. 22, is attached to the velocity units in the field so that the Calibrating Box can be switched from one unit to the other without disconnecting any cables, and so that V_1 and

V_2 can be simultaneously shorted to ground to provide a zero point signal for the tape recorder.

III. EXPERIMENTAL MEASUREMENTS AND FIELD OPERATIONS

A. General Measurements

A total of 10 field trips resulted in 5 magnetic tape reels ("Runs") recorded on 4 separate days. The altitude of investigation was varied from 7.5 cm. to 146 meters, with most of the records being for heights of 15, 70 and 240 cm. Mean wind velocities were between 2 and 8 m.p.s. Two runs were made when the air was quite unstable, one with the air very slightly unstable, and two during neutral or slightly stable conditions.

Certain of the runs are presented pictorially in Figs. 23, 24, 25, 26 and 27. In Fig. 23, for example, the velocities in each of the parts of Run 2 are photographed in such a way as to integrate the signal and show at a glance the proportion of time during which the turbulence had any given U-W or U-V values. The pictures may be termed integrated hodograph representations. They serve to show quickly how U and the fluctuations u increase with altitude, how the vertical turbulence w increases even more rapidly, and how the horizontal turbulence appears stronger than either component. The U-V turbulence ellipses are cut off at $\pm 45^{\circ}$ from the U = 0, V = 0 point because the measuring instruments were not designed to respond correctly to such large direction changes. Figs. 24 and 25 give similar pictures for Runs 3 and 4. In Fig. 26 are shown the W-T integration ellipses. The ellipses appear to be rotated clockwise slightly, denoting W-T correlation, and hence showing heat flux. Upcurrents are associated with warm air, and

downcurrents with cooler air. Fig. 27A also gives W-T correlations, and includes a case showing that the flux decreases if the high frequencies are filtered out. In Fig. 28 are plotted distribution functions which describe the turbulence during Run 1.

B. List of Measurements.

The data utilized in this report were recorded at the deserted Lancaster Airport, Lancaster, California. Each recording took place within the space of one hour.

Run 1	Feb. 11, 1951
Run 2	Feb. 7, 1952
Run 3	Feb. 16, 1952 (early afternoon)
Run 4	Feb. 16, 1952 (late afternoon)
Run 5	Feb. 25, 1952

The measurements made on each day varied with the meteorological situation and the type of recording equipment in use. Although temperature and velocity gradients were never measured directly, they could sometimes be approximated from the recorded data; Fig. 29 gives the results for Runs 2, 3, and 4. The surface temperature data are quite questionable, since they come from a thermocouple embedded in the heat meter 0.3 cm. below the ground surface. The temperature gradients were derived from data obtained with a T probe, which was calibrated at one setting to agree with the reading of the shielded thermometer shown in Fig. 30B.

In Fig. 31 are plotted vertical heat fluxes at the air-ground interface, as measured by two heat meters (6, 7). One meter acts as a radiometer to measure the net radiant energy transfer to the

earth. It is illustrated in operating position in Fig. 30B. The same figure also shows where the other heat meter was buried to measure the heat being conducted into the ground. The convective heat transfer through the air is assumed to represent the difference between the radiant energy incident on the ground and the radiant energy leaving the ground plus the heat being conducted into the ground.

Analysis Performed	RUN 1	RUN 2	RUN 3	RUN 4	RUN 5
Picture showing distribution of (U, W)		X	X	X	
Picture showing distribution of (U, V)		X	X	X	
Picture showing distribution of (W, T)			X		
Probability Density for U	X	X*	X*	X*	X*
Probability Density for W		X*	X*	X*	
Distribution function for $\frac{dU_H}{dt}$ and U_H	X				
$\overline{U}$, $\overline{u^2}$ (or $\overline{U}_H$, $\overline{u^2}_H$)	X	X	X	X	X
$\overline{v^2}$ (estimated)		X	X	X	
$\overline{w^2}$		X	X	X	
Skewness of U, V & W distributions		X	X	X	
$f(\tau)$ or $f(r)$	X		X		X
Probability density for A_u, A_v, A_w	X*	X*	X		
$\overline{A_u^2}$, $\overline{A_v^2}$, $\overline{A_w^2}$ at 2.5, 10, and 40 cps.		X	X		
Heat Flux			X		

---

*Denotes compiled but not explicitly reported herein.

RUN 1. Feb. 11, 1951. Hours 1540-1550 (estimated)

Measurements. At z = 7.5 cm., one vertical hot wire recorded U_H, the magnitude of the velocity in the horizontal plane, during a 26 second period.

Meteorological Situation. $\overline{U}$ = 5.8 m.p.s. at 7.5 cm., from the west. $T_1 = 15^{\circ}$ C. The lapse rate was very slightly unstable.

Surface. The area for 100 meters upwind of the probe was similar to the area around the pole in Fig. 32A (fairly smooth sand with small isolated grass tufts). Beyond that for a distance of 30 meters was an area containing sage brush (as in the background of Fig. 30A), with spacing of about 6 meters between bushes. Next came a flat sand and asphalt airport surface extending 2000 meters, and finally more sagebrush reaching to hills about 8 miles distant. It is estimated that the surface roughness coefficient applicable is on the order of 0.1 cm.

RUN 2. Feb. 7, 1952. Hours 1330-1430.

Measurements. At z = 15 cm., 70 cm. and 240 cm., two hot wires and one temperature probe yielded first U, W, and T, then U, V, and T, and then U, W, and T again. Each record lasted 5 minutes.

Meteorological Situation. U was just over 2 m.p.s., east northeast. Medium thick cirrus obscured the sun enough to keep the convective heat flux to a rather low value (0.002 cal/cm^2 sec). Q, T(z) andU(z) are shown on Figs. 29 and 31.

Surface. The surface relative to the pole position was identical to that shown in Fig. 32A. No calculations giving surface

roughness under these conditions were possible, and it can only be estimated that an appropriate roughness coefficient would lie between $0.2 \text{ cm.} < z_o < 5 \text{ cm.}$

RUN 3. Feb. 16, 1952. Hours 1245-1345.

Measurements. At z = 15 cm., 70 cm. and 240 cm., two hot wires and one temperature element yielded first U, W and T, then U, V and T, and then U, W and T again. Each record lasted 5 minutes.

Meteorological Situation. U at 240 cm. averaged 4.6 m.p.s., from the SW. There were no clouds and Q averaged 0.007 cal/cm^2 sec. Q, T(z) and U(z) are shown in Figs. 29 and 31.

Surface. The area upwind of the probe appears in Fig. 32C, which faces southwest. It can be described as similar to the surface of Run 1, except that here the patch of sage brush is closer to the probe. The wind profile of Run 4, during nearly neutral stability conditions, has been analyzed elsewhere in this report to define a surface roughness coefficient of $z_o = 0.07$ cm., and that coefficient should hold for this run too.

RUN 4. Feb. 16, 1952. Hours 1635-1735.

Measurements. Same as Run 3.

Meteorological Situation. Same as Run 3, except that by this late in the day the net radiant heating had dropped to zero and below and the convective heat transfer was zero or slightly negative.

Surface. Same as Run 3 ($z_o = 0.07$ cm.).

RUN 5. Feb. 25, 1952. Hours 1700-1733.

Measurements. At z = 146 meters, one vertical hot wire recorded U_H during a 33 minute run. The hot wire was supported by the tethered balloon.

Meteorological Situation. $\overline{U}$ at 146 meters was 7.7 m.p.s., from the northeast. The sky was cloudless. Due to the lateness of the hour, convective heat transfer had so decreased as to render the lower elevations stable. The surface wind at the start of the run was about 3 m.p.s. The record obtained while the balloon was ascending shows considerable turbulence and increasing wind with elevation up to an elevation estimated to be on the order of 100 meters. There the wind seemed to increase a bit to its value of 7.7 m.p.s. and its turbulence level dropped sharply. Twenty minutes after the run, while bringing the balloon down, one received the impression that the wind at an elevation of 60 meters was as strong or stronger than 7.7 m.p.s. The surface wind was negligible.

Surface. The surface is identical to the type shown in Figs. 32A and 32B for a distance of over 10 miles, and as with Run 2, it is expected that 0.2 cm. $< z_o <$ 5 cm.

C. Data Compilation

RUN 1. (1-26 second period)

Part of Run	z cm.	$\overline{U}_H$ m.p.s.	σ_{U_H} m.p.s.	σ_{U_H}/U_H
1st half	7.5	5.70	2.20	0.39
2nd half	7.5	4.40	1.90	0.43

RUN 3. (9 consecutive 5 minute periods, numbered a through i)

Part of Run	z cm.	$\overline{T}$ °C	σ_T °C	Q.10^{-3} $\frac{cal}{cm^2 sec}$
a	15	21.0	1.56	3.18
b	70	20.3	1.21	5.76
c	240	19.7	1.23	9.40

g	15	20.5	1.20	1.88
h	70	20.6	1.21	4.32
i	240	18.8	1.23	6.42

RUN 5. (1-33 minute period)

z = 146 meters $\quad \overline{U}_H = 7.73$ m.p.s. $\quad \sigma_u = 0.39$ m.p.s.

RUNS 2, 3, and 4 (Each run consists of 9 consecutive 5 minute periods, numbered a through i. U and W were measured in a, b, c, g, h, i. U and W were measured in d, e, f.)

$\overline{U}$, σ_u, and σ_v from parts d, e, and f of Runs 2, 3, and 4 are estimated roughly from the appearance of U-V photographs, without the aid of a densitometer.

The a_w values in the following table are sometimes followed by "?", denoting that the values are the closest obtainable with the rough analysis used but may be far off from the true values. Both a_w and a_u are positive for skewness such that the mode is less positive than the mean.

Part of Run	z cm	$\overline{U}$ m.p.s.	σ_u m.p.s.	σ_w m.p.s.	α_u	α_w	E(2.5) $[(cm/sec)^2\ gm^{-1}\ (c.p.s.)^{-1}]$		E(10)		E(40)	
Run 2							U	V or W	U	V or W	U	W or V
a	15	2.05	.65	.24	0	0?	190	135	21.0	25.1	1.39	4.92
b	70	2.27	.57	.32	+.27	0?	233	158	94.1	18.5	.66	2.91
c	240	2.47	.67	.39	+.40	−.21?	111	190	94.7	19.0	.52	3.03
d	15	1.80	.85				162	145	14.7	22.4	.60	1.79
e	70	2.00	.62				115	209	13.6	21.5	1.01	3.02
f	240	2.70	.86				231	355	18.1	22.3	1.51	3.60
g	15	2.17	.72	.22	0	0?	-	-	20.1	24.5	1.31	3.74
h	70	2.23	.61	.35	+.35	0?	-	-	12.7	19.0	1.21	3.03
i	240	2.68	.83	.31	0	0?	-	-	10.7	14.4	.95	2.53
Run 3												
a	15	3.29	.93	.38	+.71	0?	260	168	49.8	36.2	4.50	6.06
b	70	4.18	1.08	.64	0	0?	483	611	42.7	66.4	5.97	7.48
c	240	4.51	1.54	.72	0	−.29	360	520	40.1	47.8	6.91	6.67
d	15	3.80	1.20				515	628	67.0	56.7	8.60	7.52
e	70	4.00	1.30				285	440	30.8	48.3	4.15	4.95
f	240	5.40	1.60				624	917	48.5	19.7	7.08	6.81
g	15	3.12	.92	.36	+.18	0?	408	187	36.4	38.3	6.27	6.39
h	70	4.96	1.23	.60	+.90	0?	496	710	48.4	75.3	6.53	12.68
i	240	4.85	1.26	.70	+.18	+.48	438	630	31.5	41.1	5.68	5.42
Run 4												
a	15	4.53	1.28	.54	+.68	0?						
b	70	5.66	1.34	1.00	+.37	+.25						
c	240	6.50	1.64	.88	-.12	+.29						
d	15	4.60	1.30									
e	70	5.60	1.85									
f	240	7.40	1.77									
g	15	4.75	1.36	.56	+1.06	0?						
h	70	6.07	1.84	1.03	+.51	+.24						
i	240	7.59	1.81	1.16	-.21	+.54						

D. Field Operations.

(1) Feasibility of the Tethered Balloon as a Probe Mount.

On February 25, 1952 the final setup for balloon tethering was employed for actual measurements. The technique proved itself to be very satisfactory; the balloon rode steadily at a high elevation, and any movements of the junction point and hot wire equipment were practically imperceptible when viewed from the ground. The tethering cables took strong tension and vibrated loudly, due presumably to the forcing by the vortex streets in their immediate wakes. A high frequency signal was found to be present on the resulting tape record, but the frequency turned out to be exactly 60 c.p.s. and so was no doubt due to some electrical pickup. During analysis it was filtered out.

The tethered balloon mount seems to be steady enough for any measurements of spectra, correlation coefficients, velocity distributions, and heat flux. It is of marginal stability for momentum flux measurements.

The one grave disadvantage is that a minimum of six men are required to operate it correctly (only three if three remote controlled winders are available). Four men man the four winders, and two steady the pyramid as it nears the ground. During the February 25 experiment only three men were present, and as a result the probes were damaged, some of the Litzendraht wire shorted, and measurements made with only one wire.

The nose of the Seyfang S-600 balloon begins to be pushed in by the wind when the helium pressure in the balloon is low or

the wind is very strong. As the balloon shape becomes distorted its drag increases markedly. The pressure difference between the inside and outside of the balloon increases immediately after inflating as the helium cooled by expansion from the tanks slowly warms up; it increases as the balloon raises to higher elevations; and it increases whenever the net radiant heating of the envelope by the sun is positive. Since the balloon can only stand a pressure differential equal to about 4 inches of water, a pressure relief valve has been installed which lets the gas blow out through a 4 inch water column trapped between two concentric cylinders. When the balloon cools off, or its altitude is decreased, the nose pushes in from the wind and more helium must be added. If the balloon is flown at a constant altitude late in the afternoon the nose will start collapsing. This occurred during the February 25 run. The hemisphere pushed into the nose had a radius of two feet but did not increase the drag of the balloon in an 8 m.p.s. wind enough to cause termination of the run.

(2) Transportation.

The field equipment to be transported involved 4 large helium tanks, several hundred pounds of electronic gear, (recording equipment, tape recorder, oscilloscope, meters, etc.), winding reels, a 12' aluminum pole, two radiometers, and numerous boxes of miscellaneous gear. Fortunately a 30' closed aluminum trailer was made available and served to carry all the equipment as well as provide a shelter for housing the equipment and personnel during actual tests. The trailer appears in Fig. 32B.

(3) Field Procedure.

After all equipment has been set up, radiometer readings started, and the electronic gear has had time to heat, the velocity analogs are adjusted to the desired curves with the aid of a vacuum tube voltmeter, Simpson meter, Calibrating Box and Wind Velocity Simulator Box. Next a D. C. calibration signal is put on the tape. Then the bridges are set with proper voltages and zeroing, and finally the run can begin. Between each separate part of the run a zero signal is recorded as a reference point to mark zero velocity and provide an identification point on the tape. Another D. C. calibration signal is recorded at the end of the run. Procedure is the same no matter whether the balloon or pole mount is used.

When a new hot wire is installed on a probe, it must be annealed, calibrated in a tunnel in the laboratory (while the bridge is connected to the modulator), and its analog must be set to agree with the calibration curve.

IV. ANALYSIS

A. Analyzing Equipment

(1) General Equipment.

Fig. 14 shows the block diagram of the laboratory equipment. It has already been mentioned that the band pass filters and the power supply are the identical ones used with the field equipment. The signal from the tape recorder (high impedance, about 0.25 V R.M.S.) is first amplified and then directed through three similar amplifier units. In each unit a cathode follower is necessary to match the signal to the low impedance of the filters. The separated carriers are amplified by power amplifiers, rectified, and demodulated by Hycor low pass (pass band 0-100 c.p.s.) filters. The V_1 and V_2 signals are then added and subtracted by means of a simple analog circuit which yields $\frac{V_1 + V_2}{2}$ and $\frac{V_2 - V_1}{2}$. Thus in the laboratory three voltages are obtained which represent either V_1, V_2 and T, or U, W (or V), and T. Fig. 33 gives a detailed circuit diagram of the laboratory equipment.

It will be noted that the resistances in the analog are not of equal value, and hence would not appear to give $\frac{V_1 + V_2}{2}$ and $\frac{V_2 - V_1}{2}$ exactly. The values (except for trivial inaccuracies of $\pm$ 5 ohms), are however intentional, and their unequal magnitudes are given to counteract a bit of V_1 voltage which leaks through an imperfect V_2 filter. Fortunately this simple method provides a complete cure for the problem. There is no appreciable amount of mixing between the velocity and temperature signals at any time.

Other laboratory analysis equipment includes a Brush Pen Recorder with D. C. amplifier, a Model 640 Hickok Oscilloscope with D. C. amplifiers, a camera for photographing the screen, and a General Radio Vibration Analyzer.

(2) General Accuracy

A high degree of accuracy is fortunately not required in a preliminary investigation into trends and general ideas of a relatively new field. No attempt will be made here to define the overall accuracy of measurements. However, it should be noted that the overall variations of atmospheric turbulence characteristics for short time intervals are generally larger than any measurement errors. Where correction terms appear to be able to alter results significantly, they are applied as well as possible. Absolute values are less carefully corrected than relative values. For example, a hot wire measures mass flow, ρU, rather than merely U alone. If hot wires are calibrated at a density ρ_o and then operated at an altitude where the density is ρ, a correction term $\frac{\rho_o}{\rho}$ should be multiplied by all measured values. Such a correction is small (the elevation difference between the calibration and test sites is only around 600 meters), is applicable to all measured values equally, and has therefore been ignored in the analysis.

Calibrations are performed in such a manner that control signals are subjected to the same treatment as the turbulent signals, and the final amplifiers adjusted to give a desired response to the control signals. Thus the resulting turbulent signals are corrected in one step for inaccuracies which they have accumulated throughout their electronic manipulations. It is only possible to

counteract for inaccuracies at one signal setting, but the errors at other nearby settings are then relatively small. The calibration for any hot wire changes slightly from time to time, and the calibration of the analog circuit likewise alters a bit with time. These changes are felt mostly in the absolute magnitude of the recorded signal, and only to second order in its slope.

(3) Errors Introduced by Tape Recorder

The signals reproduced in the laboratory, V_R or W_R, U_R and T_R, are approximately proportional to the input signals, V or W, U and T, but do differ a bit because of the circuits through which the signals have traveled. The principal error is caused by the tape recorder. Errors in mean values are negligible because a steady calibration voltage, S, is put into the recording apparatus at the beginning of each tape recording, and the final output amplifiers are adjusted to give a specific mean value of output, $\overline{S_R}$, when this calibration signal is played back. Ignoring the amplification factor, $S = \overline{S_R}$ exactly. However, although $\sigma_S = 0$, $\sigma_{S_R} = \frac{.03}{\overline{S_R}}$, approximately. The existence of an $\sigma_{S_R} \neq 0$ means also that the inaccuracies of the system have introduced a frequency spectrum $F_{S_R}(\omega)$ onto the steady S signal, where $F_{S_R}(S,\omega) = \overline{S_R^2} \times G_{S_R}(\omega)$. Thus the recording-reproducing cycle has superimposed on any input signal, S, an error with standard deviation $\sigma_S = \frac{.03}{\overline{S_R}}$ and with frequency spectrum $F_{S_R}(S,\omega) = \overline{S_R^2} \times G_{S_R}(\omega)$. The statistical properties of the input signal must be inferred from the statistical properties of the output signal. The techniques for accomplishing this are given in detail in the ensuing sections.

(4) Use of pen-recorder.

In order to check for malfunctioning of the recording apparatus, as well as to permit the operator to get some "feel" for the turbulent signals to be analyzed, it is essential that a permanent visible record of the signals be made. A Brush Pen Recorder with DC amplifier proved to be ideal for this purpose. Various representative traces are shown in Fig. 16. A complete paper record was made of each tape recording, and this record used as a reference when the electrical signals were being analyzed. By getting a continuous picture of the signal being analyzed it becomes a simple matter to adjust calibration amplifications and to determine the exact position in the run.

D. Autocorrelation Analysis.

(1) Method.

The autocorrelation coefficient is defined as $f(\tau) = \frac{\overline{u(t)u(t+\tau)}}{\overline{u^2(t)}}$. Its computation involves integration of the product $u(t)u(t+\tau)$, which in turn involves storing data at time t for use later at time $t+\tau$. A magnetic tape recorder is an ideal tool for storing data over the interval τ, and the integration can be performed photographically or electrically, but for the purposes of the present analysis it was deemed advisable to use a simpler but more tedious computational approach. The turbulent signal was put on paper by the Brush Pen Recorder, the velocity values at $t = 0, \tau_1, 2\tau_1, 3\tau_1, \ldots i\tau_1, \ldots,$ etc., were determined, and each reading $U(i\tau_1)$ was put on an IBM card numbered "i". The cards were run several times through an IBM computer which calculated $\sum_{i=1}^{N} U(t_o + i\tau_1)U(t_o+(i-1)\tau_1)$ for $\tau_1 = 0, 1, 2, 4, \ldots, 128$, giving finally $f(0), f(\tau_1), f(2\tau_1), f(4\tau_1), \ldots,$

$f(128\,\tau_1)$.

The unit interval τ_1 was varied to suit the run being analyzed. $\tau_1 = 0.01$ seconds was used on Run 1, $\tau_1 = 0.4$ seconds on Run 3, and 2.0 seconds on Run 5. The paper speed in the pen recorder was varied for ease in reading off the velocity values, being 12.5 cm/sec for Run 1, 2.5 cm/sec for Run 3, and 0.5 cm/sec for Run 5.

The paper record proved much easier to read accurately if the record being put on was smoothed by an R-C circuit (acting as a low pass filter) on the pen recorder input. For Run 5, which had 2 seconds as the shortest measurement interval, the R-C filter was given a time constant of 0.3 seconds and thus its smoothing was not enough to distort the calculated f(2 seconds). Such a long time constant was required by the large amount of extraneous signal picked up during Run 5. For Run 3, where $\tau_1 = 0.4$ secs, the smoothing time constant was 0.002 seconds. No R-C circuit was employed during analysis of Run 1.

A lack of correlation between U(t) and U(t $\mp \tau$) is introduced by the inaccuracies of reading the values off the trace. This error turns out to be under 1°/o for the present analysis. A simple correction can be applied for it in cases where its magnitude may be important.

$$f(\tau) = \frac{\overline{U(t)U(t+\tau)} - \overline{U}^2}{\overline{U(t)^2} - \overline{U}^2} = \frac{\overline{u(t)u(t\mp\tau)}}{\overline{u(t)^2}}$$

Assume that any specific measured value $u_3(t)$ differs from the true u(t) by r, a quantity which has no correlation with $u_3(t)$ or with previous values of itself. Then $u_3(t) = u(t) \mp r$

$$f(\tau) = K_3 \frac{\overline{u_3(t)u_3(t+\tau)}}{\overline{u_3^2(t)}}$$

where $K_3 = \dfrac{\overline{u_3^2(t)}}{\overline{u_3^2(t)} + \overline{r^2}}$ = the correction factor. For the cases discussed here $\overline{r^2} \ll \overline{u_3^2(t)}$, and so $K_3 = 1$.

If the unit of measurement is Δ, a "rounding off" correction gives the distribution of r, called D(r), as follows:

$$D(r) = 0, \qquad r < -\frac{\Delta}{2}$$

$$D(r) = \frac{1}{\Delta}, \qquad -\frac{\Delta}{2} < r < +\frac{\Delta}{2}$$

$$D(r) = 0, \qquad \frac{\Delta}{2} < r$$

$$\int_{-\infty}^{\infty} D(r)dr = 1$$

$$\overline{r^2} = \int_{-\infty}^{\infty} r^2 D(r)dr = \frac{\Delta^2}{12}, \text{ so in general}$$

$$K_3 = \frac{\overline{u_3^2(t)}}{\overline{u_3^2(t)} + \frac{\Delta^2}{12}}$$

Fig. 16D shows part of the pen recording, from Run 3, which was actually used in the $f(\tau)$ analysis.

(2) Results. Fig. 34 compares all four autocorrelation curves found, while Figs. 35, 36, 37 and 38 give the details of each.

In the "inertial subrange" defined in Kolmogoroff's Similarity Hypothesis the autocorrelation function, f(r), is shown by dimensional reasoning to have a form like $f(r) = 1 - Br^{2/3}$ (the so-called "2/3 law").

In each of the four curves plotted, there is a range between r = 0 and $r = r_c$ where this formula can reasonably be applied. The "K_3" correction just described was not used for these curves. It is of such a direction and magnitude as to make the theoretical and experimental curves agree more closely than shown on Fig. 38. In several instances the critical point where the formula becomes obviously inapplicable is sharply defined.

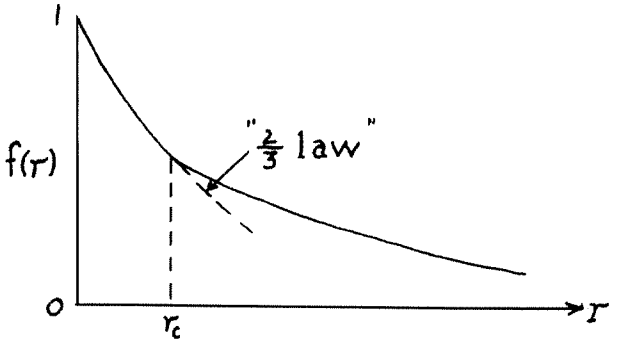

RUN	z	r_c	$\frac{r_c}{z}$	Stability at z
1	7.5 cm.	29 cm.	3.9	Slightly unstable
3	15 cm.	304 cm.	20	Very unstable
3	240 cm.	432 cm.	1.8	Moderately unstable
5	146 meters	139 meters	.95	Slightly stable

It appears that the ratio r_c has a strong dependence on the thermal stability.

C. Energy Spectrum Analysis

(1) Spectrum from Vibration Analyzer readings.

Since $\overline{u^2}$ is twice the total mean turbulent energy in the x direction per unit mass, and

$$\overline{u^2} = \int_0^\infty E(k)dk = \int_0^\infty E(\omega)d\omega = \int_0^\infty E(n)dn,$$

$E(\omega)d\omega$ may be called twice the contribution to $\overline{u^2}$ of the energy in turbulent frequencies between ω and $\omega + d\omega$. The first problem is to find $E(\omega)$ from the output of a filter into which the turbulent signal flows.

Let Y = reading of the General Radio Vibration Analyzer (the narrow band pass filter whose characteristics are given in Fig. 39)

V(t) = voltage into the analyzer (proportional to the turbulent signal) = $K_4 u(t)$

V(t) = $L(y)$ where $L(y)$ means a linear operator acting on y.

Let y^2 have a "power spectrum" $g(\omega)$, so that $\overline{y^2} = \int_0^\infty g(\omega)d\omega$.

Likewise $V^2 \longrightarrow h(\omega)$ such that $\overline{V^2} = \int_0^\infty h(\omega)d\omega$.

It follows that $\overline{y^2} = \int_0^\infty \frac{h(\omega)}{|Z(\omega)|^2} d\omega$ where $Z(\omega)$ is defined as the impedance of the filter.

With the filter set with the pass band centered at ω_1,

$\overline{y_1^2} \cong h(\omega_1) \left[\int_0^\infty \frac{d\omega}{|Z(\omega)|^2}\right]$ since $h(\omega_1)$ is effectively contant over the range where $\frac{1}{|Z(\omega)|^2} \neq 0$

$\therefore \overline{y_1^2} = h(\omega_1) \times \left[\begin{array}{l}\text{Area under filter curve} \\ \text{(Fig. 39) when input freq.} = \omega_1\end{array}\right]$

For calibration, put a known constant frequency (ω_3) signal of amplitude V_c into the filter. Define y_c = y max, and tune the filter to give y_c (the filter will then be "tuned" to ω_3).

Then $h(\omega) = 0, \quad \omega \neq \omega_3$

$h(\omega) = \infty \quad \omega = \omega_3$, and

$$\int_0^\infty h(\omega)d\omega = \overline{V_c^2}$$

making

$$\overline{y_c^2} = \int_0^\infty \frac{h(\omega)d\omega}{|Z(\omega)|^2} = \frac{\overline{V_c^2}}{|Z(\omega_3)|^2}$$

$$\frac{1}{|Z(\omega_3)|^2} = \frac{\overline{y_c^2}}{\overline{V_c^2}} = \text{const. for an } \omega_3$$

This constant gives the magnitude of the ordinate of the filter response curve, in correct units, and so

$\overline{y_1^2} = h(\omega) \dfrac{\overline{y_c^2}}{\overline{V_c^2}} A$, where A is the area under a filter curve having a maximum height of unity. For the particular wave analyzer used, it can be seen (Fig. 39) that $A = K\omega$, where K is a constant, and so

$$h(\omega_1) = \overline{y_1^2} \left[\frac{\overline{V_c^2}}{\overline{y_c^2}} \quad \frac{1}{K\omega_1} \right]$$

$\overline{V^2} = \int_0^\infty h(\omega)d\omega$ and $V(t) = K_4 u(t)$, so

$$E(\omega) = \frac{h(\omega)}{K_4^2} = \overline{y_1^2} \left[\frac{\overline{V_c^2}}{\overline{y_c^2}} \quad \frac{1}{K_4^2 K \omega_1} \right]$$

Thus $E(\omega_1)$ is calculated from the mean square reading of the needle on the vibration analyzer.

(2) Corrections for tape recorder noise.

It was shown in a preceding section that the tape recorder

itself, when playing back a steady AC signal S, produces a frequency spectrum

$$F_{S_R}(S, \omega) = \overline{S_R^2}\, G_{S_R}(\omega)$$

If

$$\overline{A^2} = \int_0^\infty a(\omega)\, d\omega$$

and $\overline{B^2} = \int_0^\infty b(\omega)\, d\omega$ are the mean square values of two uncorrelated functions and with their respective power spectra,

$$\overline{A^2} + \overline{B^2} = \int_0^\infty \left[a(\omega) + b(\omega)\right] d\omega$$

or $$\overline{C^2} = \int_0^\infty c(\omega)\, d\omega \qquad \text{where } \overline{A^2} + \overline{B^2} = \overline{C^2}$$

and

$$a(\omega) + b(\omega) = c(\omega).$$

Let A refer to the noise from the tape recorder, B the response from the turbulence signal, and C the response of the two together (C is what if finally measured by the reading on the Vibration Analyzer).

Then

$$E(\omega_1) = \overline{y_1^2} \left[\frac{\overline{V_c^2}}{\overline{y_o^2}} \quad \frac{1}{K_4 K \omega_1} \right] - \overline{(\text{signal})^2}\, G_{S_R}(\omega_1).$$

When a steady calibration signal S_R from the tape is analyzed, $E(\omega)$ is zero, so

$$G_{S_R}(\omega_1) = \left[\frac{\overline{y_1^2}}{\overline{S_R^2}} \cdot \frac{\overline{V_c^2}}{\overline{y_c^2}} \quad \frac{1}{K_4 K \omega_1} \right]$$

Thus the error term $G_{S_R}(\omega)$ is readily found at various

frequencies, and it is then simple to find the true $E(\omega)$ energy spectrum.

The correction term varies between 1 percent of $E(\omega)$ at 2.5 c.p.s. and a maximum of 10 percent of $E(\omega)$ at 40 c.p.s.

All the $E(\omega)$ for 40 c.p.s. have been multiplied by 1.6 to correct them for the lag of the hot wires at that frequency.

(3) Calculation of Probability Density Function.

The indicator needle of the vibration analyzer wavers so broadly when a turbulent signal is put into the analyzer that $\overline{y^2}$ cannot be estimated directly. Therefore the probability density, D(y), must be found.

$$\int_0^\infty D(y)dy = 1$$

$$\overline{y^2} = \int_0^\infty y^2 D(y)dy$$

D(y) dy represents the proportion of time that the needle is between y and y + dy, so obtaining it requires that an integration be performed over the length of the run. This can be found by photographic integration of the signal into the meter, in just the same way as D(U), D(V) and D(W) are found. However, this method, requiring taking numerous pictures and making densitometer traverses across the negatives, is extremely tedious -- particularly when the curves differ so from Gaussian that approximation methods cannot be used to give $\overline{y^2}$.

As a direct calculation for D(y), the meter reading is noted every 3 seconds, and a mark put at the appropriate y position on a graph. The number of marks put above each y is an indication of the

percentage of time the needle was at y. For accuracy the meter scale was divided into 12 units. Smooth curves were drawn representing D(y). Fig. 40 shows some of these, normalized to make $\int_0^\infty D(y)dy = 1$. When runs were repeated, their results agreed, to a remarkable degree of accuracy, even though the meter readings were not made at exactly corresponding times during the run.

Calculation of $\overline{y^2}$ was performed on computing machine, using the formula

$$\overline{y^2} = \sum_{i=0} y_i^2 D(y_i) \Delta y.$$

(4) Results.

(a) Energy Spectra.

As in the case of the "2/3 law", dimensional reasoning for the "inertial subrange" permits derivation of the formula $E(n) \sim n^{-5/3}$ (the so-called "-5/3 law"). On Fig. 41 is plotted the energy spectrum for all runs for which such measurements were made. It can be seen that the average spectrum is close to the "-5/3 law". Energies at 2.5, 10, and 40 cycles per second were measured in each case. The upper range of eddy sizes for which the "-5/3 law" seems to be reasonably well verified coincides with the upper range of eddy sizes for which the "2/3 law" fits.

(b) Isotropy.

Fig. 42 presents the calculated integrated energy spectrum curve which shows the energy in all frequencies greater than n for a typical case averaged from the Run 3 spectra data ($E(2.5) = 480$, $E(10) = 48$, $E(40) = 4.8 (cm/sec)^2 gm^{-1} (c.p.s.)^{-1}$. It is interesting to see that the W energy and the U energy are the same for high fre-

quencies, but start to separate at just under 2 c.p.s. The curves in this low frequency range are merely estimated, but since they must be smooth there are sufficient points to determine their shape closely. Due to the present measurement technique, the energy spectrum E(n) for turbulent components parallel to the mean wind is different from the energy spectrum, say G(n), for the transverse turbulent components, even for isotropic turbulence. Where $E(n) \sim n^{-5/3}$, $G(n) = \frac{4}{3} E(n)$, (see Reference 17), and so the indicated isotropy of turbulent energy must be viewed with regard to this relationship. In plotting Fig. 42 it was assumed that equal energies yield equal numbers (i.e., transverse energy $= \frac{3}{4} G(n)$ for $2.5 < n < 40$ c.p.s.).

Remembering that $G(n) = \frac{4}{3} E(n)$, the energy spectra data for Runs 2 and 3 (pg. 43) can be examined for isotropy. Run 3 indicates isotropy rather well at the three frequencies. For Run 2 the isotropy is not apparent at 40 c.p.s. It is believed the lack of isotropy is more likely due to an error in adjustment of the analysis equipment than to anisotropy of the turbulence.

(c) Isotropy from probability density curves.

On Fig. 40 are plotted the probability density curves for the signals from the vibration analyzer. To obtain energies from such curves it is necessary to find the mean square meter reading $(\overline{A^2})$, and multiply it by a calibration constant times the reciprocal of the frequency. Remembering $G(n) = \frac{4}{3} E(n)$, the U and W curves are generally similar except that at n = 2.5 c.p.s. (representing the largest eddies) and particularly for z = 15 cm., the vertical turbulent energy is less than the horizontal. This transition from isotropy to anisotropy occurs at an elevation and eddy size which is fairly consistent with the transition region demonstrated by the integrated energy spectrum and

the "2/3 law".

(d) Intermittency and maximum values.

The D(U) and D(W) curves of Fig. 40 show that the amount of 40 c.p.s. energy tends to be rather constant over time (and therefore horizontal space). This can be inferred from the thinness of the D curves. On the other hand, the 2.5 c.p.s. eddies have very broad D curves implying that the distribution of these eddies is irregular. These gusts must therefore be more closely related to the forcing function than are the smaller ones. The D curves are also valuable in showing the maximum energy at a particular frequency during a given run. An intermittency factor might best be defined here as $\frac{\sigma_A}{\bar{A}}$. Similar intermittency has been noted in the turbulent flow in wakes (8).

(e) Panofsky (9) has suggested that the vertical velocity energy spectrum be given by

$$E_1(\omega) = \frac{2\pi\,\omega\,z^2}{\left(\frac{\omega z}{\sigma_w} + 2\pi\right)^3}$$

The energies given by this equation have been checked at frequencies of 2.5, 10 and 40 c.p.s. for z = 70 cm. with the typical measured single velocity component energies used during the calculation of the integrated energy spectrum curve.

Panofsky Spectrum $E_1(\omega)$		Average Measured Spectrum $E(n)$	
$E_1(2\pi.2.5)$ = 32.6(cm/sec)^2	$\frac{1}{\text{gm rad/sec}}$	E(2.5)=38.2(cm/sec)^2	$\frac{1}{\text{gm rad/sec}}$
$E_1(2\pi.10)$ = 4.02		E(10) = 3.82	
$E_1(2\pi.40)$ = 0.301		E(40) = .382	

D. Momentum Flux and Heat Flux Analysis

(1) General:

The horizontal shearing stress P, which can be referred to as the momentum flux through a horizontal plane, is given by

$$P = - \rho \overline{uw} \qquad \text{(10, pg. 461)}$$

$$= - 1.23.10^{-3} \overline{uw} \text{ dynes/cm}^2 \text{ for w and u in cm/sec.}$$

The heat flux Q through a horizontal plane is given by

$$Q = C_p \rho \overline{wT}$$

$$= 0.295.10^{-3} \overline{wT} \text{ cal/sec cm}^2 \text{ at S.T.P., for w in cm/sec and T in } ^{o}C.$$

Both fluxes require the calculation of a mean value of a product of two variables. The distribution of u and w is graphically illustrated by Figs. 23, 24, and 25, while that for w and T is shown in Fig. 26.

The fluxes represented by these pictures can be calculated by finding the distribution functions D(uw) and D(wT) from densitometer readings of the negatives from which the pictures were made. It would take an excessively long time to perform this accurately. It was decided that sufficient accuracy could be obtained by graphical means, working with the photographs directly, and assuming the distribution to be adequately represented by a double Gaussian function.

Method a. (12, pg. 20-21). Assume the photograph has coordinates x and y, and that the ellipse on it has the distribution function

$$D(xy) = f(x, y) = \frac{1}{2\pi \sigma_x \sigma_y \sqrt{1 - r^2}} e^{-\frac{1}{2(1-r^2)}\left(\frac{x^2}{\sigma_x^2} - \frac{2rxy}{\sigma_x \sigma_y} + \frac{y^2}{\sigma_y^2}\right)}$$

where σ_x and σ_y are the conventional standard deviations.

All constant density lines are concentric ellipses.

$$\int_{-\infty}^{\infty}\int_{-\infty}^{\infty} f(x, y)dx\, dy = 1, \text{ and}$$

$$\overline{xy} = \int_{-\infty}^{\infty}\int_{-\infty}^{\infty} xy\, f(x, y)\, dx = r\, \sigma_x\, \sigma_y$$

r is the correlation coefficient.

If the scales are so adjusted that $\sigma_x = \sigma_y$, the principal axes of the ellipse must be at 45° angles to the x axis, by symmetry. Let these new axes define the ' (primed) plane, in which plane there is no correlation. σ_x' and σ_y' are the standard deviations of the distributions in the new system. By the geometrical properties of ellipses,

$$\sigma_x^2 + \sigma_y^2 = \sigma_x'^2 + \sigma_y'^2$$

Also,

$$1 - r^2 = \frac{\sigma_x'^2\, \sigma_y'^2}{\sigma_x^2\, \sigma_y^2} \qquad (13, \text{ pg. } 242)$$

but $\sigma_x = \sigma_y$, so

$$r = \frac{+\ \sigma_x'^2 - \sigma_y'^2}{\sigma_x'^2 + \sigma_y'^2}$$

and $\overline{xy} = \dfrac{\left(\sigma_x'^2 - \sigma_y'^2\right)\sigma_x\, \sigma_y}{\sigma_x'^2 + \sigma_y'^2}$ which is simply a function of the known σ_x σ_y and the relative dimensions of the principal axes of the ellipses.

This calculation method requires varying scale sensitivities to make $\sigma_x = \sigma_y$ and so was not used in this research, but it is a convenient method for other cases.

Method b. This second method is as accurate as the first and simpler to apply under these special circumstances.

Assume the same $D(xy) = f(x, y)$ as before.

Then $\overline{xy} = S_{xx} \sigma_x^2 = S_{yy} \sigma_y^2$ where S_{xx} is the slope, relative to the x axis, of the line connecting the mean values in the y direction of the elements of thickness dx at any x. The equation for this line is $y = r \frac{\sigma_y}{\sigma_x} \chi$ (13, pg. 222), and therefore

$$S_{xx} = r \frac{\sigma_y}{\sigma_x}$$

so $\overline{xy} = r \sigma_x \sigma_y = S_{xx} \sigma_x^2 = S_{yy} \sigma_y^2$.

It is easy to estimate the slope of the line of the means (regression line) from the pictures. For slender ellipses the line of means is almost identical to the principal axis of the ellipse.

(2) Heat Flux Method.

The measuring techniques of this project introduce no hidden correlations between w and T into the photographs. In case W or T_1 is given the wrong mean value, there is no change of measured heat flux by the graphic method.

If the center line of the hot wires had been set at a slight angle to the horizon, the W signal would include a slight U dependence, but not enough to interfere with any results.

(3) Total Heat Flux Results.

During Run 3, measurements of heat flux were made at 15, 70 and 240 cm. by correlating the instantaneous signals of tempera-

ture and vertical velocity (Fig. 25). The results are presented in Fig. 43. The values calculated agree fairly well with the radiometer measured flux, and show fair consistency in that the later run at each elevation invariably indicates a decrease of flux, and the flux increases with altitude. At first this latter statement might appear to be a paradox when one considers that large amounts of heat cannot be created in the air. A possible explanation for the result is that the low elevation heat flux is representative of that due to the turbulent mixing from the smooth surface immediately surrounding the pole, while the flux at higher elevations is caused by the roughness elements some distance (say $z \cdot \frac{\overline{U}}{\sigma_w}$) away, which in this case were sagebrush bushes separating the local smooth area from the airport. This explanation points out the large effect that surface conditions may have on convection. It is assumed that the heat flux is higher than average at the lower elevations at the sagebrush area downwind of the pole.

(4) High Frequency Heat Flux Results.

The conventional heat flux W-T correlation picture is shown on Fig. 27A together with a picture of the same run differing only in that an R-C filter is put on the W input to eliminate the high frequencies. The time constant of the filter is 0.52 seconds, and the picture shows that approximately half of the heat flux is eliminated by the filter. Thus about half of the heat flux at 70 cm. appears to be carried by eddies with periods less than 2 seconds. This is in disagreement with the results of Swinbank (11), who reports negligible flux is lost when the response time of the measuring instrument is several seconds. $\overline{U}$ during his measurements was the same as for

these, and $Q \sim 1.4.10^{-3}$ cal/cm^2 sec. His site was open, level grassland, and he used z = 137 cm. It is not felt that the differences in surface, total flux, or elevation are large enough to account for the different conclusion.

(5) Momentum Flux Method.

The obtaining of $\overline{uw}$ is very difficult with any equipment, despite the fact that for a normal case of P = 1 dyne/cm^2 and σ_U = 1 m.p.s., the slope S_{xx} = 0.08, which should be observable on the ellipse picture. The nature of simultaneous measurements of U and W is bound to introduce an experimental correlation between the two velocities merely because the axis of the instrument cannot be absolutely horizontal. The hot wire - tape recorder method does offer a simple way of correcting for the error. Briefly, if $\overline{W} = 0$ really holds for the time interval during which the integration takes place, then $\overline{uw}$ as calculated from the ellipse picture is almost exact provided the picture also shows that the apparent $\overline{w} = 0$. If the picture shows that $\overline{w} \neq 0$, then one of the amplifiersshould be readjusted, and another picture made, until, by trial and error, $\overline{w} = 0$.

These conclusions can be derived in the following way.

Let U and W represent the true wind velocities related to earth coordinates. Assume the central axis of the hot wire probe is pointing upward at an angle θ . Call V the total wind, and φ the angle it makes with the x axis.

V_1 = velocity of wind on hot wire 1 (upper wire)

V_2 = velocity of wind on hot wire 2 (lower wire)

$V_3 = \frac{V_1}{1-a}$ = voltage from the V_1 amplifier

$V_4 = \frac{V_2}{1+a}$ = voltage from the V_2 amplifier.

a = a correction term.

$$V_1 = V\cos\left(\frac{\pi}{2} - \varphi + \theta\right) = \frac{1}{\sqrt{2}}\left[U(\cos\theta - \sin\theta) + W(\sin\theta + \cos\theta)\right]$$

$$V_2 = V\cos\left(\frac{\pi}{2} + \varphi - \theta\right) = \frac{1}{\sqrt{2}}\left[U(\cos\theta + \sin\theta) + W(\sin\theta - \cos\theta)\right].$$

Let $(\cos\theta + \sin\theta) = A = 1 + \theta + 0(\theta^2)$

$(\cos\theta - \sin\theta) = B = 1 - \theta + 0(\theta^2)$

$A^2 + B^2 \cong 2 + 0(\theta^2)$

$$U = \frac{1}{\sqrt{2}}\left[V_3(1-a)B + V_4(1+a)A\right]$$

$$W = \frac{1}{\sqrt{2}}\left[V_3(1-a)A - V_4(1+a)B\right]$$

(if $\theta = a = 0$, $U = \frac{1}{\sqrt{2}}(V_3 + V_4)$ and $W = \frac{1}{\sqrt{2}}(V_3 - V_4)$.

Assume $\overline{W} = \overline{w} = 0$, and assume the amplifiers have been adjusted to give an apparent $\overline{w} = 0$ on the photograph (i.e., $\overline{V_3 - V_4} = 0$). Then

$$W = \frac{(V_3 - V_4)}{2} \times (1-a)A$$

$$W_{actual} = W_{photograph} \times (1-a)(1+\theta) = W_k.$$

Therefore, correction of the hot wire amplifier sensitivities to cause $\overline{W}_{photograph} = 0$ makes $W_{photograph}$ very close to the true W, provided $\overline{W} = 0$.

If $W_{photograph} \neq 0$, there appears to be no simple way to calculate $\overline{uw}$ from the picture.

If the analog circuits are grossly misadjusted, a W-U correlation will be introduced which cannot be canceled by the above method except over a very narrow velocity range.

(6) Momentum Flux Results

The only photographs which show this characteristic that $\overline{W}_{photograph} = 0$ are the first ones for Run 2 and Run 3. No correlation is evident in the Run 3 pictures. The correlation required for a typical shear force in this case would be represented by a slope of the correlation ellipse axis of about 0.10. This amount should be large enough to detect and measure. Since none is apparent either the measurements are incorrect or the shear force is much less than usual.

The correlation pictures for Run 2 do indicate momentum flux,

$$P_{o\ 15\ cm} = 0.21 \text{ dynes/cm}^2$$

$$P_{o\ 70\ cm} = 0.52$$

$$P_{o\ 240\ cm} = 1.50$$

These values demonstrate the same dependence on height exhibited by the heat flux measurements, and perhaps for the same reason.

E. Mean Values, and Total Isotropy

(1) Photometry

It is necessary to obtain the means, standard deviations and skewnesses of the various velocity components, and for this the probability densities must first be obtained in some form. These require some type of time integration to show the relative length of time during which the signal representing the component is between particular velocities. An electronic counting circuit (14) can give the distributions directly, but it was not available for this project.

Therefore, photographs of the signal, say U(t), were made by photographing the screen of an oscilloscope having U(t) on the vertical axis and a steady high frequency sweep on the horizontal axis. Fig. 27B shows a picture made from a typical negative (on which 3 signals were put). The lines at the bottom are the U = 0 calibrations.

A special track was built on which the negatives could be moved through the densitometer in such a way that the density was always read midway between the oscilloscope grid lines. The densitometer consists of a conventional photomultiplier tube, dry battery high voltage supply, microammeter, and a light of variable intensity operated off line voltage through a Sola constant voltage transformer.

Fig. 27B shows a typical densitometer calibration picture such as is taken and developed with each set of negatives. A rectangle of light on the oscilloscope screen (from a high frequency sine wave on the vertical axis, and linear sweep on the horizontal axis) is photographed for one minute, moved, photographed another minute, etc., until parts of the film have exposures corresponding to 0, 1, 2, 3, 4, and 5 minutes. Thus points are obtained on an exposure vs densitometer reading curve, from which D(U) can be found from densitometer readings on the distribution negative. Over a wide range the density "d" of the plate = $\gamma \log_{10} e$, where e = exposure and γ is a constant depending on the film and type of development. It follows that, since the densitometer reading $R = K_1 10^{-d}$, $R = Ke^{-\gamma}$. This formula fits the points found by the above method, and permits their extrapolation.

(2) Photometry errors.

No check as to the accuracy of these procedures has

been made, but the resulting probability densities obtained are smooth consistent curves showing expected characteristics and yielding data of reasonable values.

The darkening of a photographic plate is a function of the exposure which it is given. The Eberhard effect, caused by localized action of the developer during development, appreciably darkens dark areas immediately adjacent to light ones, and lightens light areas next to dark ones. This causes no difficulty in the present case because densitometer measurements were not made in regions having high density gradients.

The formula e = It, where I = intensity of illumination, and t = time of exposure, is not always correct (termed "Reciprocity Failure"). At very long or very short exposures ($t < \frac{1}{500}$ sec. or $t > 5$ secs) the error becomes appreciable. Since for all negatives a broad (2 mm. thick) sweep line is used, and the vertical motions of the line are of low amplitude at high frequencies, the oscilloscope light reaching a given point comes in units of time greater than $\frac{1}{500}$ sec. Observations of the signal showed it rarely stayed in one spot for over 5 seconds. Therefore the reciprocal law holds, as applied here.

The "Pre and Post-Exposure Effect" is one wherein the density of the film is shown to depend on whether the total exposure it received was due to one long exposure or many short ones. Again, for this analysis, the error so caused is found to be negligible.

(3) Calculation of $\overline{U}$, $\sqrt{\overline{u^2}}$, and α

Assume D(U) has been found by the photographic method, and plotted.

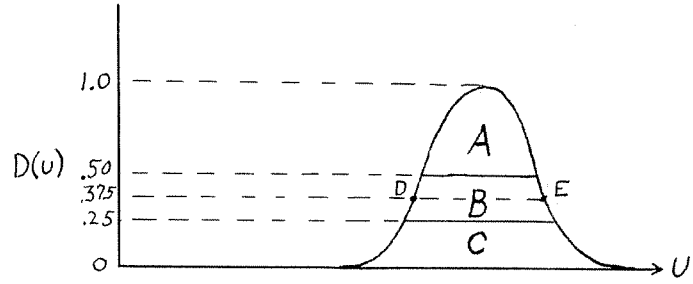

$\overline{U}$ is found approximately by estimating the centers of the areas A, B, and C, and averaging the U values of these centers.

$\sqrt{\overline{u^2}}$ is assumed to represent the standard deviation σ_U of a normal curve. For such a curve, the distance DE(on the line which is 37-1/2 percent of the maximum height of the curve) = $\frac{\sigma_U}{0.357}$

$$\sqrt{\overline{u^2}} = 0.357(D-E)$$

α , for a Pearson Type III curve which is a close approximation to any of the skew distributions, = 2 $\left[\frac{\text{mean-mode}}{\sigma_U}\right]$ (15, pg. 106). The mean and σ_U have already been found. The mode is the value of U having the highest D(U).

When D(U) is plotted from a very few points, α cannot be found, but $\overline{U}$ and $\sqrt{\overline{u^2}}$ can still be obtained reasonably accurately.

(4) Correction for $\sqrt{\overline{u^2}}$

As noted elsewhere, if the tape recorder records a steady carrier voltage S, it plays it back as a varying voltage S_R having mean $\overline{S_R}$ and standard deviation $\sigma_{S_r} = \frac{.03}{\overline{S_R}}$. If a turbulent signal is recorded, its standard deviation σ_2 as measured on

playback will therefore be larger than the true standard deviation σ_1 of the recorded signal. If all standard deviations come from Gaussian distributions, it can be shown that

$\sigma_1^2 = \sigma_2^2 - \sigma_{S_R}^2$, which is the correction formula by which σ_1 is obtained. The correction is small enough to be ignored except for the temperature measurements.

Proof: If the tape recorder alone causes a signal with distribution function $f(p) = B\exp\left(\frac{-P^2}{2\sigma_{S_R}^2}\right)$, and if the input turbulent signal can be represented by $f(x) = A\exp\left(\frac{-x^2}{2\sigma_1^2}\right)$, then the distribution function $q(x)$ of the resultant output is given by

$$q(x) = \int_{-\infty}^{\infty} \left[Ae^{-\frac{x_1^2}{2\sigma_1^2}}\right]\left[Be^{-\frac{(x-x_1)^2}{2\sigma_{S_R}^2}}\right] dx.$$

This reduces to $g(x) = Ke^{-\frac{x^2}{\sigma_1^2 + \sigma_{S_R}^2}}$, so

$$\sigma_2^2 = \sigma_1^2 + \sigma_{S_R}^2 .$$

(5) Errors from incorrect densitometer techniques.

If the densitometer technique for finding $D(x)$ is very poor and gives a) a value of $\left[D(\bar{x})\right]$ which is too high by 20 percent and b) a value of $\left[D(2\sigma)\right]$ which is too low by 20 percent, then the standard deviation which is found will be 10 percent too small. The mean and skewness will be negligibly affected. This numerical example is intended to demonstrate the maximum errors that might be expected, and it is seen they are not of such magnitude as to materially harm the results.

(6) Total Isotropy Results

When all eddy sizes are considered the turbulence near the surface is very anistropic. Figs. 23, 24 and 25 illustrate this clearly.

On Fig. 44 the isotropy energy ratios $(\frac{\sigma_W}{\sigma_U})^2$ are plotted vs. elevation. There is too much scatter to permit worthwhile generalizations other than to note the ratio first increases linearly with altitude, and then stays surprisingly constant, and there is no definite correlation with stability. The anistropy is quite pronounced at all the elevations to 240 cm. The equivalent ratios, $(\frac{\sigma_V}{\sigma_U})^2$, were not calculated but can be estimated from the pictures (Figs. 23, 24 and 25). They vary from 1 to 2 with no observable relation between the ratio and elevation or heat flux.

The ratios $(\frac{\sigma_i}{\overline{U}})$ are given on Fig. 45, and demonstrate in another manner the same things Fig. 44 shows. Corresponding points from two parts of one run have rather similar $\frac{\sigma_i}{\overline{U}}$ values.

G. I. Taylor (16, pg. 61) in 1927 found $\sigma_U = \sigma_V = \sigma_W$ at z = 130 feet, $\frac{\sigma_V}{\sigma_W} = 3$ at z = 2 feet, and $\frac{\sigma_V}{\sigma_W} = 1.4$ at 8 feet. Also $\frac{\sigma_U}{\sigma_V} = 1$ over large σ_U ranges. In the same reference Scrase's results are listed. He found $\frac{\sigma_V}{\sigma_W} = 1.6$ at z = 2 feet, and the ratio was nearly constant to 15 feet. At 60 feet, $\frac{\sigma_V}{\sigma_W} = 1.2$. All of these results were for zero temperature gradient. They agree in general with the values listed in this report.

$\frac{\sigma_T}{\sigma_W}$ are plotted in Fig. 46 for very unstable lapse rate conditions, and for reference, $\frac{\sigma_U}{\sigma_W}$ are also shown. The striking simi-

larity of both curves suggests that the mechanisms and coefficients for transfer of momentum and heat are rather similar for these conditions.

F. Roughness Coefficient.

For an adiabatic atmosphere, the velocity profile is accurately given near the ground by (10)

$$\overline{U} = \frac{1}{k}\sqrt{\frac{P_o}{p}}\,\log\left(1 + \frac{z}{z_o}\right)$$

where k is the von Karman coefficient = 0.40, P_o is the surface shear, and z_o a roughness coefficient.

Run 4 (see Fig. 29) was the only one made at low level during near-adiabatic conditions. For $\overline{U}_{15\,cm}$ = 4.64 m.p.s., $\overline{U}_{70\,cm}$ = 5.97 m.p.s., and $\overline{U}_{240\,cm}$ = 7.04 m.p.s., z_o turns out to be z_o = 0.07 cm. The velocities given follow the logarithmic profile, and are the average values during parts a, b, c, g, h, and i of Run 4 except that $\overline{U}_{70\,cm}$ has been increased 2 percent over the true average to give a consistent z_o.

If ε_1 is the height of the surface roughness elements, Prandtl (10) suggests that $z_o = \frac{\varepsilon_1}{30}$ meaning the roughness elements are about 2 cm. high at the site of Run 4. Paeschke (10) finds $\varepsilon_1 \cong 2$ cm. for a fallow field. In the present case, the upwind surface consists mostly of smooth sand and airport with a clump of 1 meter diameter sagebrush a distance upwind. The sagebrush has thin branches and few leaves. ε_1 = 2 cm. appears to be of a logical order of magnitude for this case.

The ground shear can be simply calculated from the given velocity profile. It has a reasonable value,

$$P_o(\text{calculated}) = 1.41 \text{ dynes/cm}^2$$

The surface under these flow conditions is termed "Aerodynamically Rough" by Calder's definition (6).

G. Kolmogoroff's Similarity Hypothesis.

Consider a typical energy spectrum curve representing the energy per unit mass and unit wave number (k, number of waves per unit length).

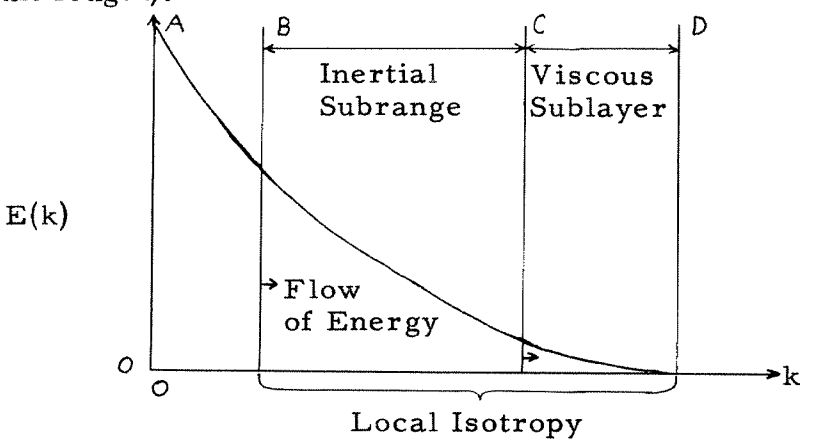

The eddy sizes can conveniently be divided into several ranges. (17, 18) A-B is comprised of eddies of dimensions on the same order as the size of the forcing device by which they are first produced. For example, behind a wind tunnel grid the dimension would correspond to that of the grid spacing.

B-D is Kolmogoroff's region of local isotropy. It is assumed that as eddies in A-B decay, they lose their correlation with their surroundings and the pressure forces tend to "randomize" them and make them isotropic.

C-D is the viscous sublayer of small eddies whose kinetic

energy of turbulent motion is being dissipated into heat through the action of viscosity. Viscosity puts an effective upper limit on the maximum wave number. Turbulent characteristics in this region must depend on the kinematic viscosity and the energy dissipation $\varepsilon = \frac{-d}{dt}(\frac{3}{2}\overline{u^2})$. The energy dissipation must be continually fed into this region from the B-C region. There is thus a constant flow of energy along increasing wave numbers as the eddies break down into smaller ones.

B-C is the inertial sublayer of the local isotropy region. In it the inertial forces are much greater than the viscous ones(i.e., the Reynolds Number is large) and therefore the turbulent characteristics must depend only on ε, the rate of energy flow across a wavenumber.

For the inertial subrange, dimensional reasoning requires that

$$f(r) = 1 - \frac{C_1}{\overline{u^2}}(\varepsilon r)^{2/3}; \text{ the so-called "2/3 law",}$$

and $$E(k) = C_2 \varepsilon^{2/3} k^{-5/3}; \text{ the so-called "-5/3 law".}$$ C_1 and C_2 should be universal constants.

Energy spectrum measurements in this report have shown a reasonable degree of isotropy of turbulent energy at frequencies between 2.5 and 40 cycles per second, corresponding to eddy dimensions of about 10 cm. to 1.6 meters. At z = 15 cm. the 2.5 c.p.s. energy starts demonstrating anistropy. The Kolmogoroff "inertial subrange" evidently does apply to eddies of these sizes. The preceding "2/3 law" and "-5/3 law" "verifications" of the inertial subrange extend over even larger eddy ranges, but it must be remembered that

they are merely necessary, not sufficient, conditions for the existence of such a subrange. If the range of agreement between the autocorrelation coefficient and the "2/3 law" does actually correspond to the entire inertial subrange then the measurement at 146 meters suggests that the subrange may be quite large in the atmosphere.

The direct measurements of f(r), E(k), and the isotropy of turbulent energy suggest that the range of the inertial subrange may sometimes be extended in atmospheric turbulence to eddies having dimensions as much as 20 times larger than the characteristic dimension considered to represent the forcing function. The height z of measurement of the eddies would appear to be a logical dimension to provide an upper end to the inertial subrange. From the experimental results it seems that the actual size of the largest isotropic eddies increases with increased thermal instability. This is explained by assuming that the presence of the ground tends to damp out the vertical component of mechanically induced turbulence for eddies of size up to z, but then the thermal instability adds vertically directed energy which keeps the measured energy close to isotropic.

H. Dissipation and total atmospheric Energy

(1) Energy Dissipation

Since $f(r) = 1 - \frac{C_1}{\overline{u^2}} (\varepsilon r)^{2/3}$ in the initial subrange defined by Kolmogoroff, and since C_1 should be a universal constant and f(r) and $\overline{u^2}$ are known for several runs, it is possible to calculate the rate of dissipation of total turbulent energy into heat. In Ref. 19 a value of $C_2 = 1.33$ was found for

$g(r) = 1 - \frac{2C_2}{\overline{3u^2}} (\varepsilon r)^{2/3}$. Also, for isotropic turbulence,

(17, 19)

$$g(r) = f(r) + \frac{1}{2} r \frac{\partial f}{\partial r}$$

so

$$f(r) = 1 - \frac{1}{2} \frac{C_2}{\overline{u^2}} (\varepsilon r)^{2/3}, \quad C_1 = \frac{C_2}{2} = 0.67$$

Using this value for C_1, it is found that:

run	elevation	$(cm^2 sec^{-3}) = -\frac{d}{dt}(\frac{3}{2} \overline{u^2})$
1	7.5 cm.	138.10^3
3	15 cm.	$1.8.10^3$
3	240 cm.	$3.04.10^3$
5	146 meters	$0.0020.10^3$

It can be seen that the dissipation drops off rapidly with elevation.

If a smooth curve is fitted to the above data and the energy dissipation integrated up to 200 meters, its order of magnitude is found to be:

Total dissipation $\sim 2.10^4$ ergs/sec cm^2

Consider a column of air extending from the ground to an elevation of 1000 meters and having properties typical of those existing on an average sunny afternoon when convection is rising to 1000 meters. Let $\overline{U}$ = 4.8 m.p.s., and near the ground $\sigma_U^2 = \sigma_V^2 = 1.44$ $(mps)^2$ and $\sigma_W^2 = 0.36$ $(mps)^2$, tapering off rapidly with altitude.

The kinetic energy of the mean motion is $1.42.10^7$ ergs/cm^2.

The kinetic energy of the turbulent motion is about $1.4.10^5$ ergs/cm^2.

The power being expended in overcoming a surface shear force of 1 dyne/cm^2 is about 5.10^2 ergs/sec cm^2.

The viscous dissipation, which dies off very rapidly with altitude, is about 20.10^3 ergs/sec cm^2 as calculated from the auto-correlation curves (above).

Heat balance - Rate at which heat energy is going into the ground $\sim 8.4.10^4$ ergs/sec cm^2.

- Rate at which more radiation is being received than lost $\sim 38.10^4$ ergs/sec cm^2.

- Rate at which heat moves up into the atmosphere by convection $\sim 29.6.10^4$ ergs/sec cm^2.

Thus in one minute convection transfers as much energy as already exists in the form of kinetic energy. Most of this energy goes to heat the air directly, but some of it is represented by potential energy which can become the kinetic energy of mechanical motions which only turns into heat through the action of viscosity.

If there were no net radiant heating or cooling, the viscous dissipation would be 5.10^2 ergs/sec cm^2, matching the energy required to overcome the surface shear stress. With thermal heating the viscous dissipation as calculated is an order of magnitude larger, implying that the turbulent kinetic energy put into the atmosphere by the thermal instability is much greater than that put in by the kinetic energy of the mean flow. It should be remembered that the value of C_1 or C_2 which determines the value of the dissipation has never been shown to hold over the wide eddy range considered here. Thus these generalizations concerning the dissipation may eventually prove to be misleading.

REFERENCES

1. Willis, J. B.: Review of Hot Wire Anemometry. Report ACA-19, Australian Council for Aeronautics. Oct., 1945.

2. Anderson, L. J., and Heibeck, H. L.: A Tau-Meter for Rapid-Response Temperature Recording Systems. Bulletin of the A. M. S., Vol. 32, No. 2, Feb., 1951, pg. 67-70.

3. Weske, J. R.: A Hot Wire Circuit With Very Small Time Lag. NACA-TN No. 881. Feb., 1943.

4. Myers, R. F.: A Low-Level Temperature Sounding System for Routine Use. Bulletin of the A. M. S., Vol. 33, No. 1, Jan., 1952. Pg. 7-12.

5. Liepmann, H. W., Laufer, J., and Liepmann, Kate: On the Spectrum of Isotropic Turbulence. NACA-TN No. 2473, Nov., 1951.

6. Vehrencamp, John E.: An Experimental Investigation of Heat and Momentum Transfer At a Smooth Air-Earth Interface. Department of Engineering, University of California at Los Angeles, May, 1951.

7. Halstead, M. H. and Mather, J. R.: Micrometeorology of the Surface Layer of the Atmosphere. Interim Report No. 15. The Johns Hopkins University Laboratory of Climatology, Seabrook, New Jersey, Sept., 1951.

8. Townsend, A. A.: Momentum and Energy Diffusion in the Turbulent Wake of a Cylinder. Proc. Roy. Soc. Vol. 197. (1949) Pg. 124.

9. Panofsky, H. A.: A Working Hypothesis for the Vertical Velocity Spectrum in the Friction Layer. Symposium on Atmospheric

Turbulence in the Boundary Layer. M.I.T., June, 1951.

10. Stewart, H. J.: Kinematics and Dynamics of Fluid Flow. Handbook of Meteorology. Berry, Bollay & Beers. McGraw-Hill, New York. 1945. Pg. 412-500.

11. Swinbank, W. C.: The Measurement of Vertical Transfer of Heat and Water Vapor by Eddies in the Lower Atmosphere. Journal of Meteorology, Vol. 8, No. 3, June, 1951. Pg. 135-145.

12. Liepmann, H. W., and Laufer, John: Investigations of Free Turbulent Mixing. NACA-TN No. 1257. August, 1947.

13. Yule, G. U., and Kendall, M. G.: An Introduction to the Theory of Statistics. Hafner Publishing Co., New York, 1950.

14. Liepmann, H. W.: On the Use of Counting Methods for the Measurement of Mean Values in Turbulence Research. Submitted to the NACA in Partial Fulfillment of Contract NAw-5777. Guggenheim Aeronautical Laboratory, Calif. Institute of Tech., Nov., 1950.

15. Kenney, J. F.: Mathematics of Statistics, Part I. D. Van Nostrand Co., New York. 1939.

16. Taylor, G. E. & Sutton, O. G.: Discussion, Atmospheric Turbulence, Qt. Journal Roy. Met. Soc. No. 58, Jan., 1932.

17. Chuang, F. K., Cole, J. D. and Roshko, A.: On the Statistical Theory of Turbulence. Submitted to the NACA in partial fulfillment of Contract NAw-5777, Guggenheim Aeronautical Laboratory, Calif. Inst. of Tech., July, 1951.

18. Batchelor, G. K.: Kolmogoroff's Theory of Locally Isotropic Turbulence. Proc. Camb. Phil. Soc., Vol. 43, 1947, Pg. 533-559.

19. Batchelor, G. K., and Townsend, A. A.: Decay of Isotropic Turbulence in the Initial Period. Proc. Roy. Soc. (London), ser. A., Vol. 193, No. 1035, July 21, 1948, pp. 539-558.

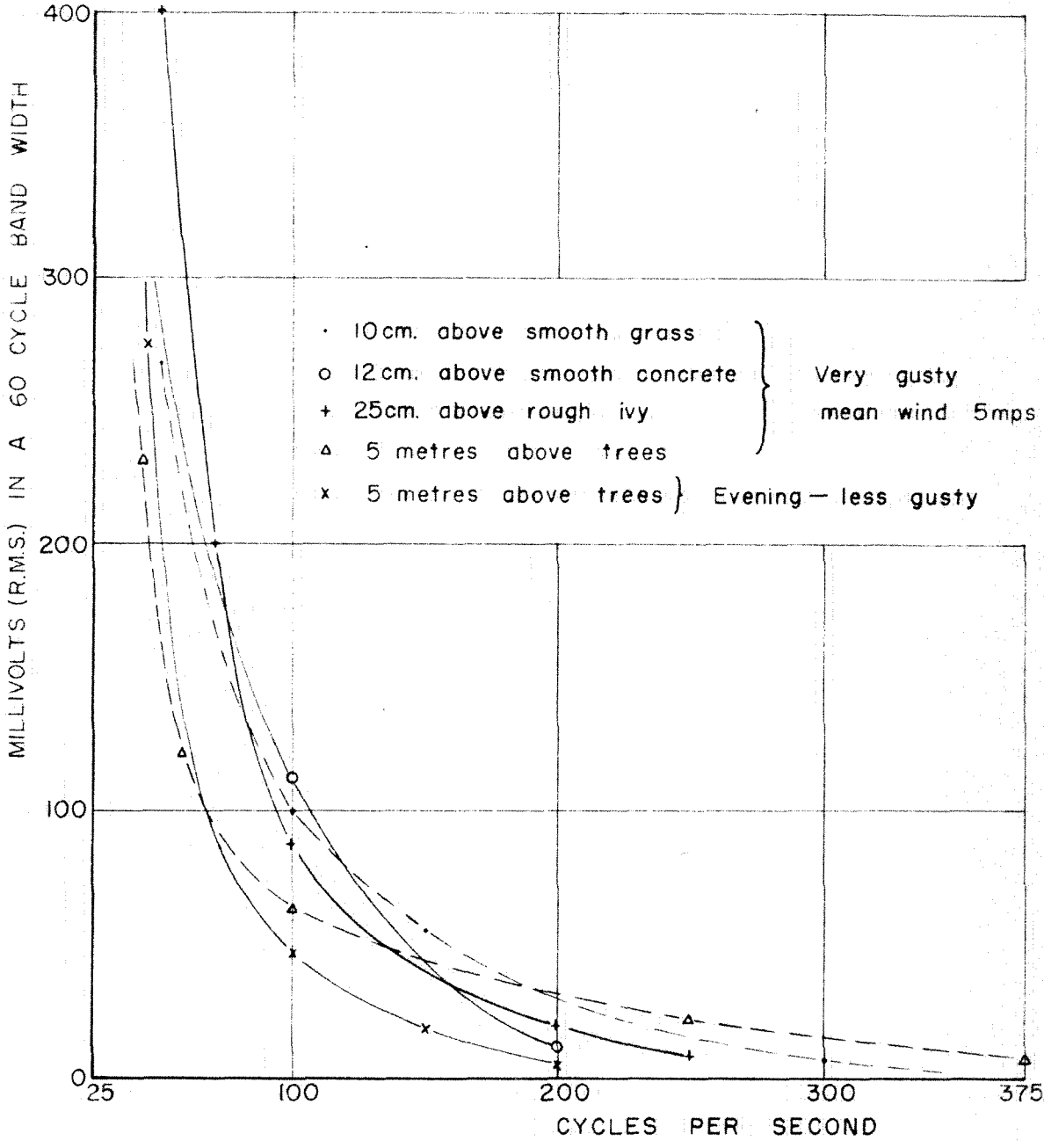

FIG. 1 FREQUENCY SPECTRUM

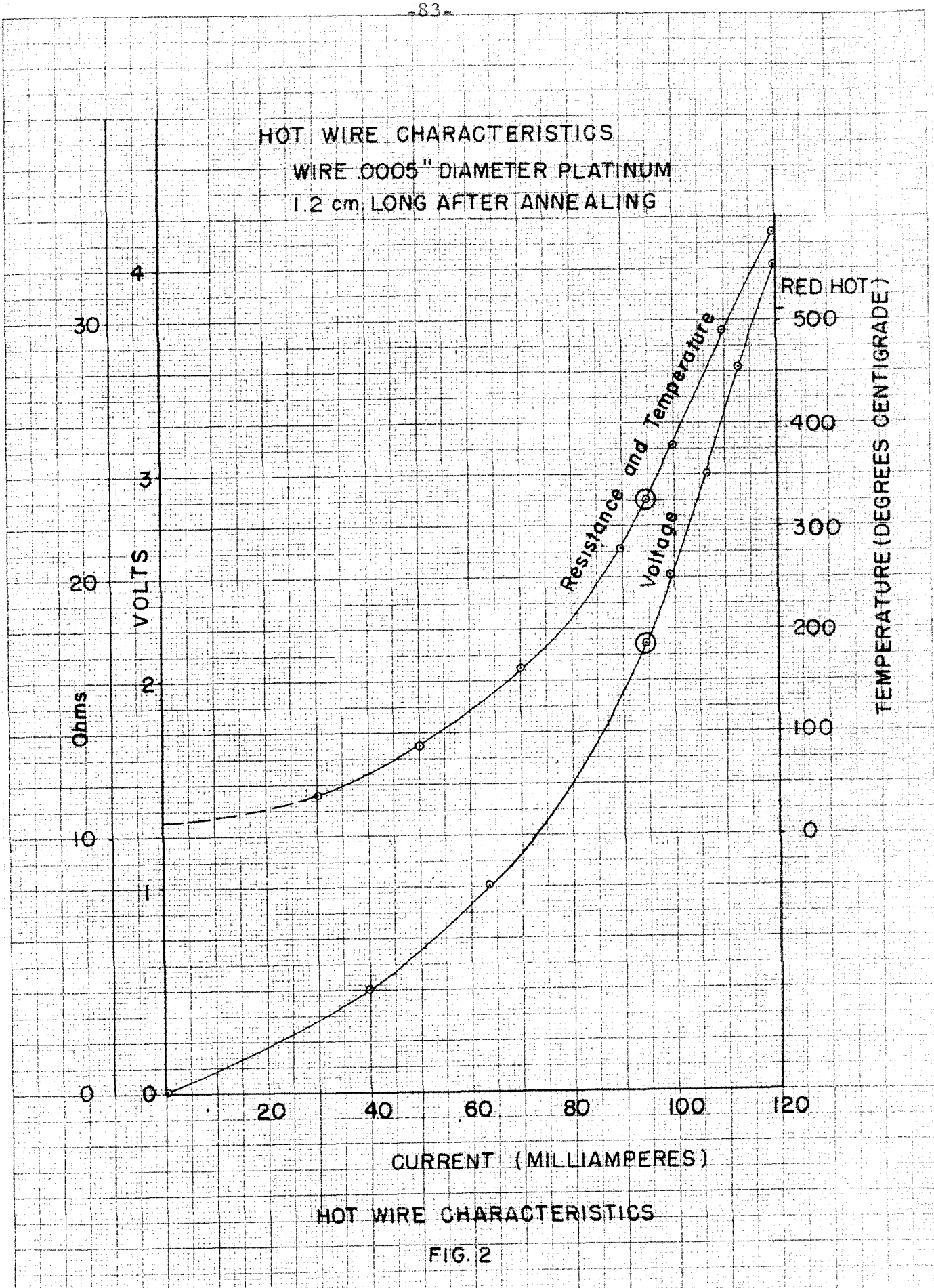

HOT WIRE CHARACTERISTICS

FIG. 2

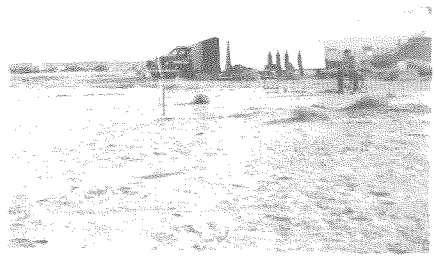

Fig. 3 A Support Pole and Field Equipment

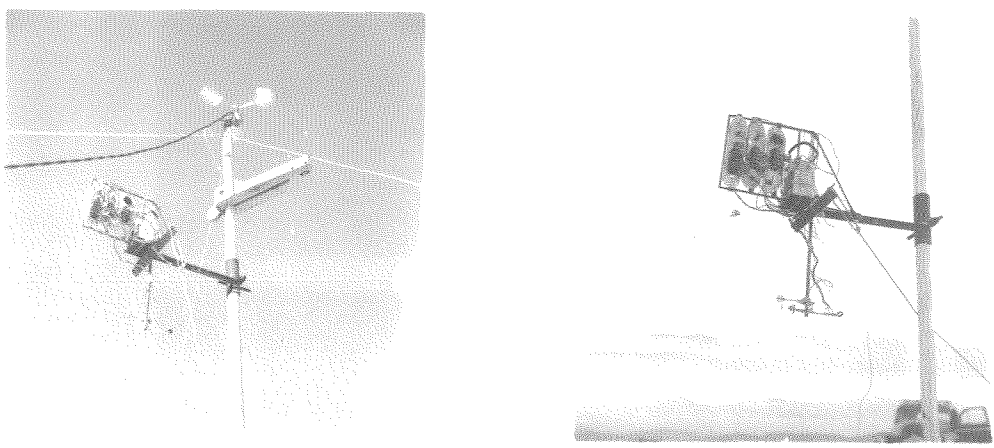

Fig. 3 B Support Pole (Closeup)

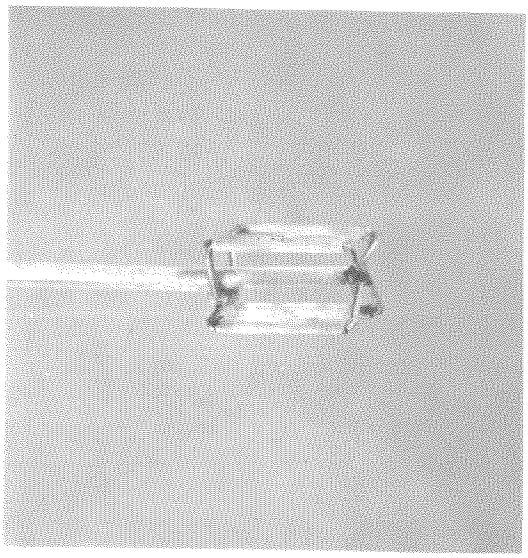

Fig. 4A Temperature Probe

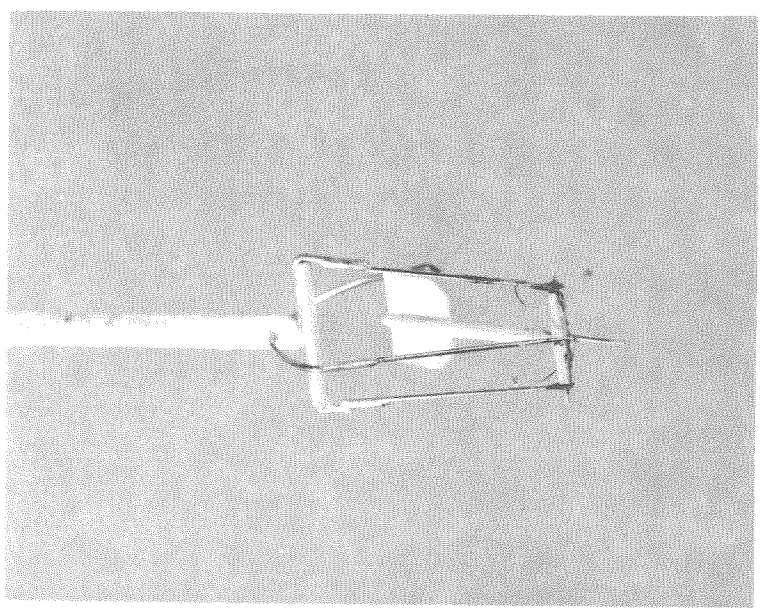

Fig. 4B Velocity Probe

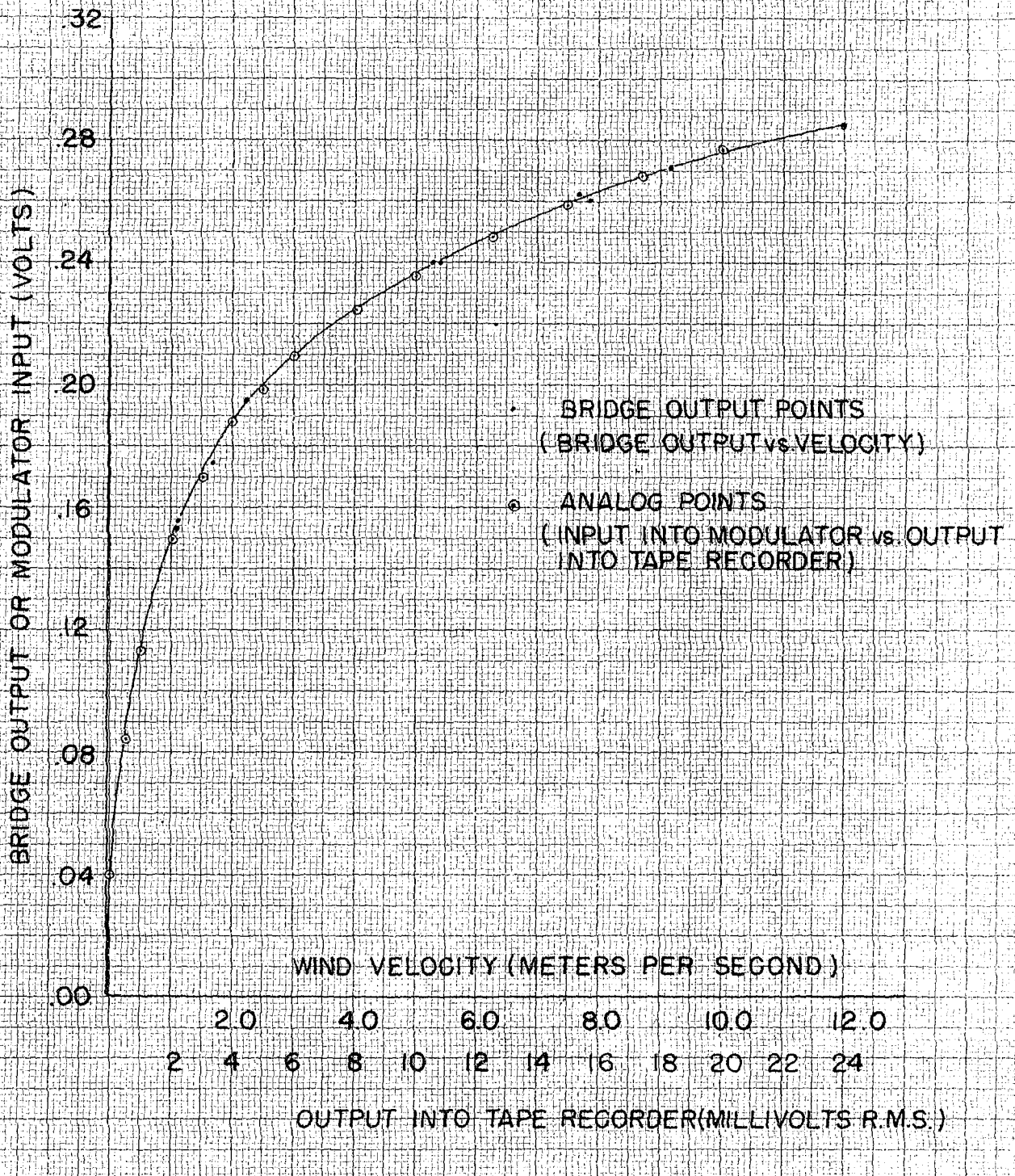

HOT WIRE RESPONSE AND ANALOG CURVES

FIG. 5

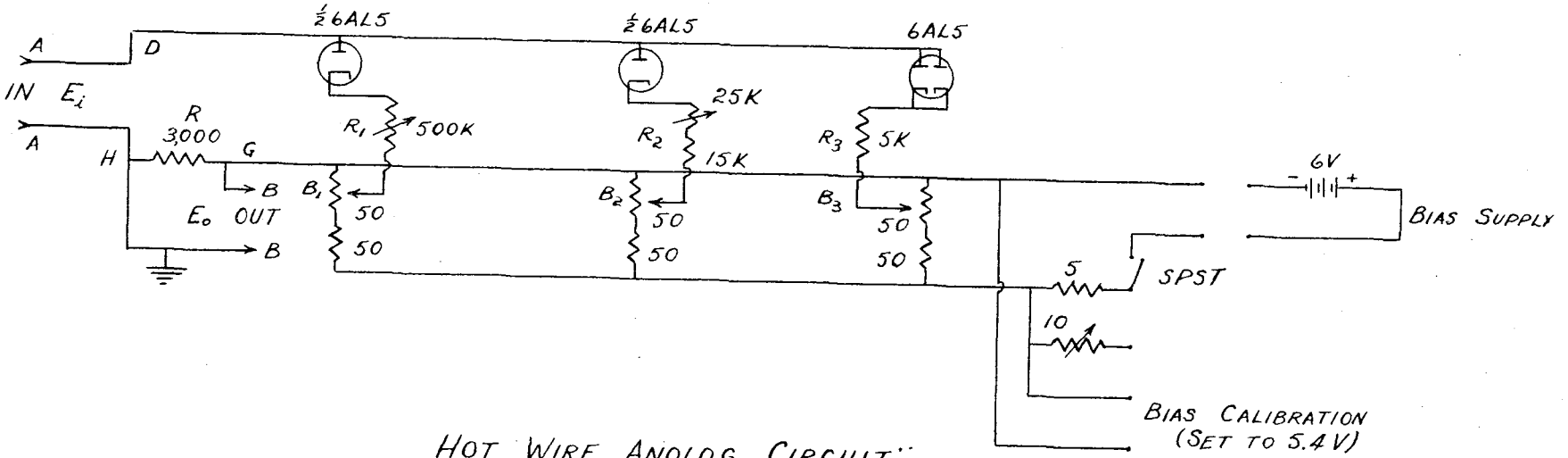

HOT WIRE ANOLOG CIRCUIT

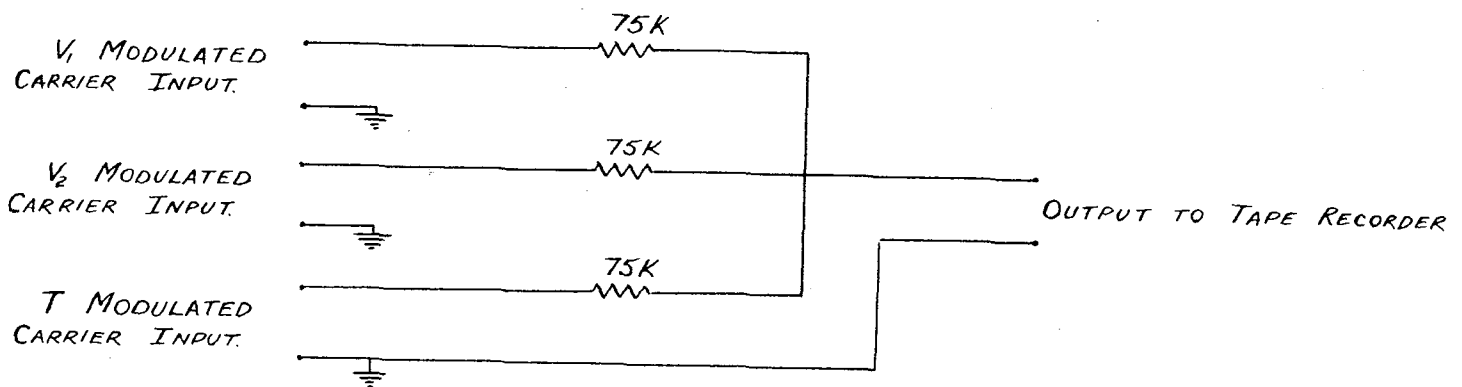

MIXING ANALOG CIRCUIT

FIG. 6 ANALOG CIRCUITS

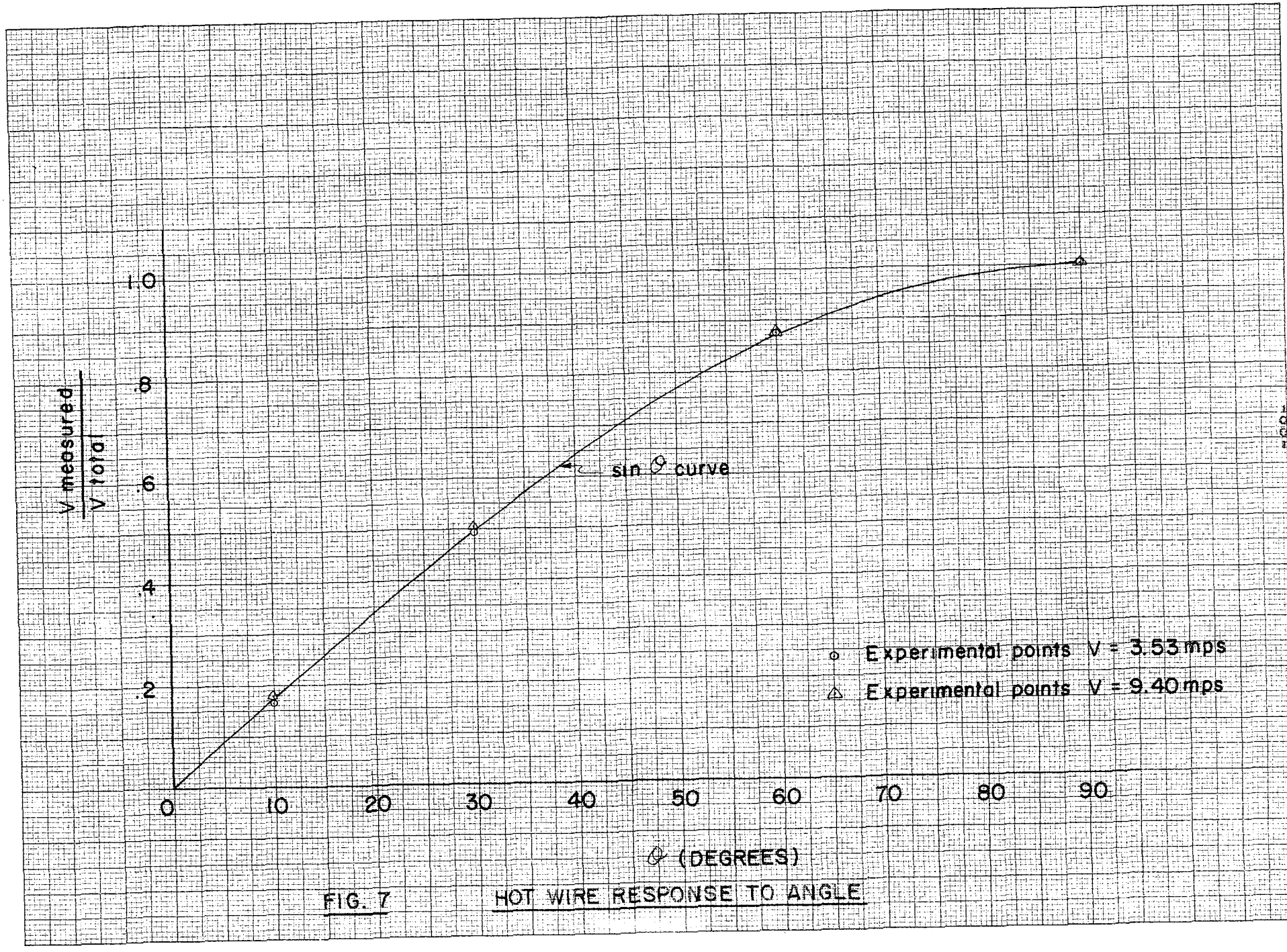

FIG. 7 HOT WIRE RESPONSE TO ANGLE

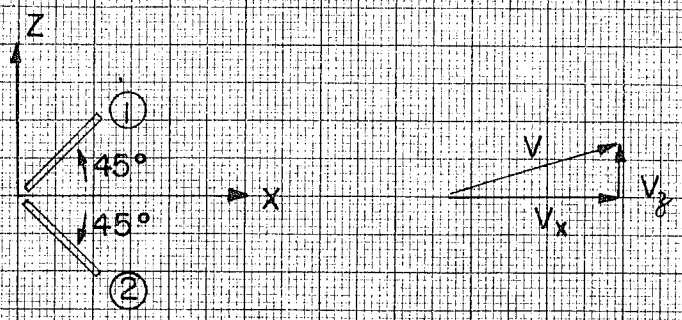

TWO DIMENSIONAL CASE
PROBE A DIAGRAM
FIG. 8A

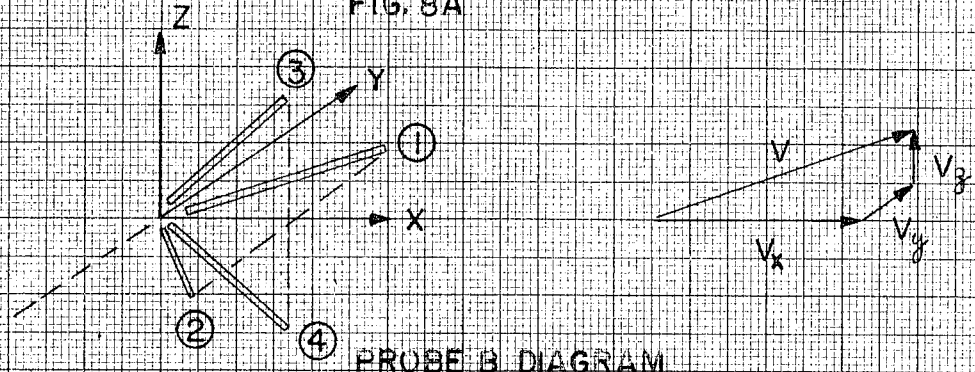

PROBE B DIAGRAM
FIG. 8B

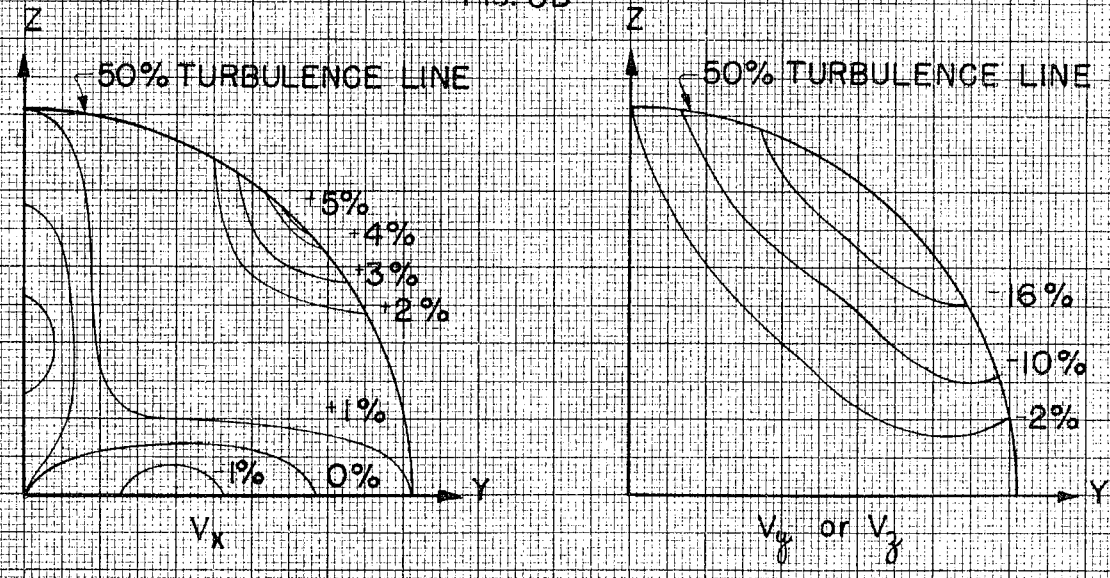

APPROXIMATE CONSTANT ERROR CONTOUR
LINES FOR PROBE B

PROBE B ERROR DIAGRAMS
FIG. 8C

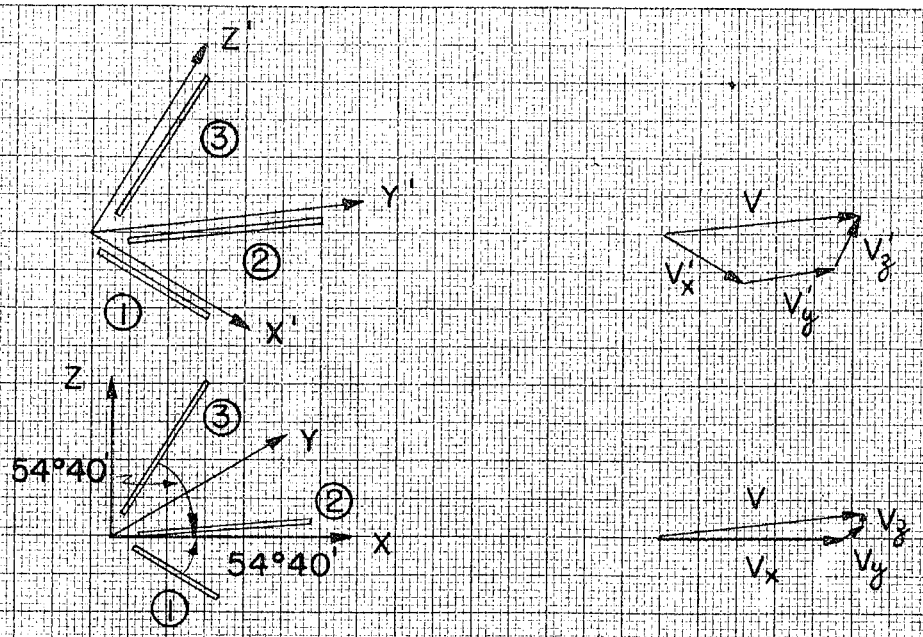

PROBE E DIAGRAM

FIG. 9A

TEST SET-UP

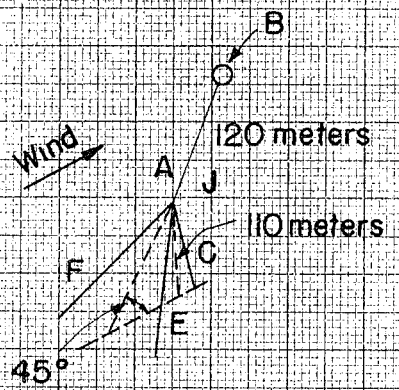

Rayon Strings

Balloon - diameter 5' 9"

lift 5 lbs.

For velocities to 8 m.p.s.

FINAL SET-UP

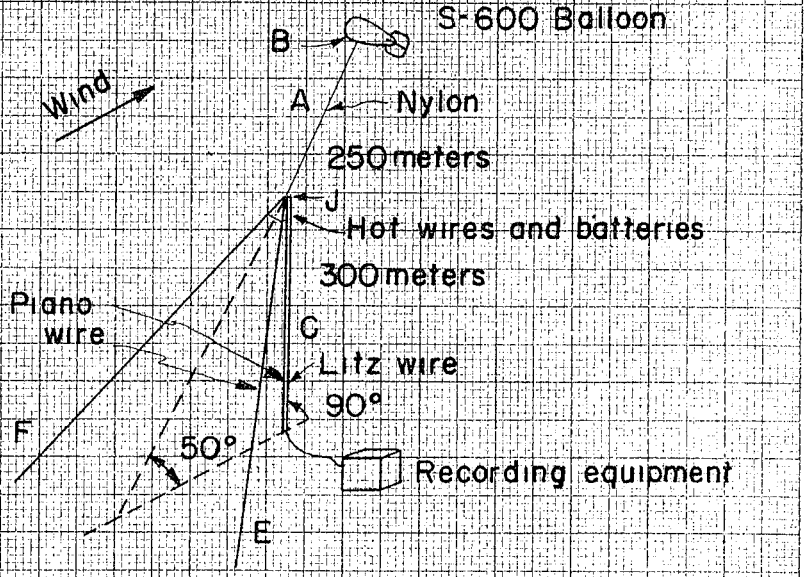

Shown at maximum height

Balloon - streamline, 22' long, lift 12 lbs.

Hot wires and batteries $3\frac{1}{2}$ lbs.

For velocities to 12 m.p.s.

FIG. 9B BALLOON TETHERING DIAGRAMS

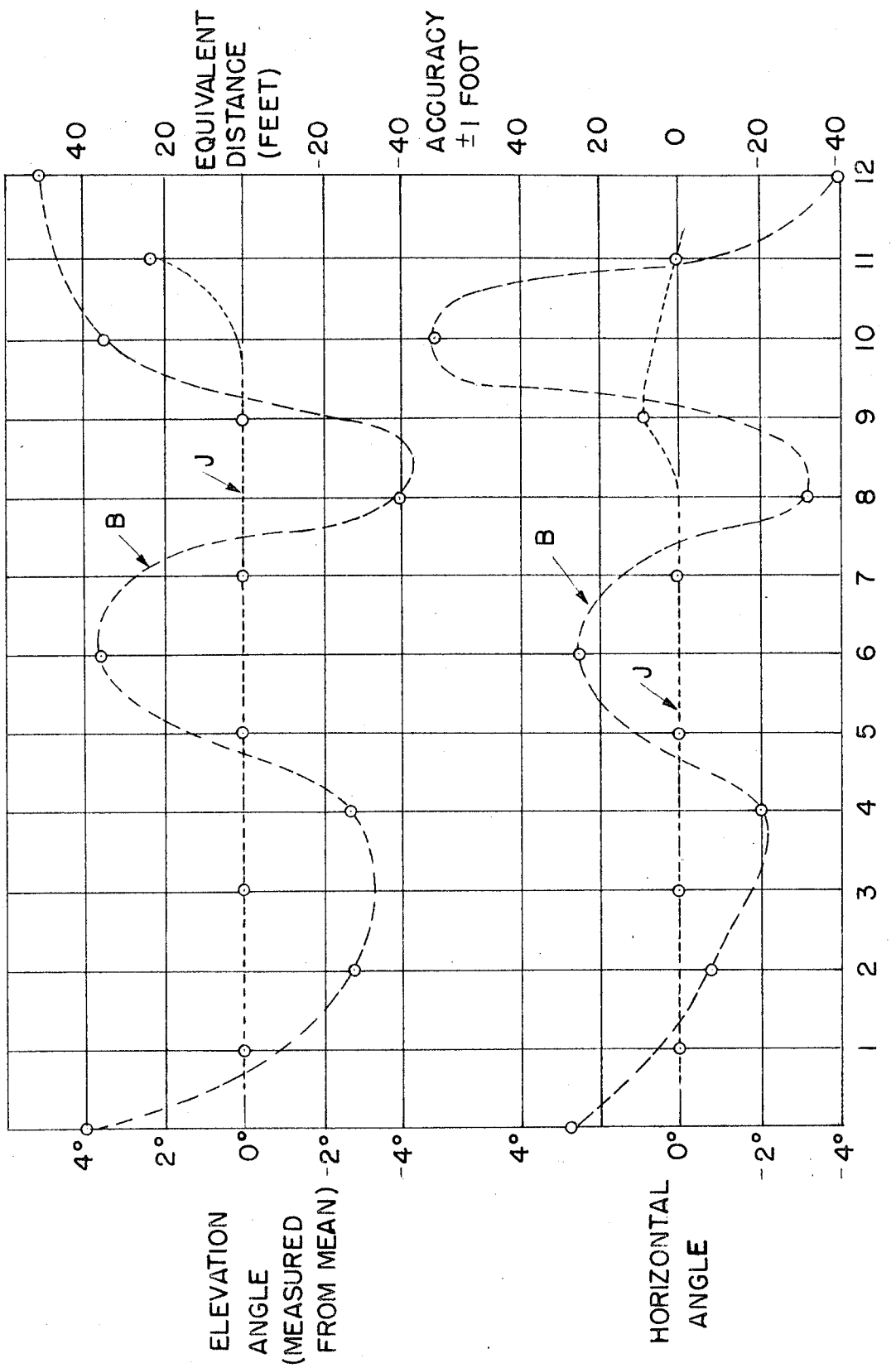

FIG.10 BALLOON MOVEMENTS

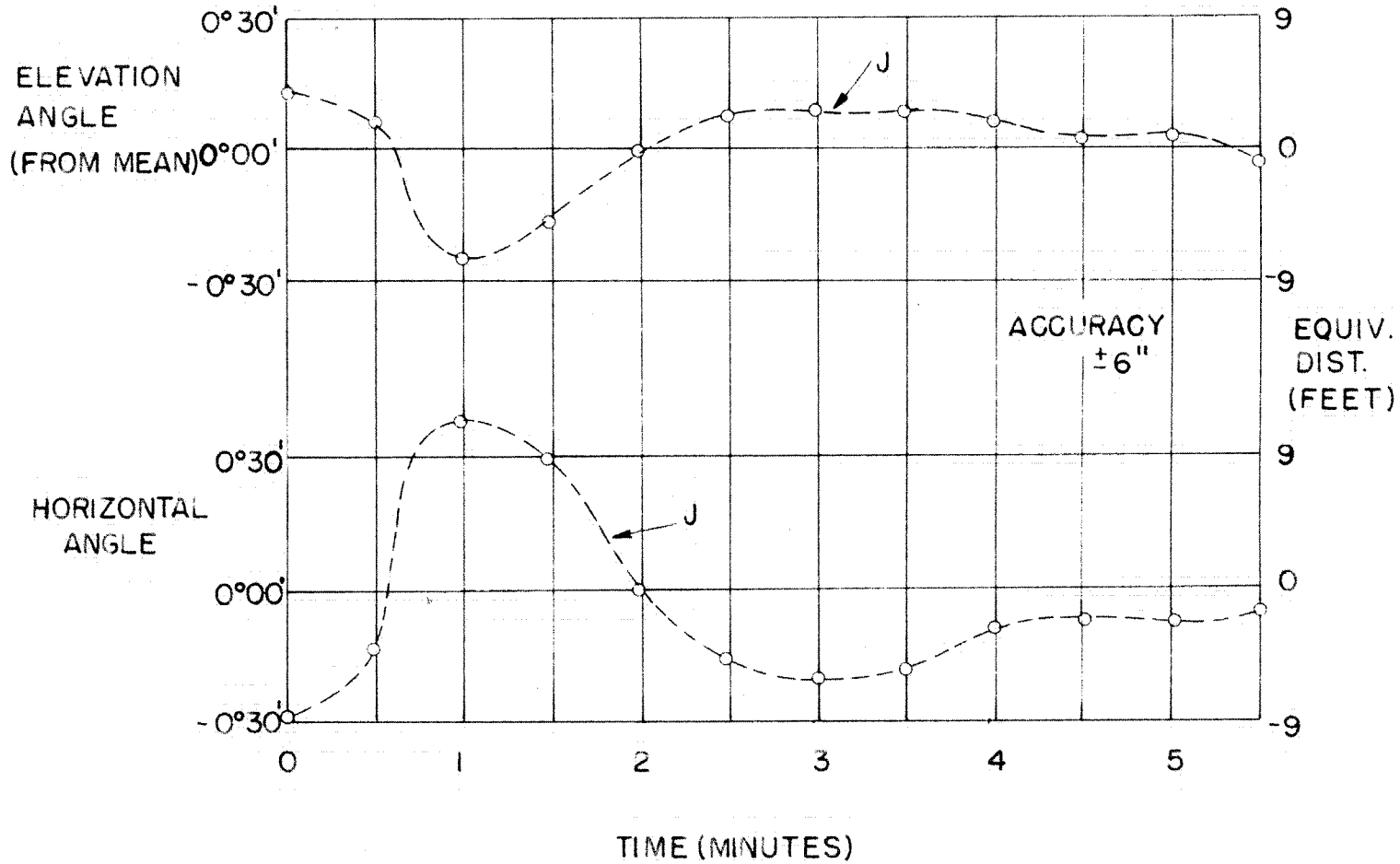

FIG. 11 JUNCTION POINT MEASUREMENTS

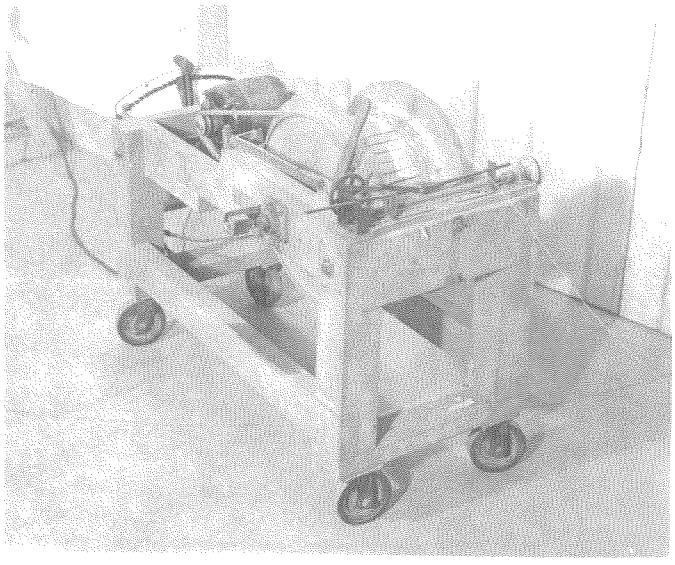

Fig. 12B Winder for Litzendraht Conductor

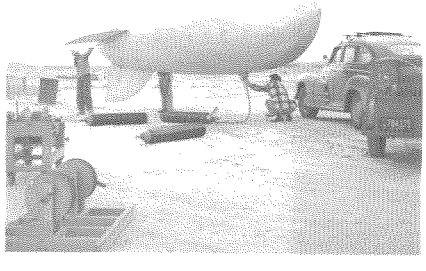

Fig. 12A Balloon

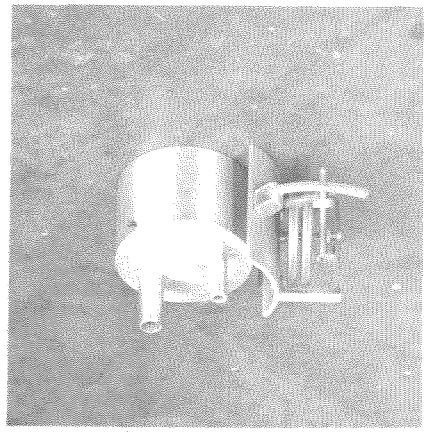

Fig. 12C Altitude Operated Helium Valve

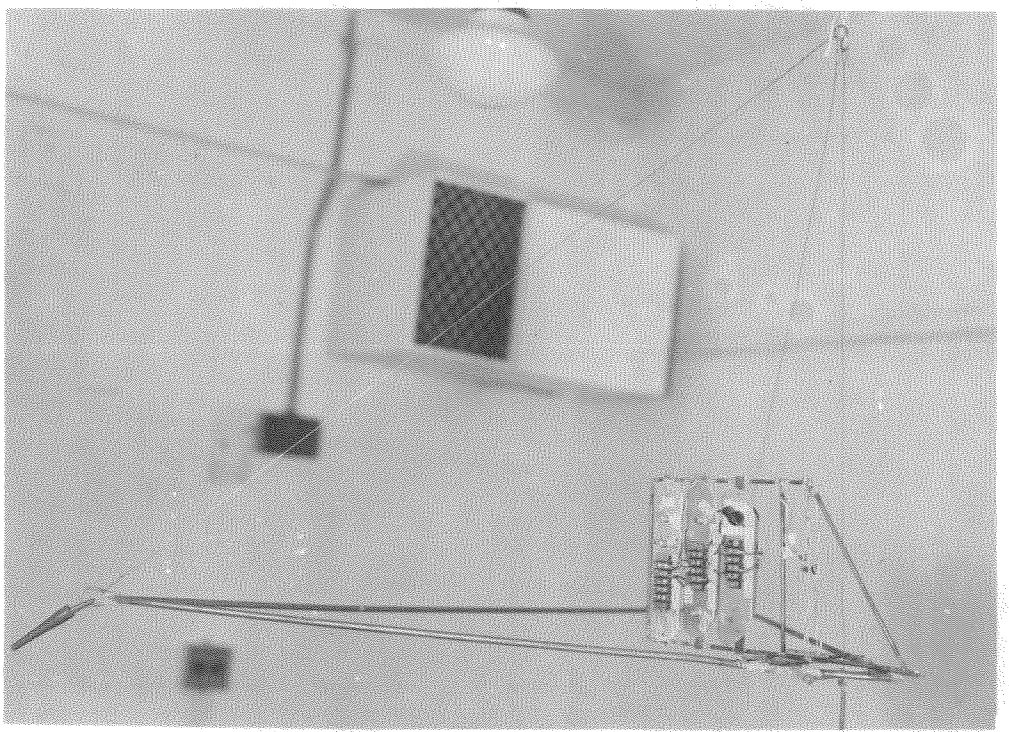

Fig. 13A Pyramid (Junction Point)

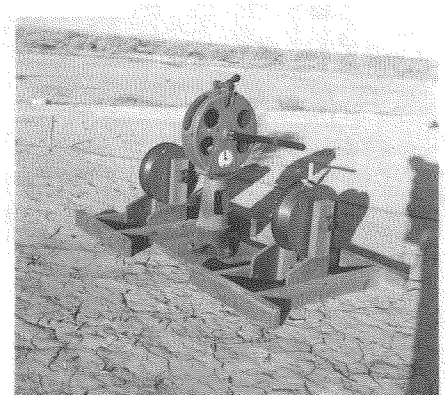

Fig. 13B Winders

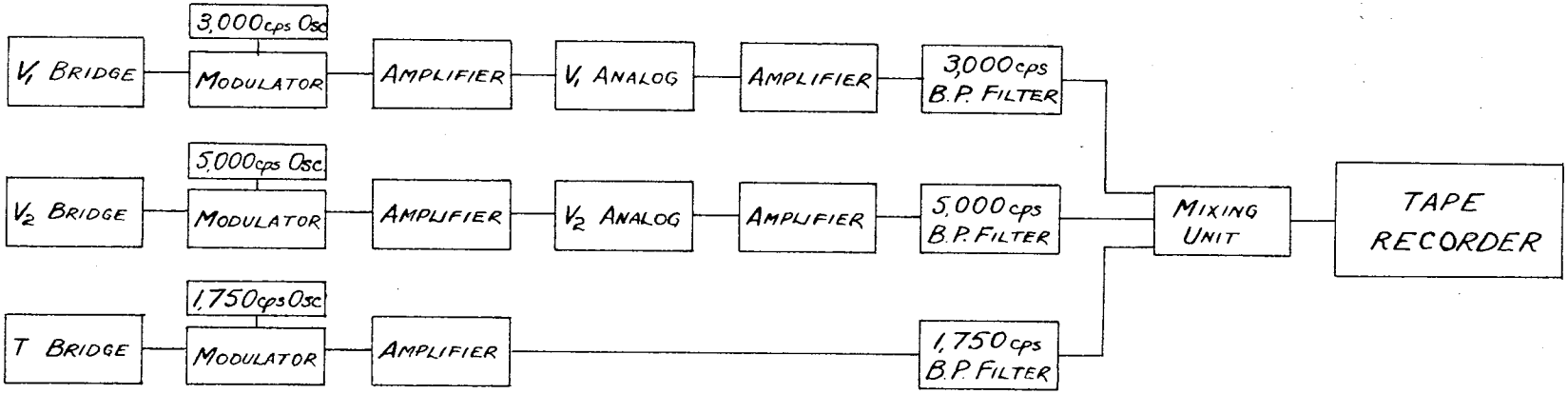

FIELD EQUIPMENT

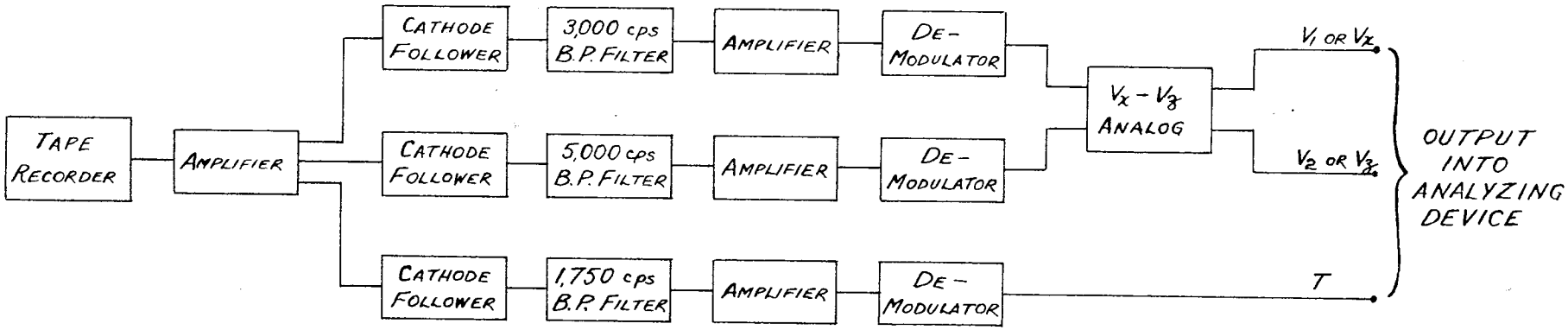

LABORATORY EQUIPMENT

FIG. 14 BLOCK DIAGRAM ELECTRONICS

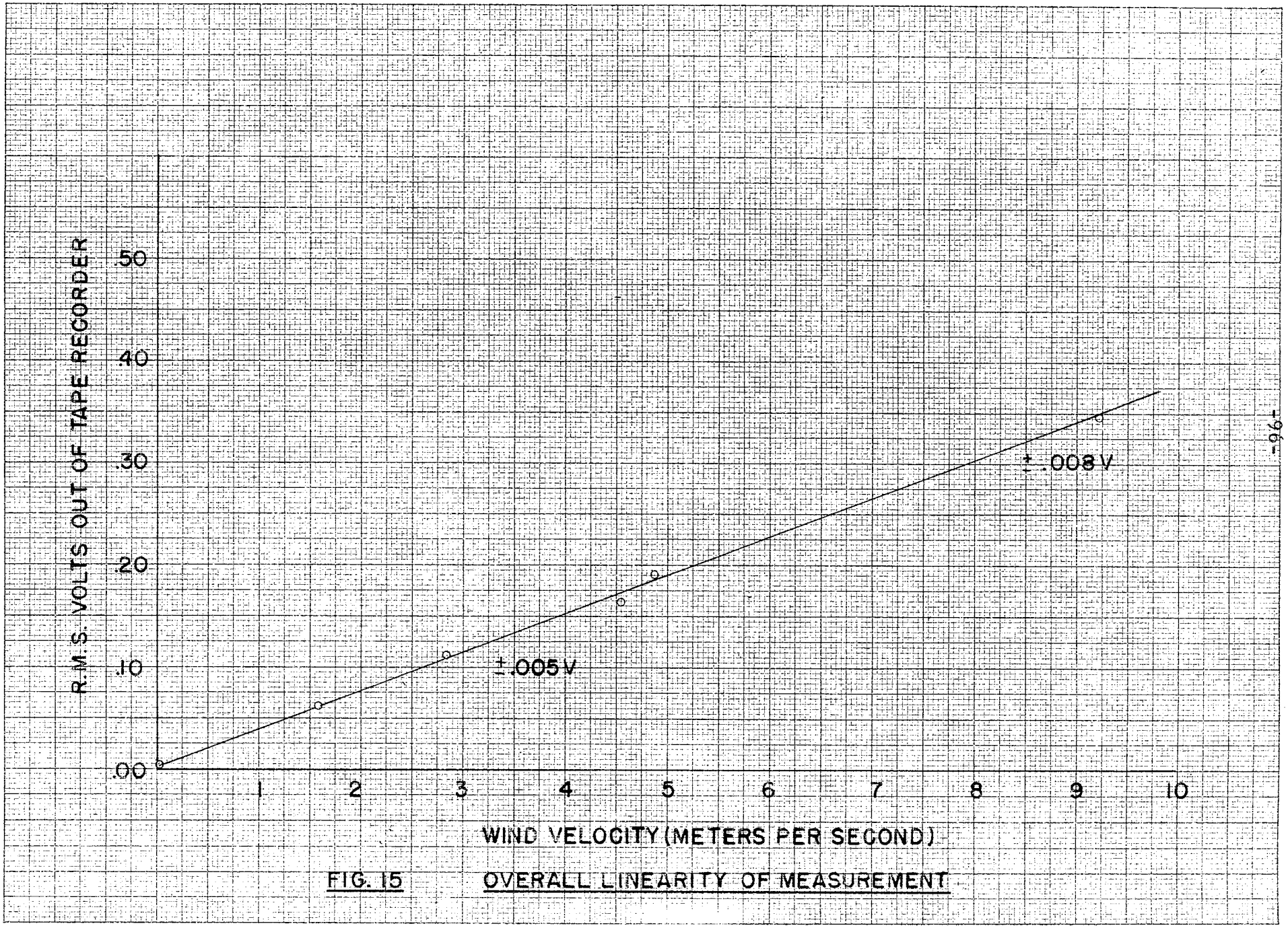

FIG. 15 OVERALL LINEARITY OF MEASUREMENT

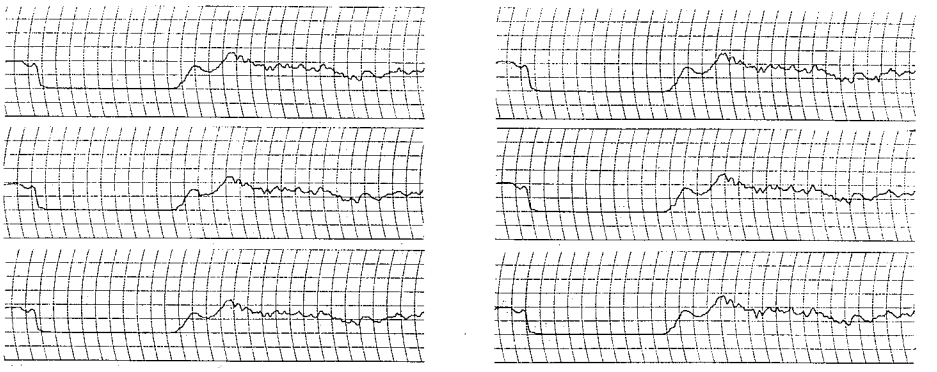

E SIGNAL REPRODUCIBILITY TEST (Paper speed = 1/2 cm./sec.)

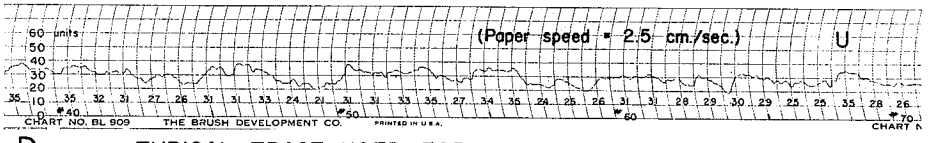

D TYPICAL TRACE USED FOR $f(\tau)$ CALCULATIONS (RUN 3, 15 cm.)

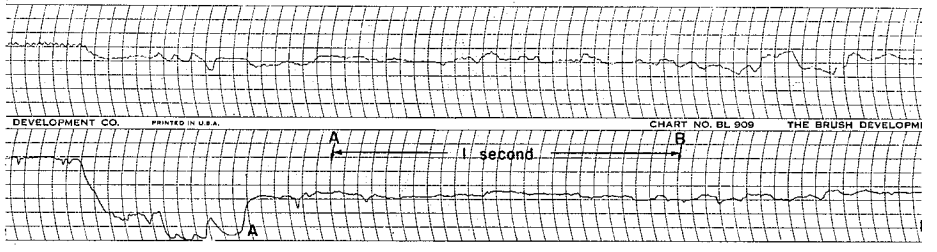

C SAME SIGNAL AS IN B, AT 12.5 cm./sec.

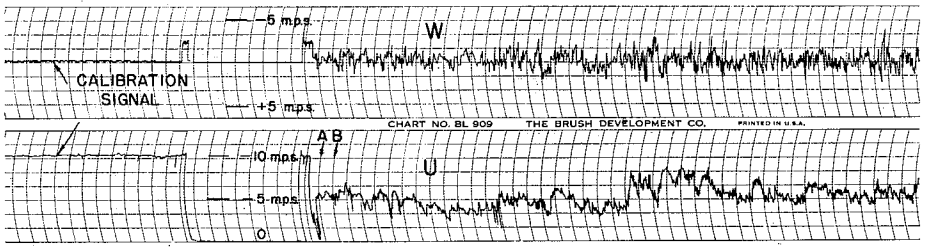

B TYPICAL U-W TRACE AT 1/2 cm./sec. (RUN 3, 70 cm.)

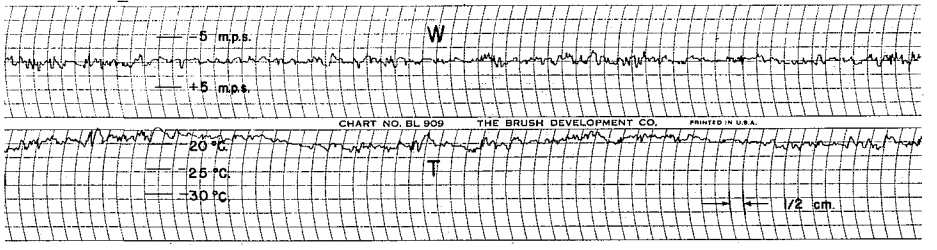

A TYPICAL W-T TRACE AT 1/2 cm./sec. (RUN 3, 70 cm.)

FIG. 16 PEN RECORDINGS

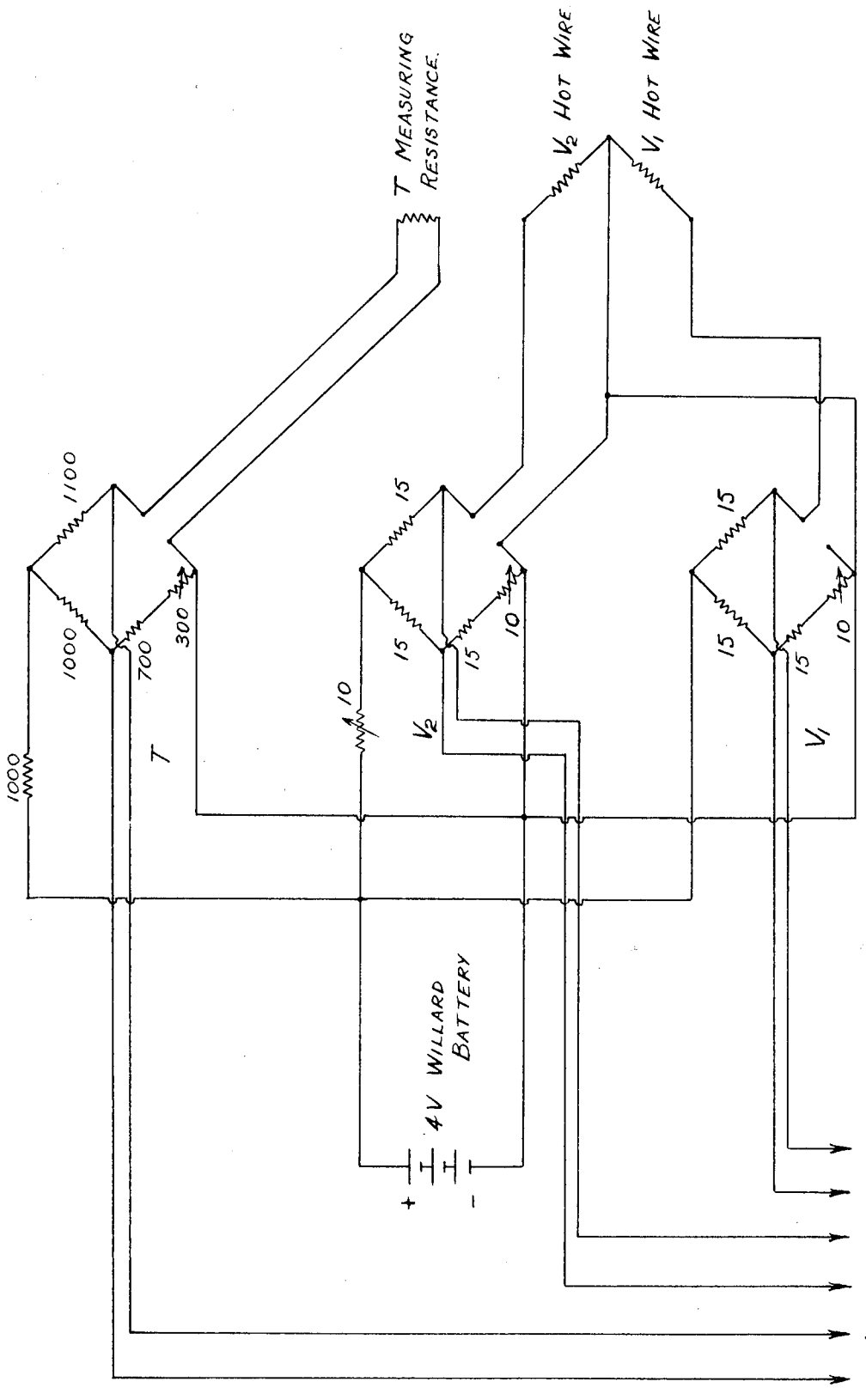

FIG. 17 V_1, V_2, AND T MEASURING BRIDGES

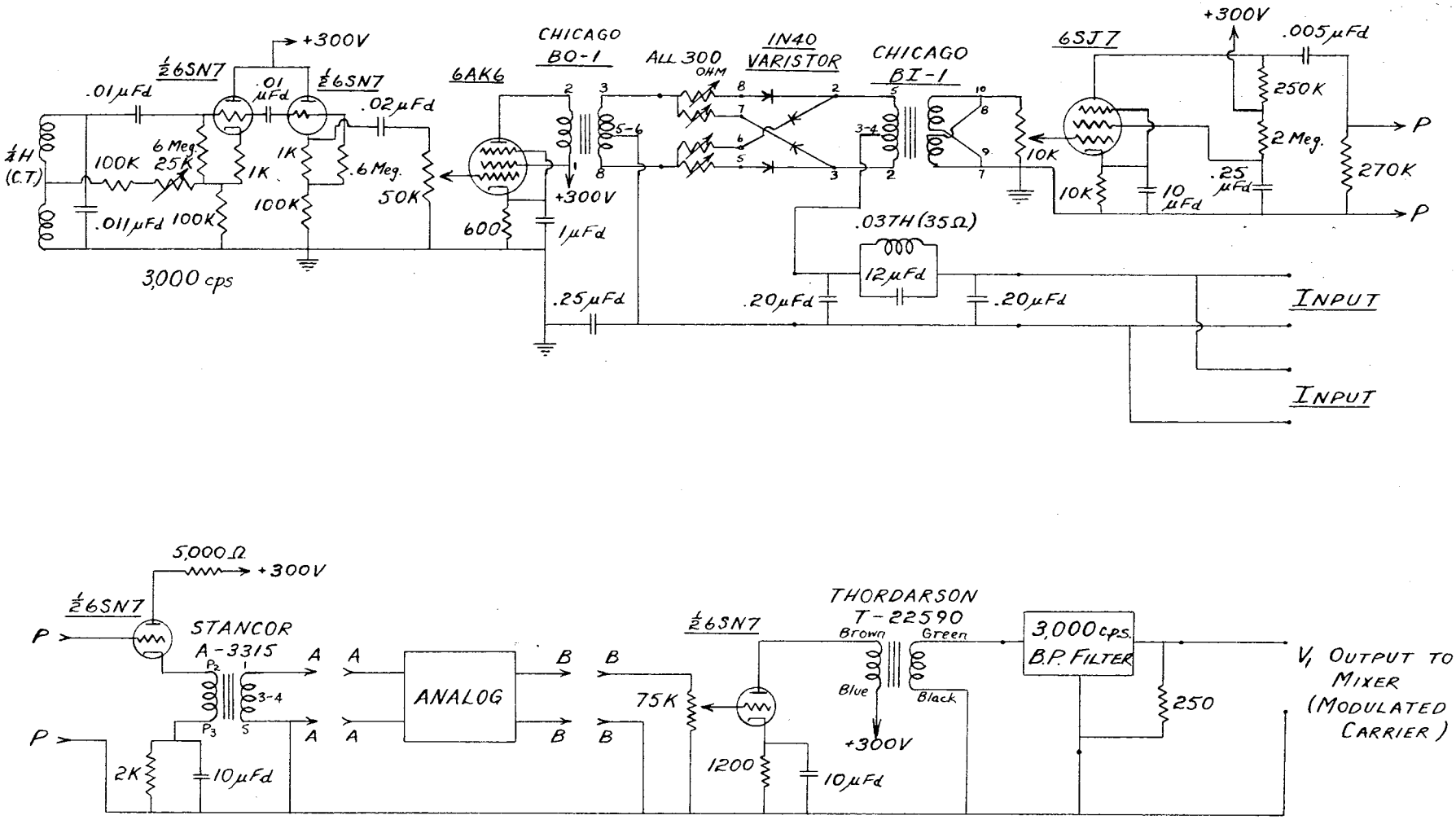

FIG. 18 V1 RECORDING UNIT

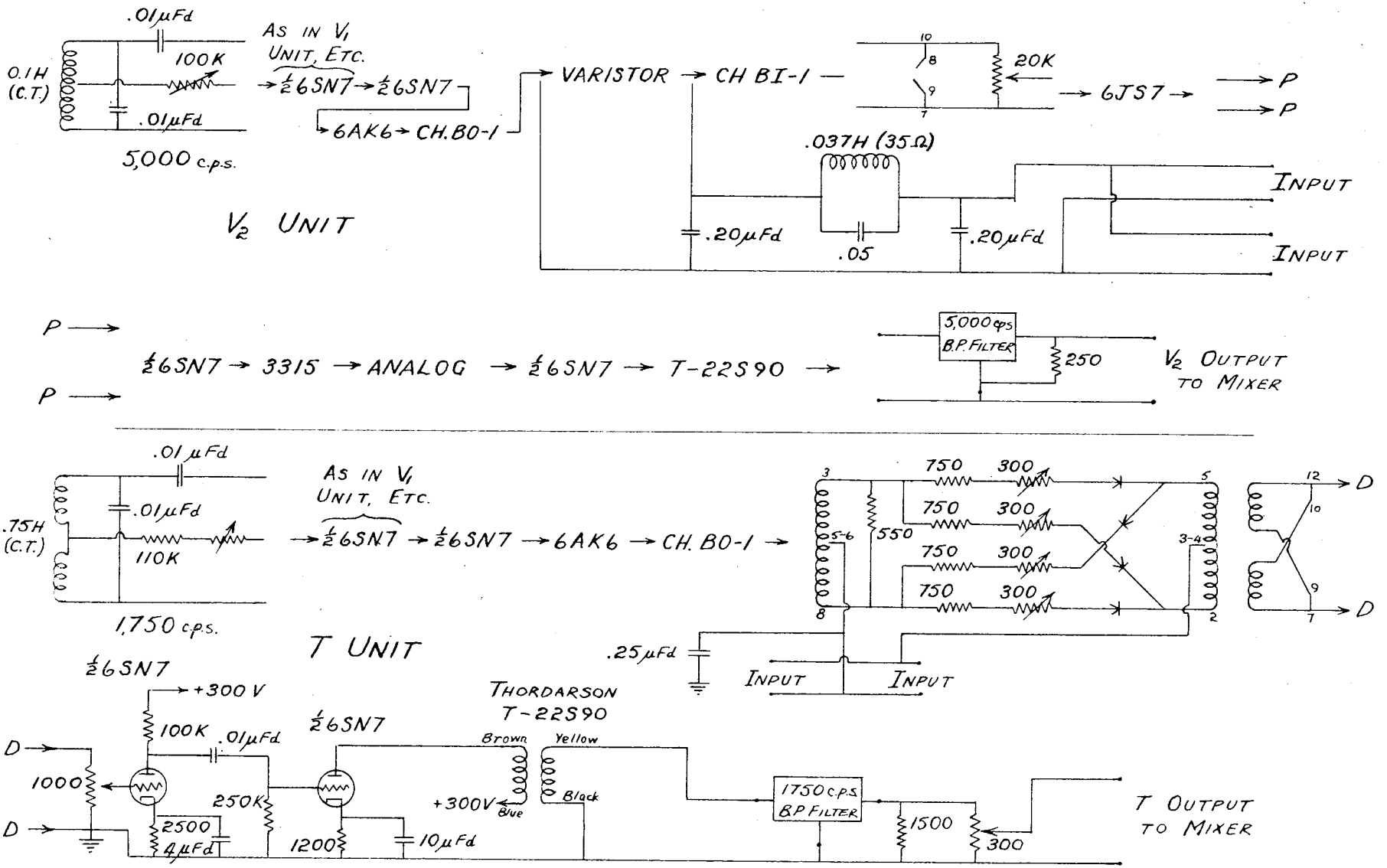

FIG. 19 V_2 AND T RECORDING UNITS

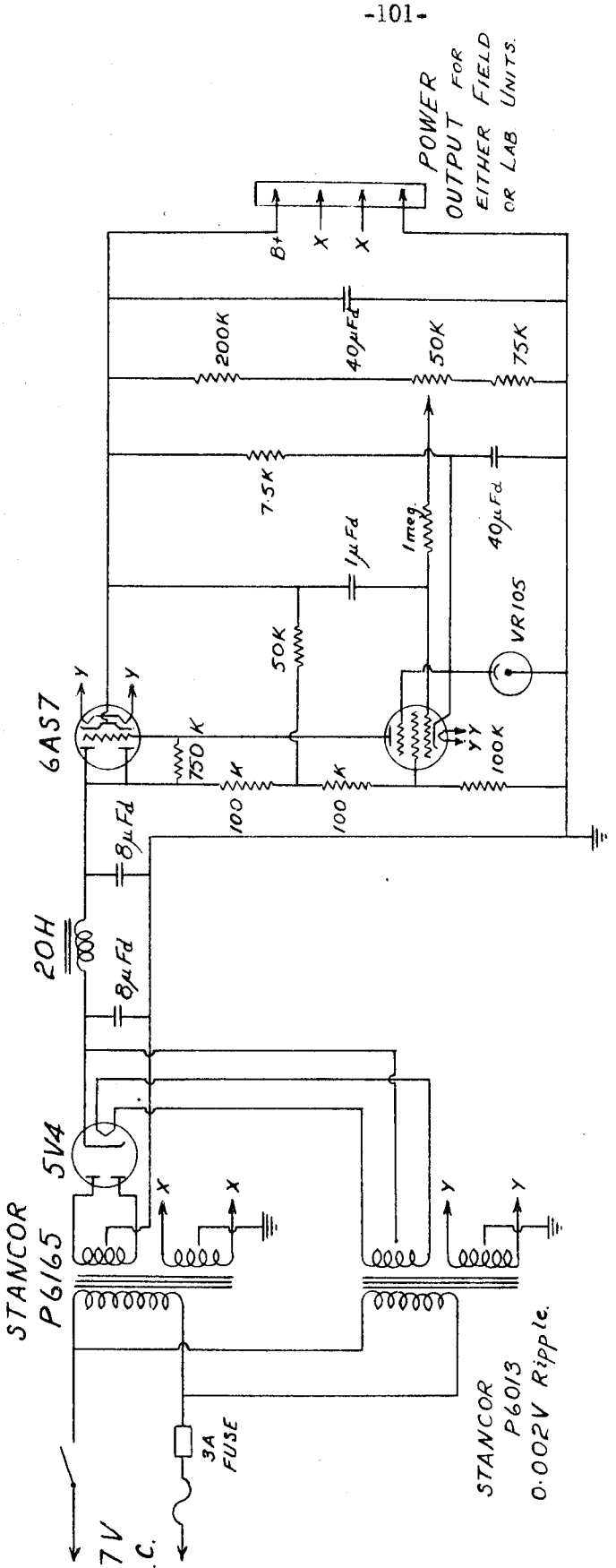

FIG. 20 POWER SUPPLY

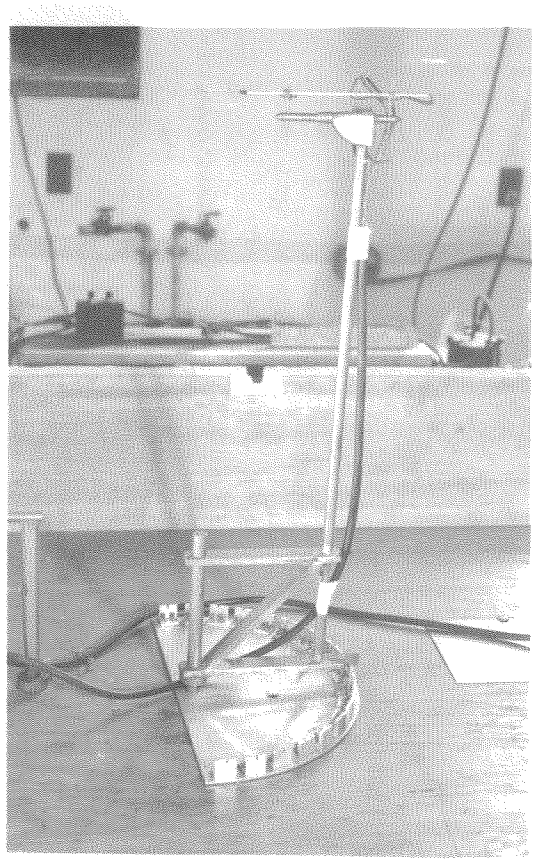

Fig. 21A Hot Wire Test Holder

Fig. 21B Closeup of Test Holder

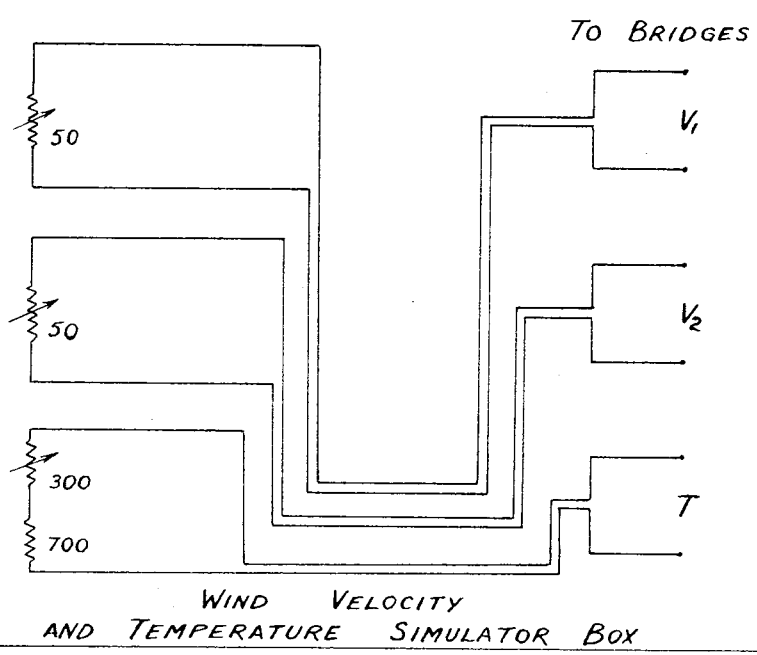

Wind Velocity and Temperature Simulator Box

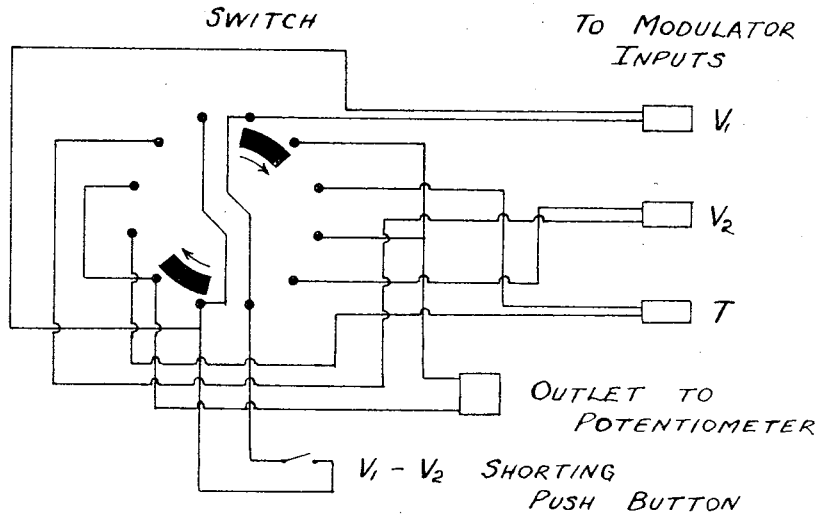

Shorting Switchbox

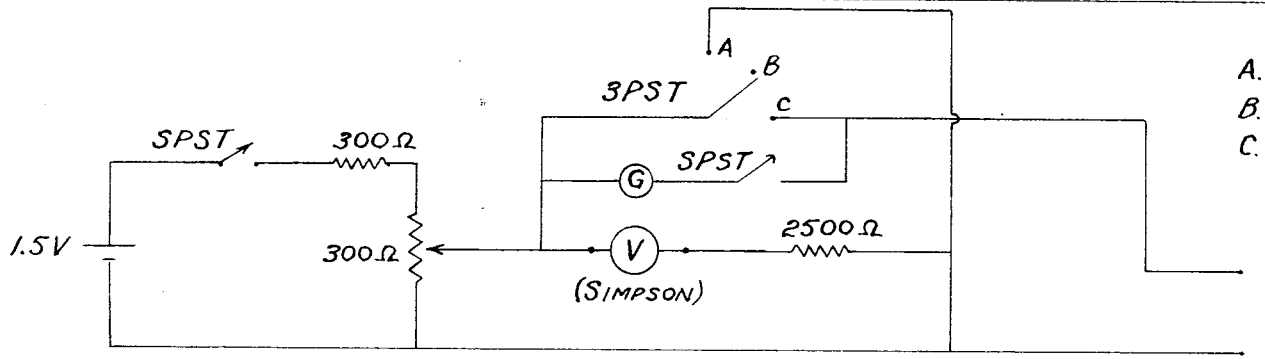

A. Null Indicator
B. Potentiometer
C. Voltage Supply

Calibrating Box

Fig. 22 Calibrating Aids

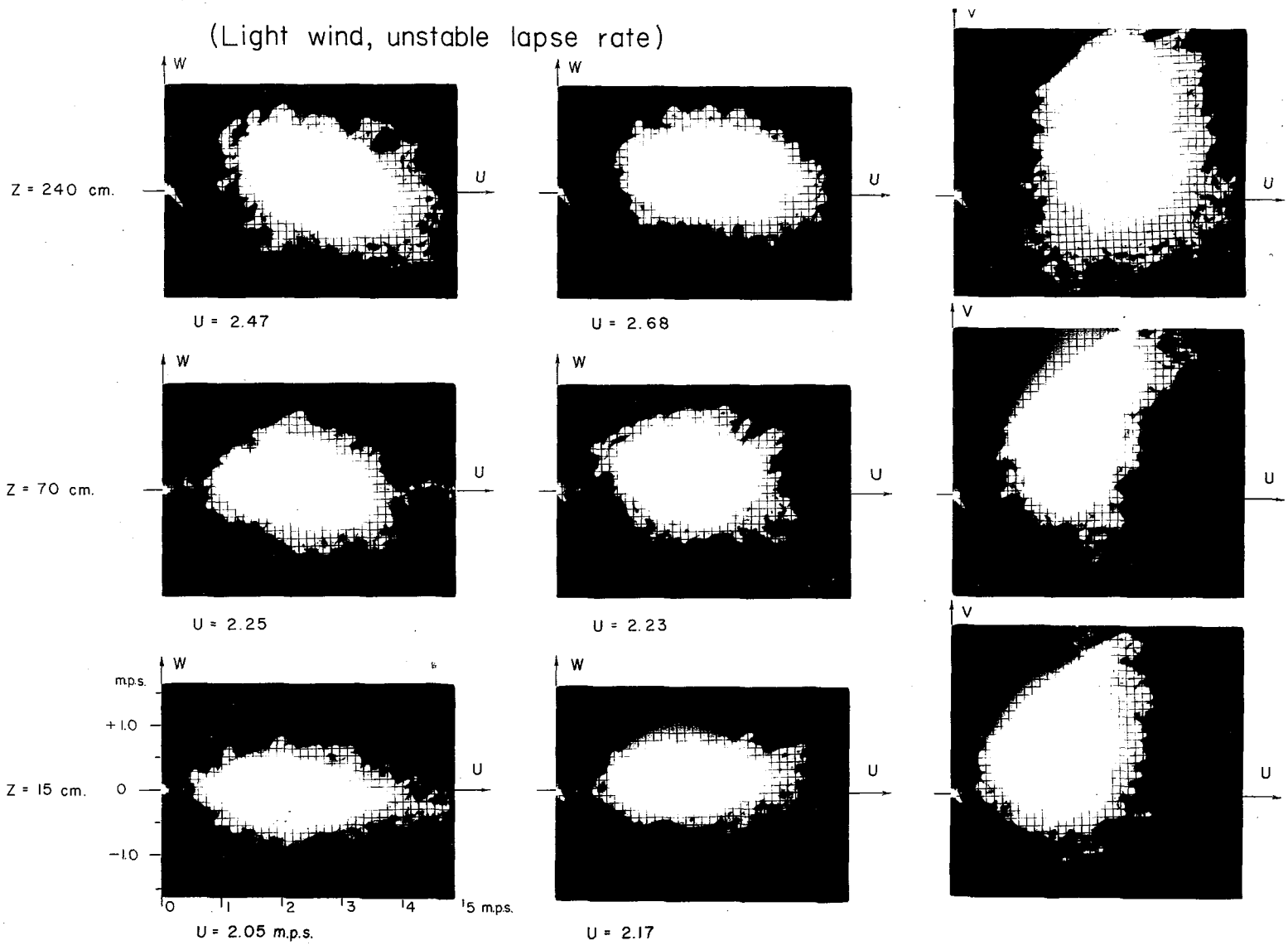

FIG. 23 VELOCITY PICTURES RUN 2

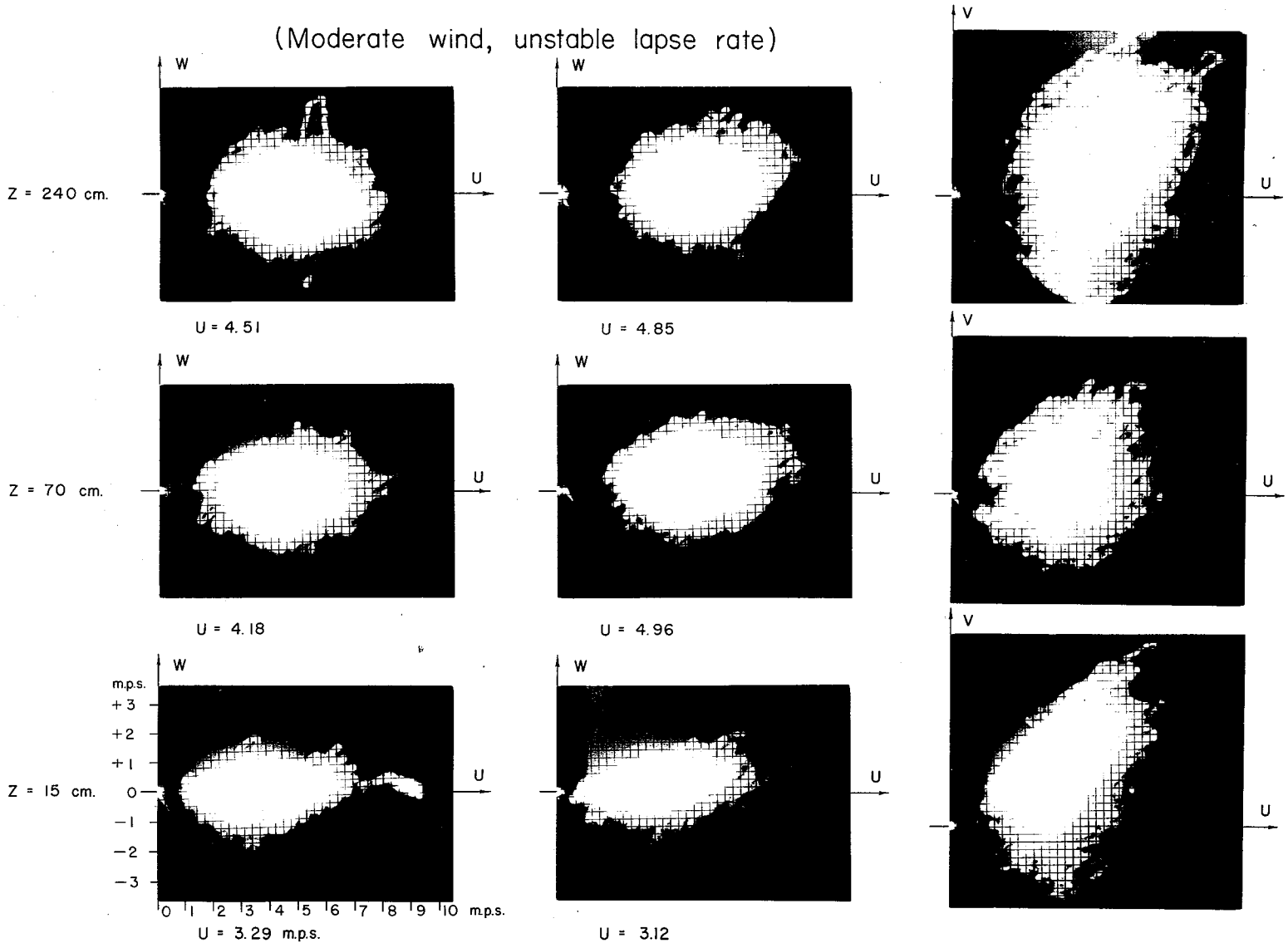

FIG. 24 VELOCITY PICTURES RUN 3

(Moderate wind, neutral lapse rate)

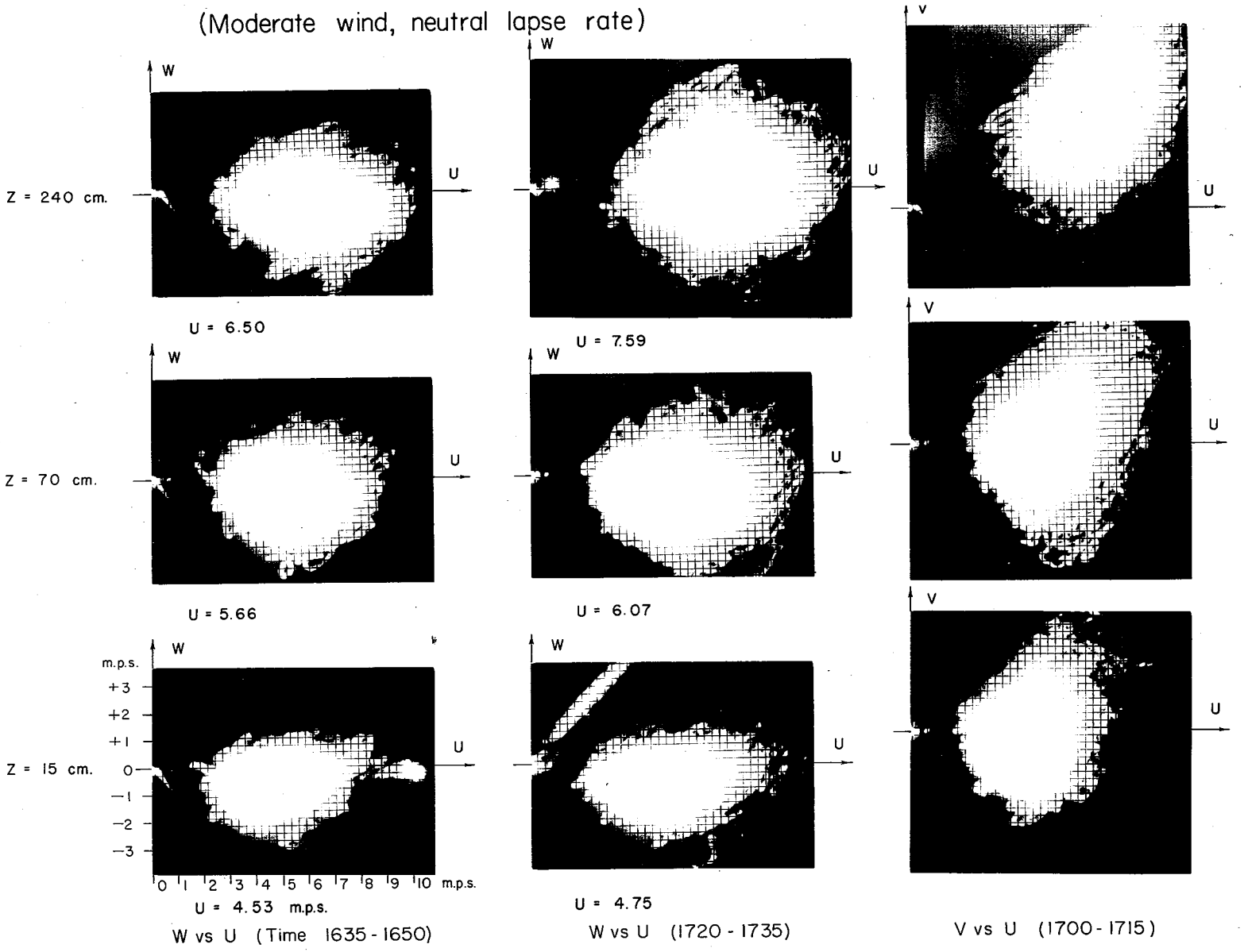

U = 6.50 | U = 7.59

U = 5.66 | U = 6.07

U = 4.53 m.p.s. | U = 4.75

W vs U (Time 1635 - 1650) | W vs U (1720 - 1735) | V vs U (1700 - 1715)

FIG. 25 VELOCITY PICTURES RUN 4

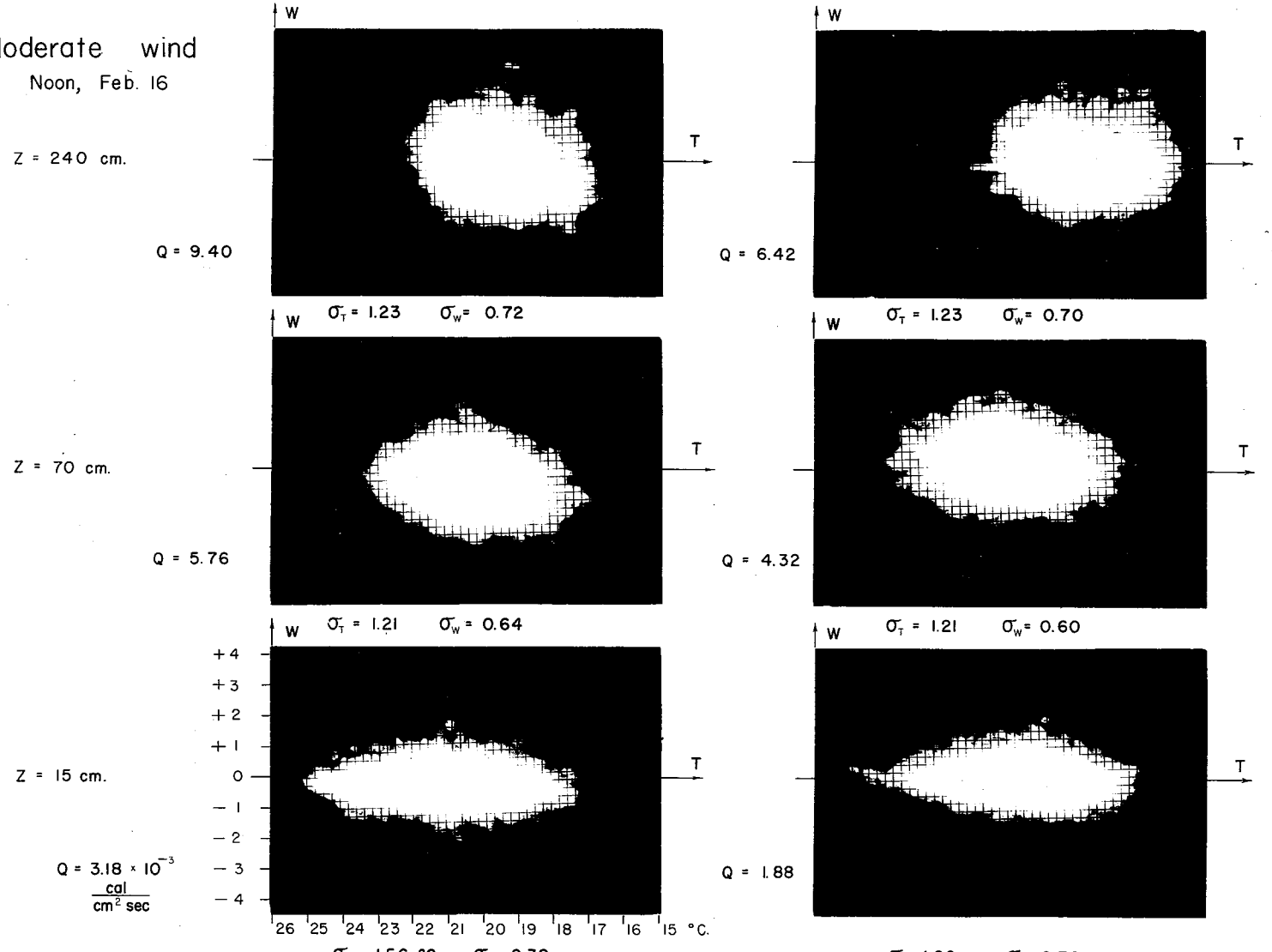

FIG. 26 TEMPERATURE - VELOCITY CORRELATION PICTURES RUN 3

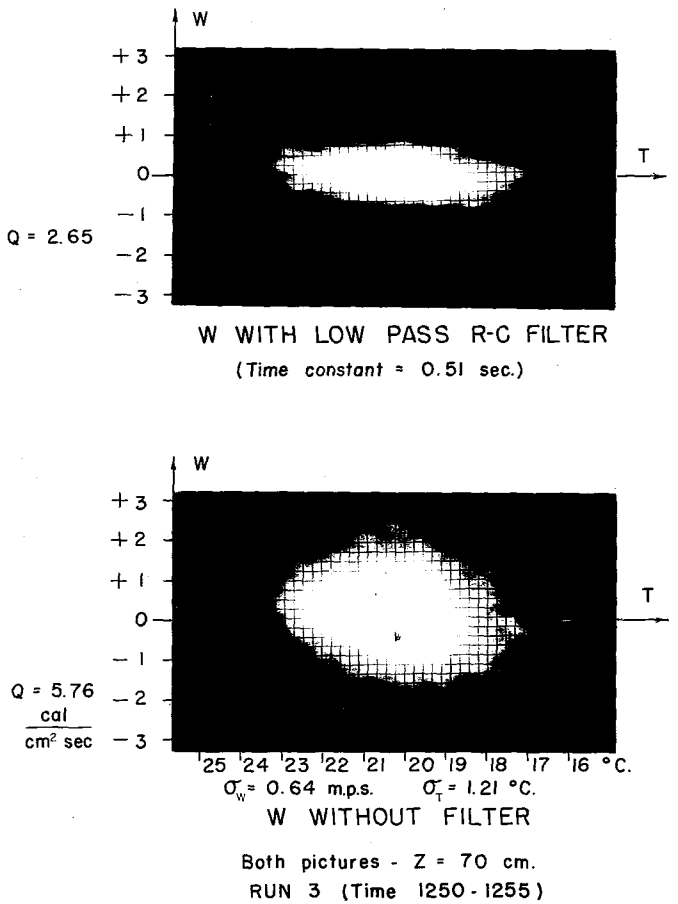

HEAT FLUX vs FREQUENCY

FIG. 27 A

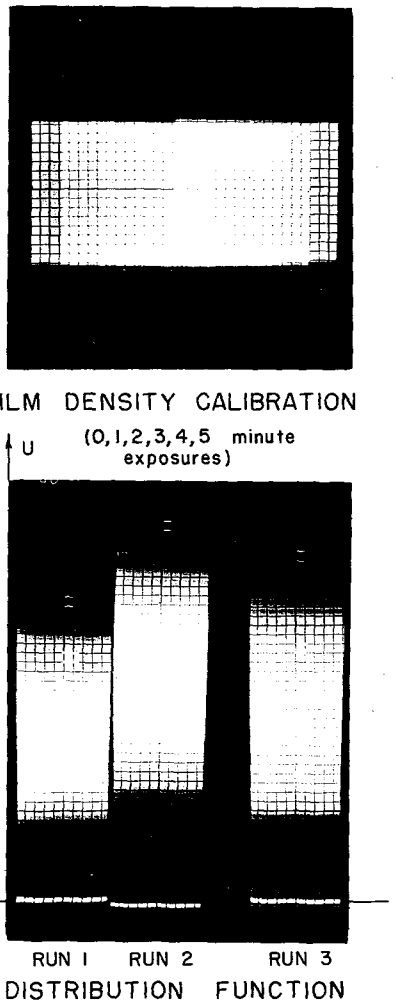

CALIBRATION PICTURES

FIG. 27 B

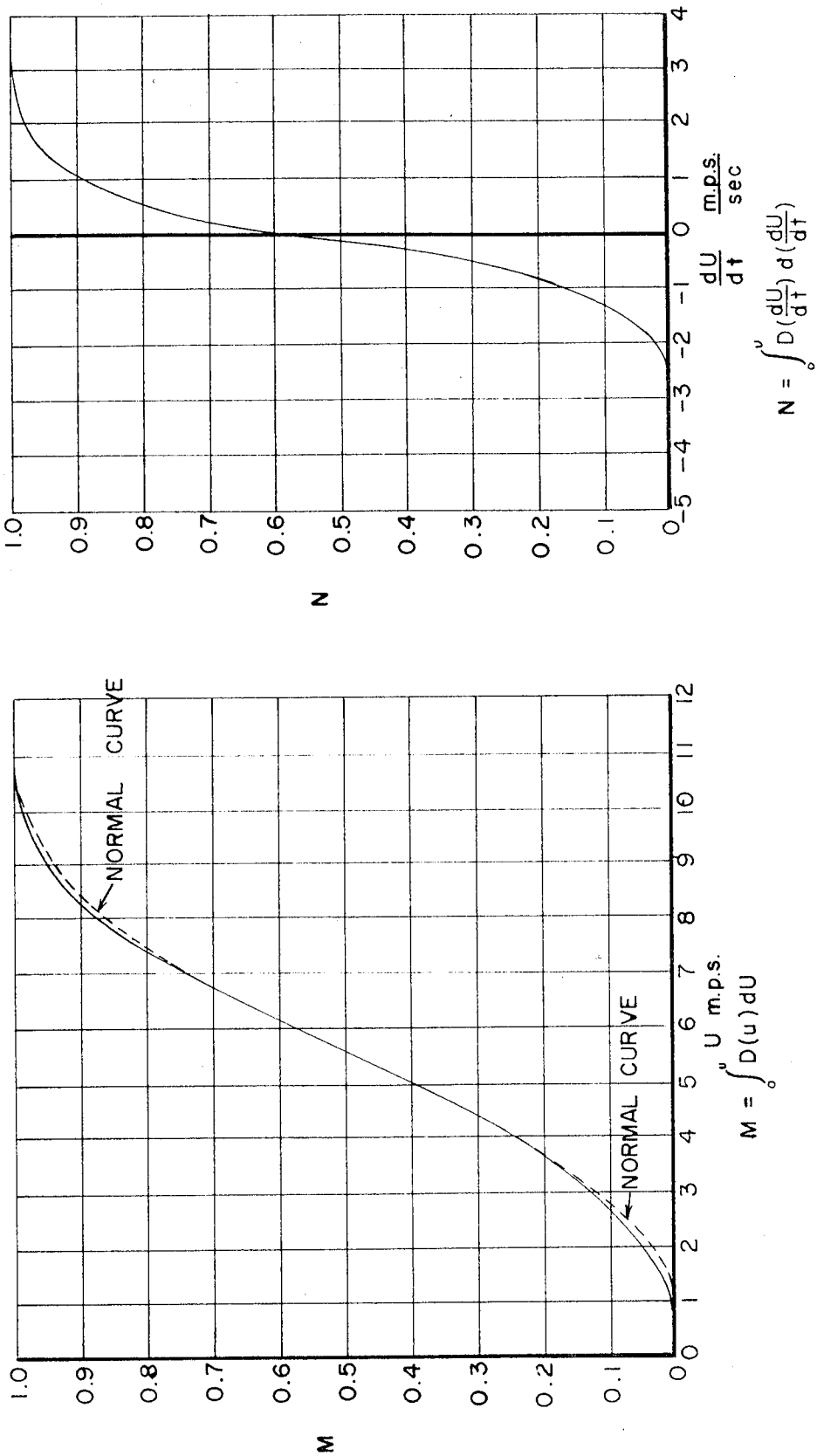

FIG. 28 DISTRIBUTION FUNCTIONS, U AND $(\frac{dU}{dt})$, FIRST HALF RUN 1

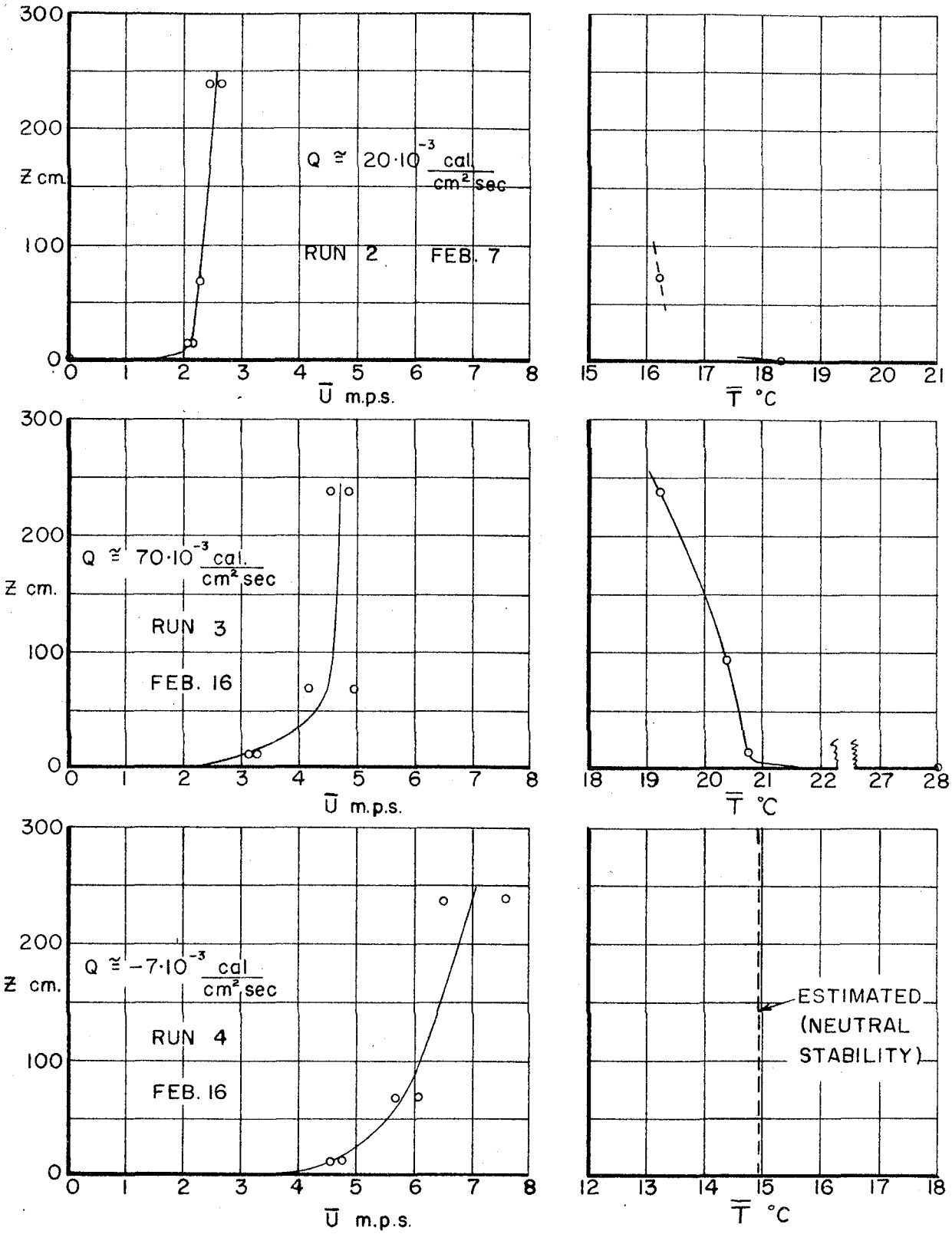

FIG. 29 WIND AND TEMPERATURE GRADIENTS

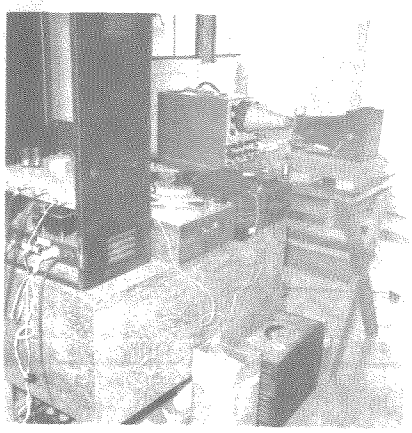

Fig. 30A Analyzing Equipment

Radiometer

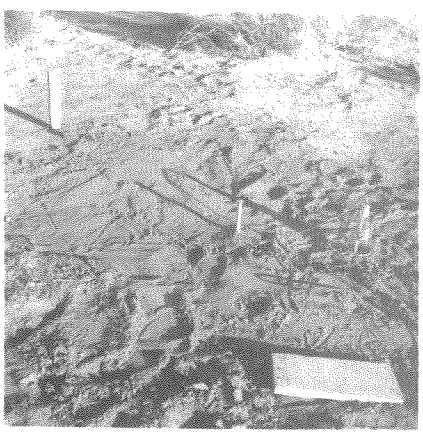

Ground Heat
Meter Site

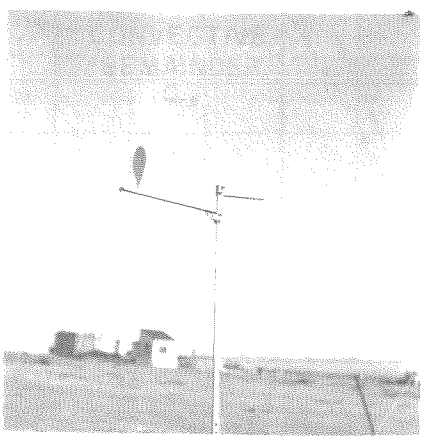

Thermometer and Shield

Fig. 30B Field Equipment

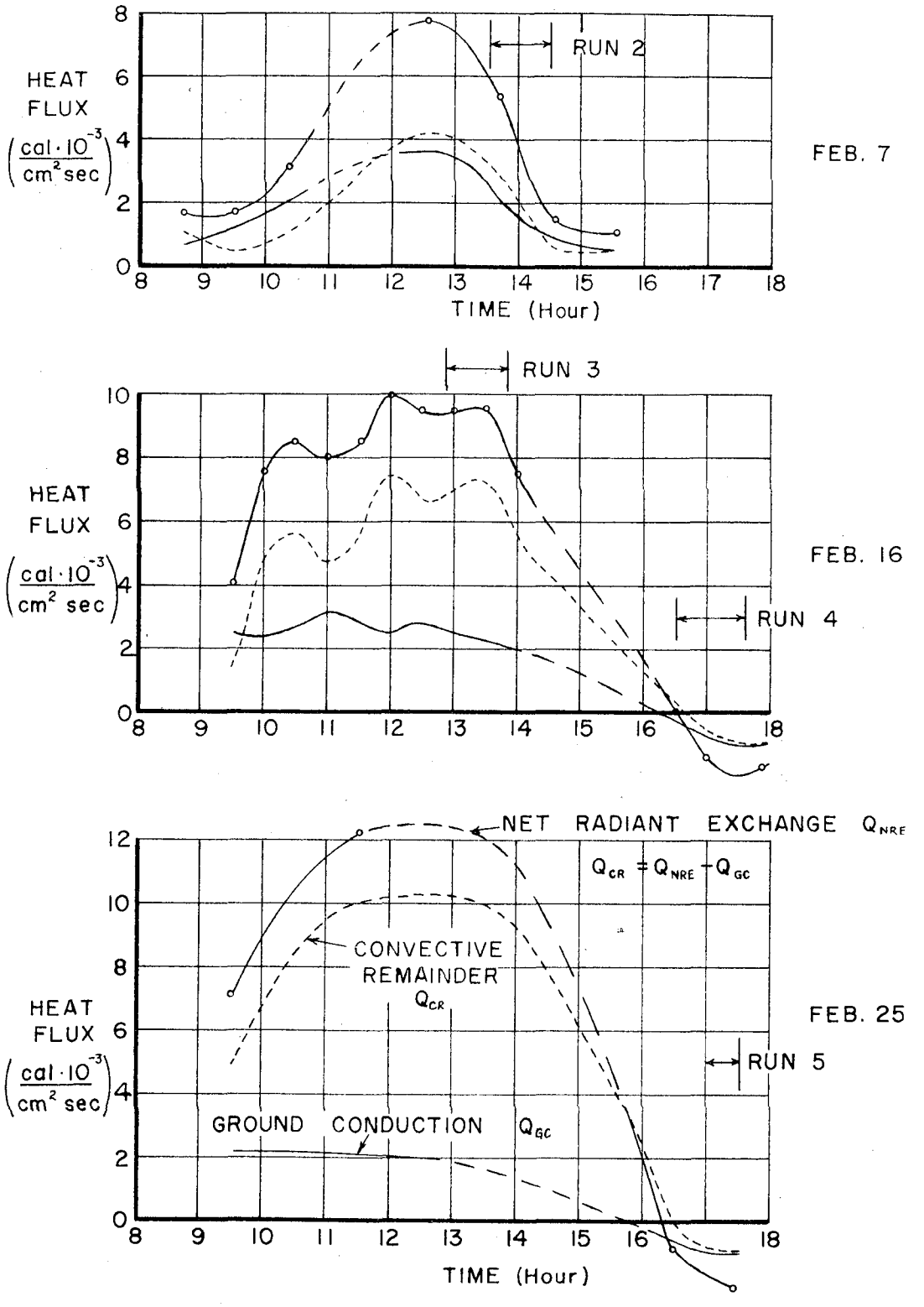

FIG. 31 RADIOMETER HEAT FLUX

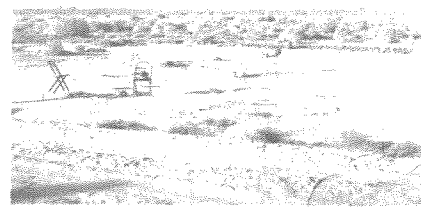

A - Looking N

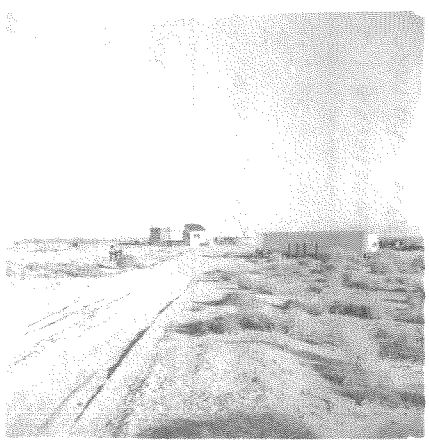

B - Looking NE

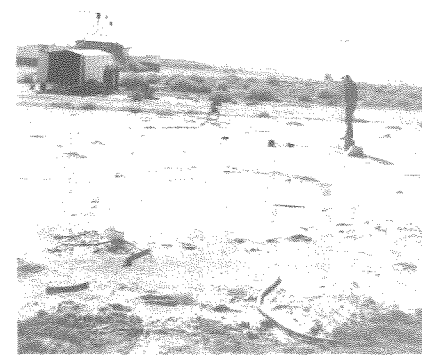

C - Looking SW

Fig. 32 Site Photographs

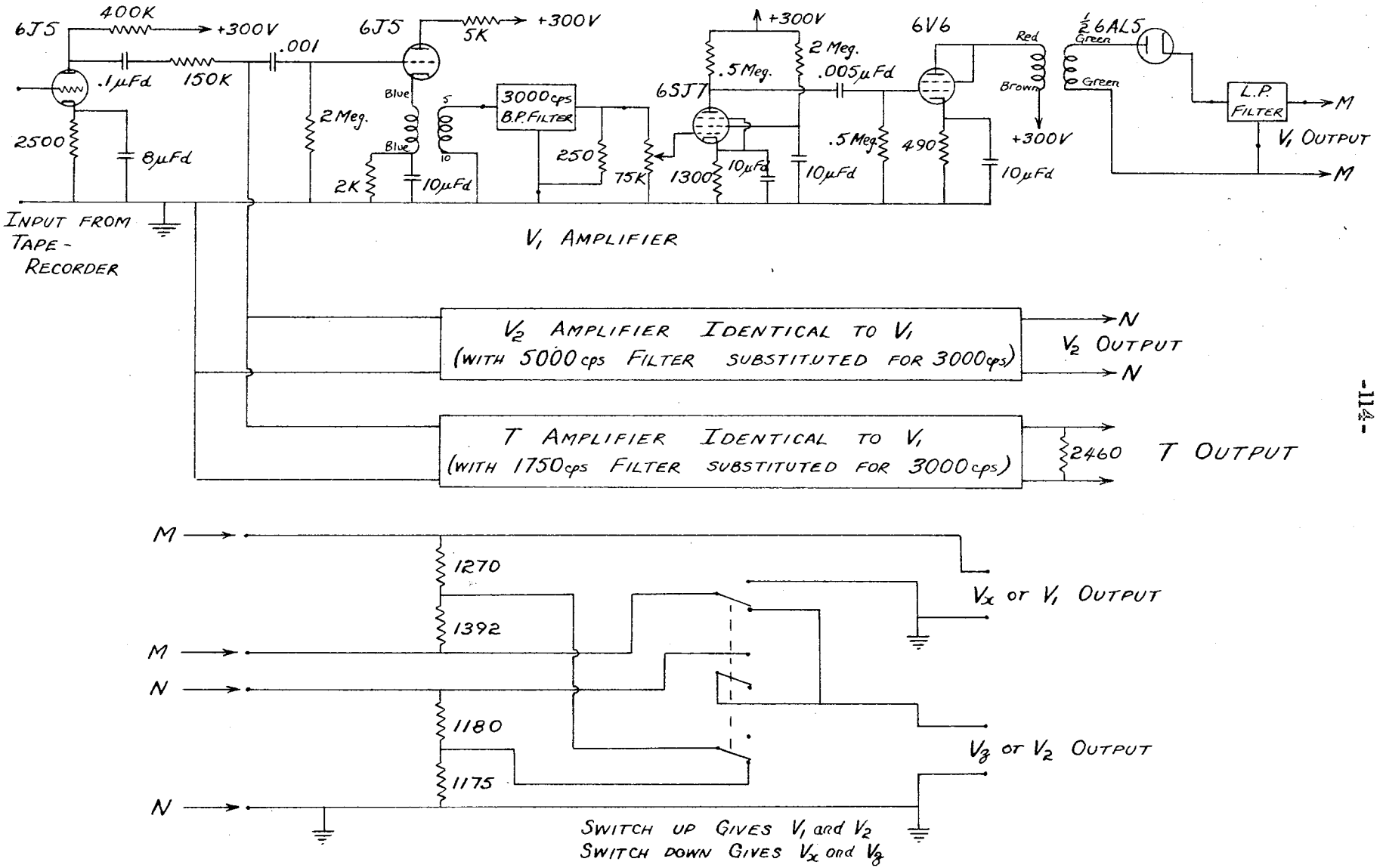

FIG. 33 LABORATORY AMPLIFIERS AND ANALOG

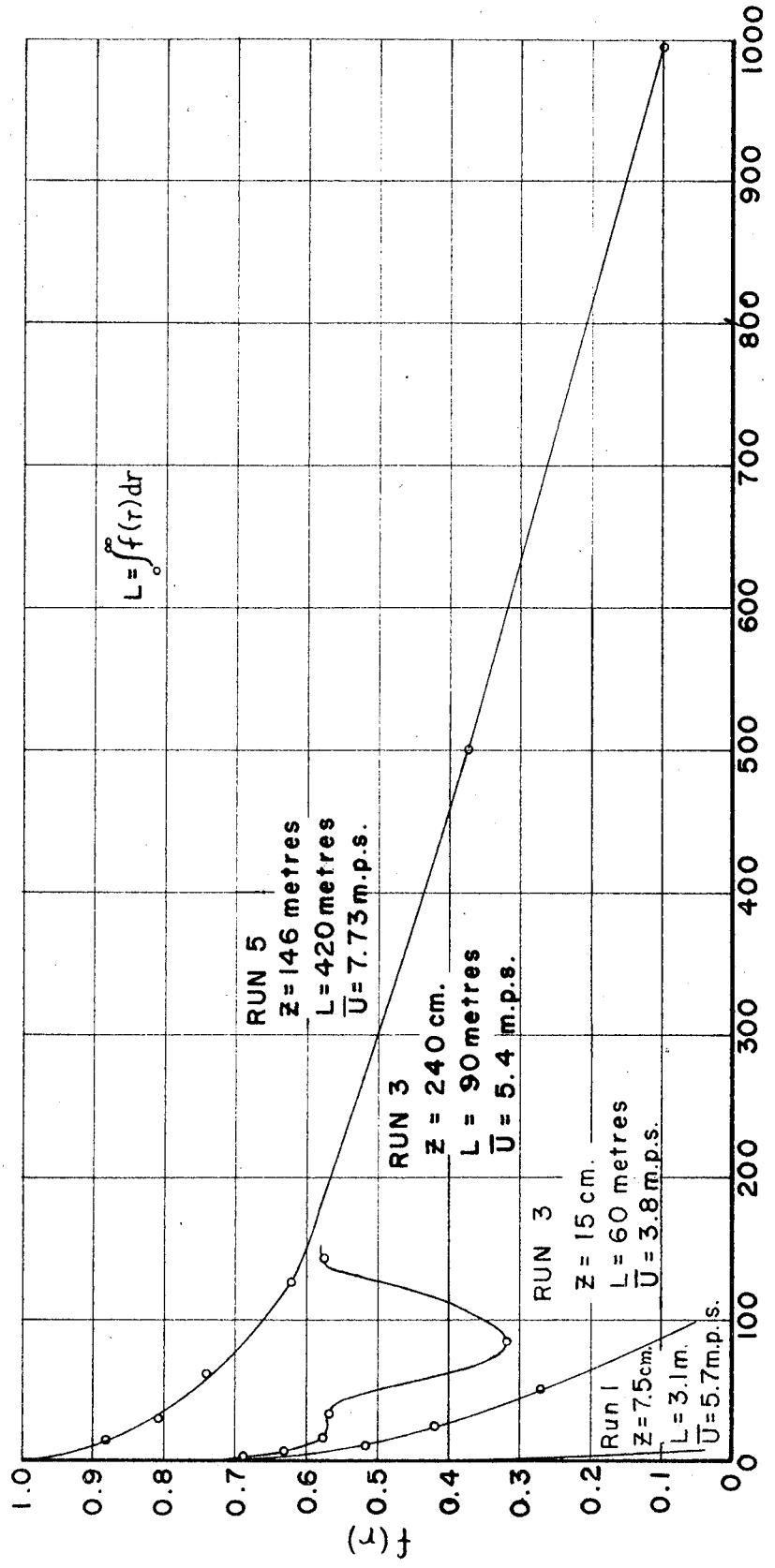

FIG. 34. COMPARISON OF AUTOCORRELATION CURVES

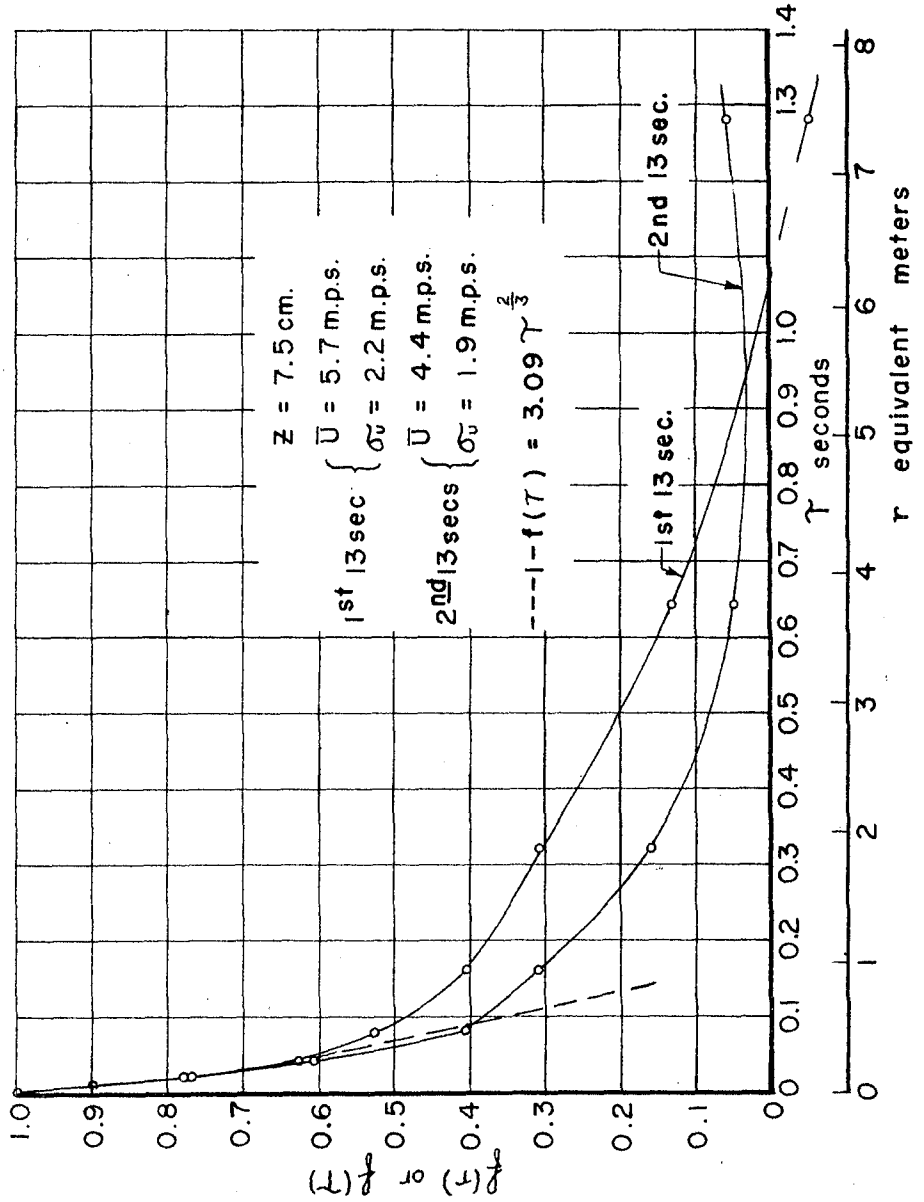

FIG.35 AUTOCORRELATION CURVE RUN 1 (Z = 7.5 CMS.)

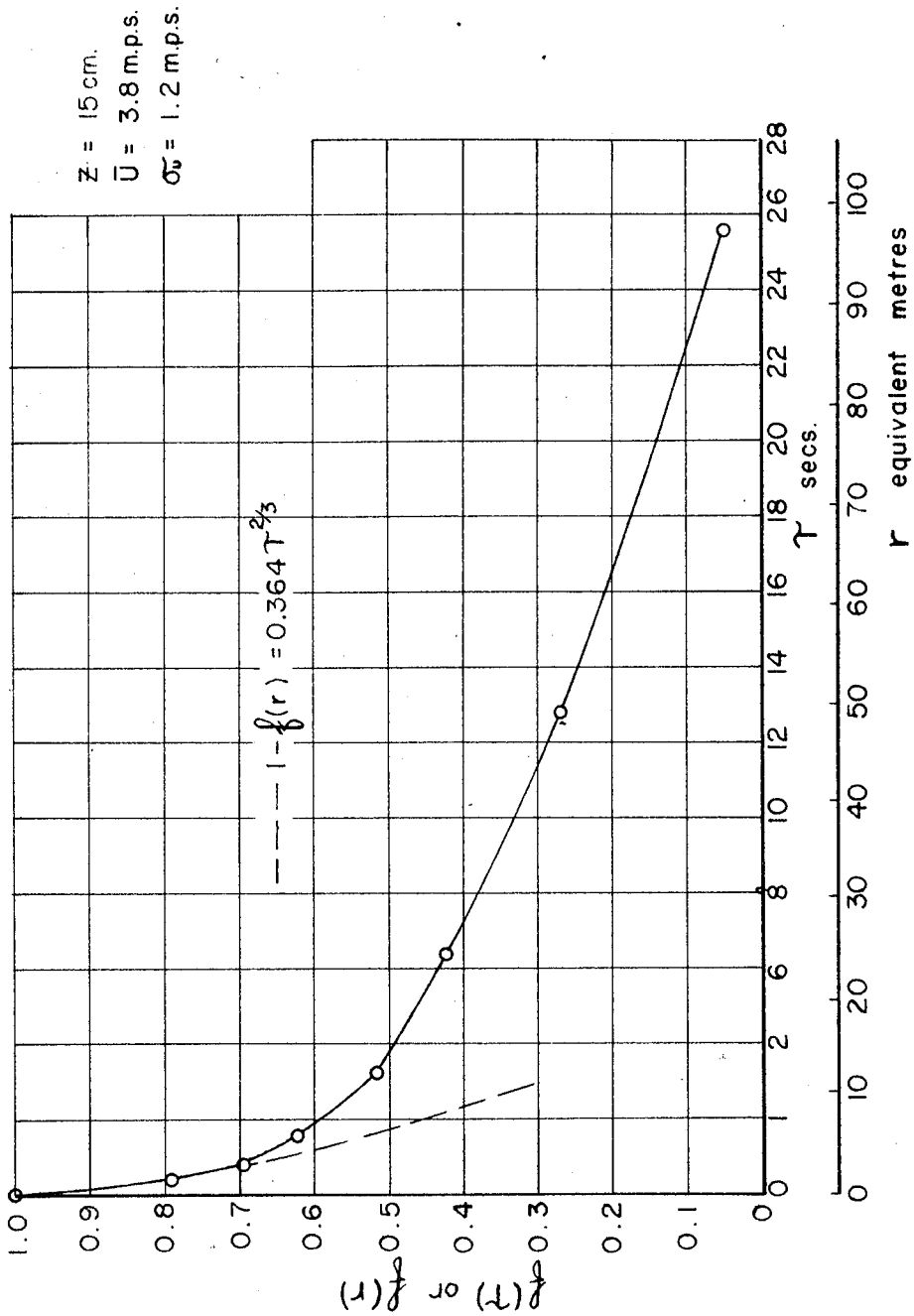

FIG. 36 AUTOCORRELATION CURVE RUN 3 (z = 15cm.)

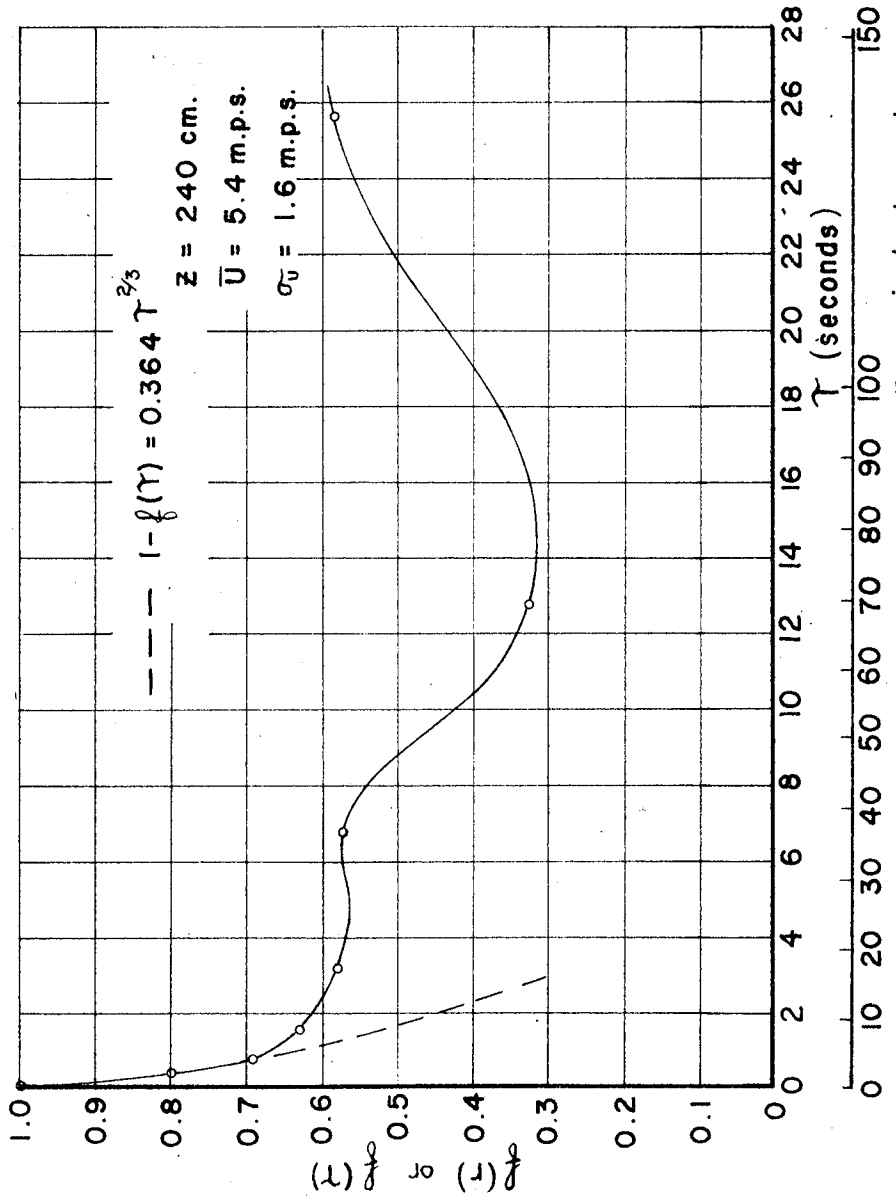

FIG. 37. AUTOCORRELATION CURVE RUN 3 (Z = 240 CMS.)

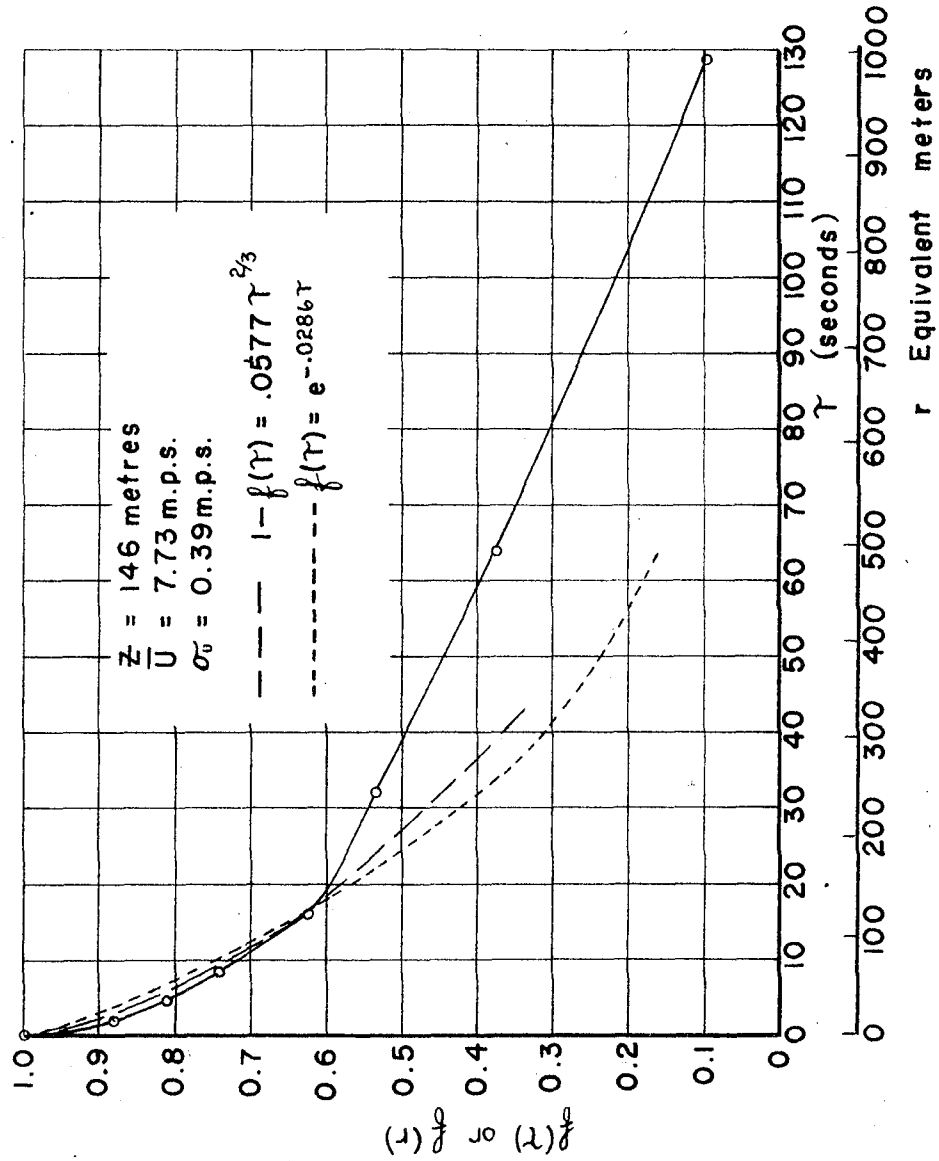

FIG. 38 AUTOCORRELATION CURVE RUN 5 ($\bar{z}$ = 146 METRES)

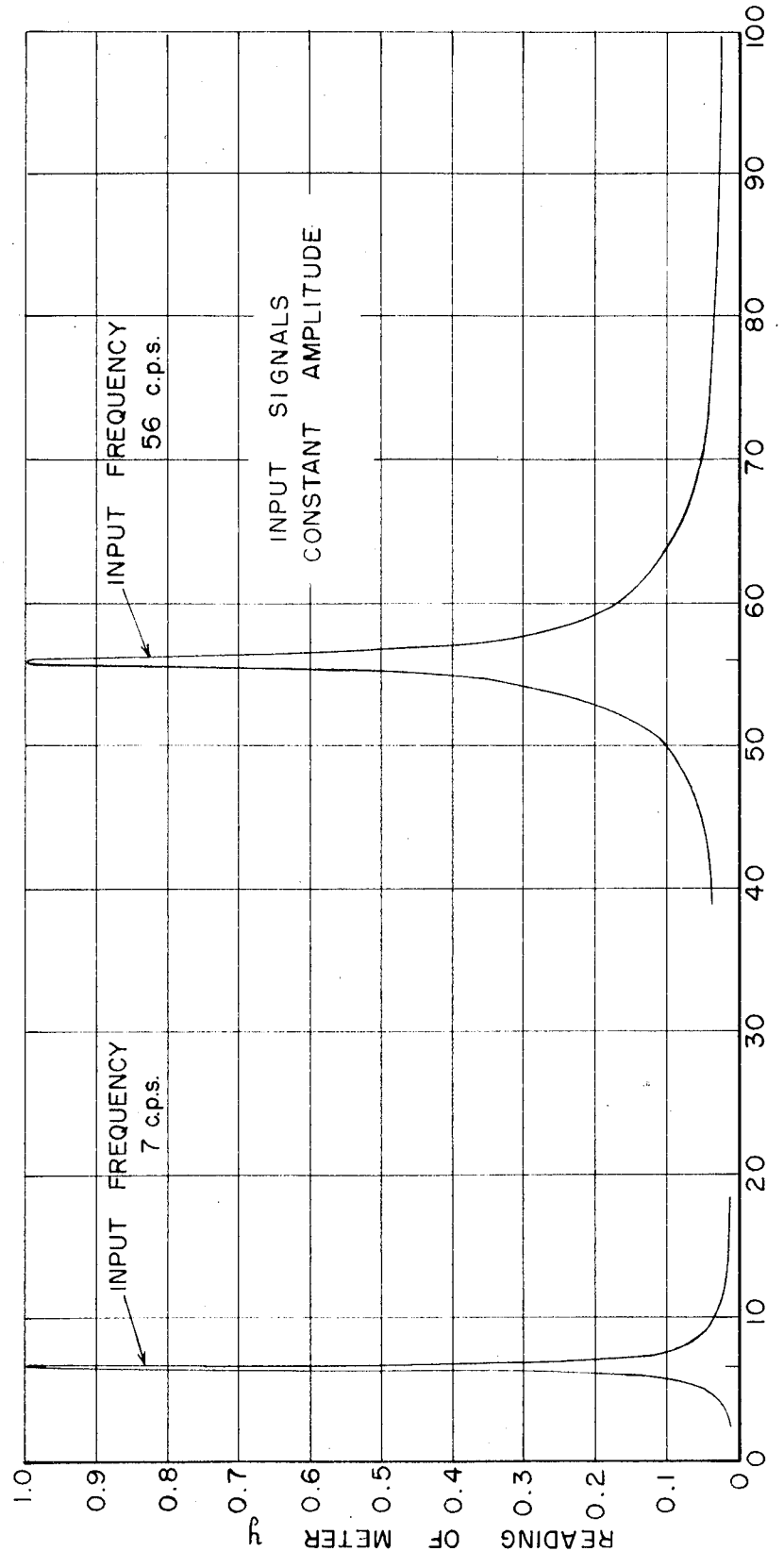

FIG. 39 VIBRATION ANALYZER CHARACTERISTICS

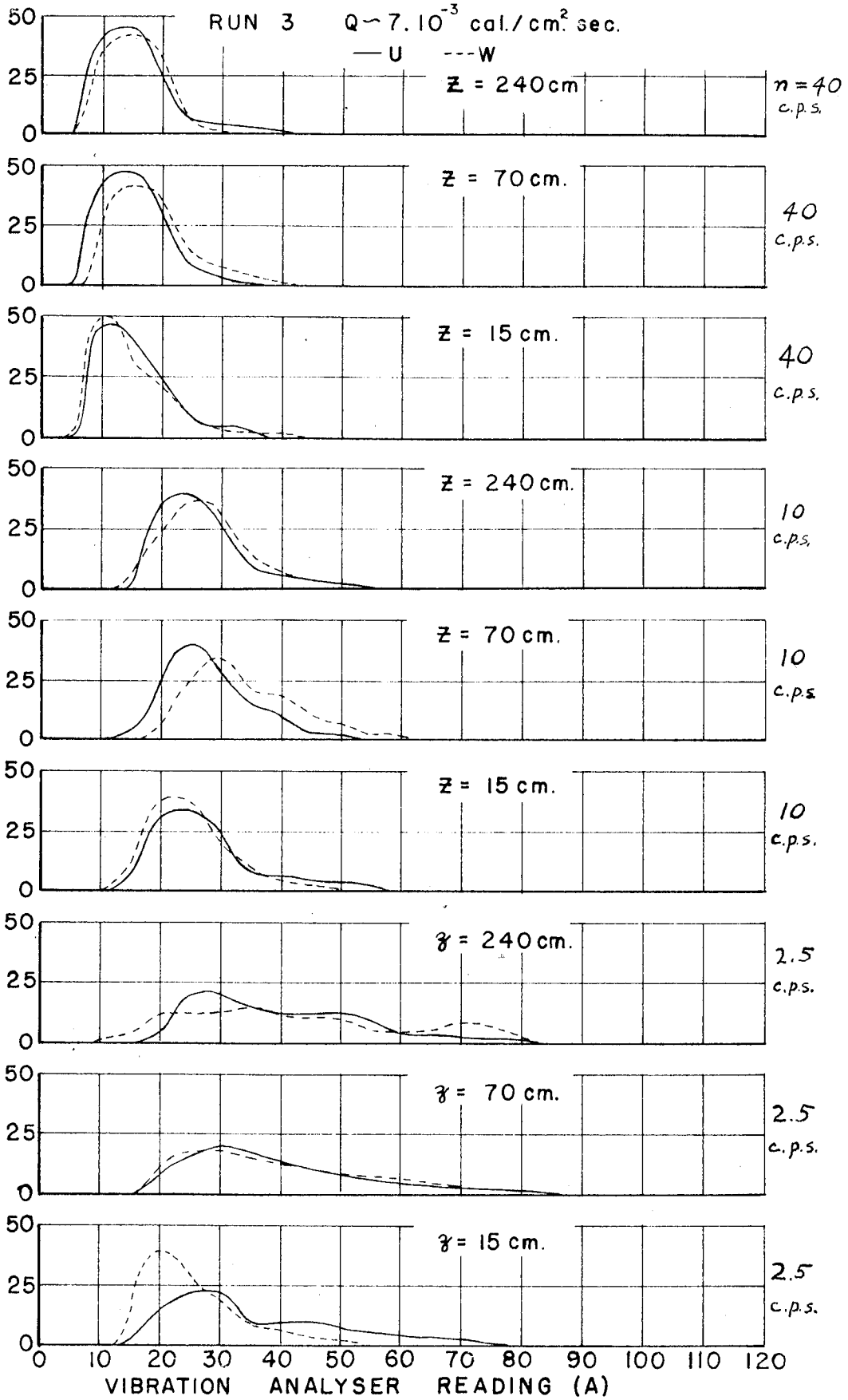

FIG. 40 PROBABILITY DENSITIES FROM VIBRATION ANALYSER

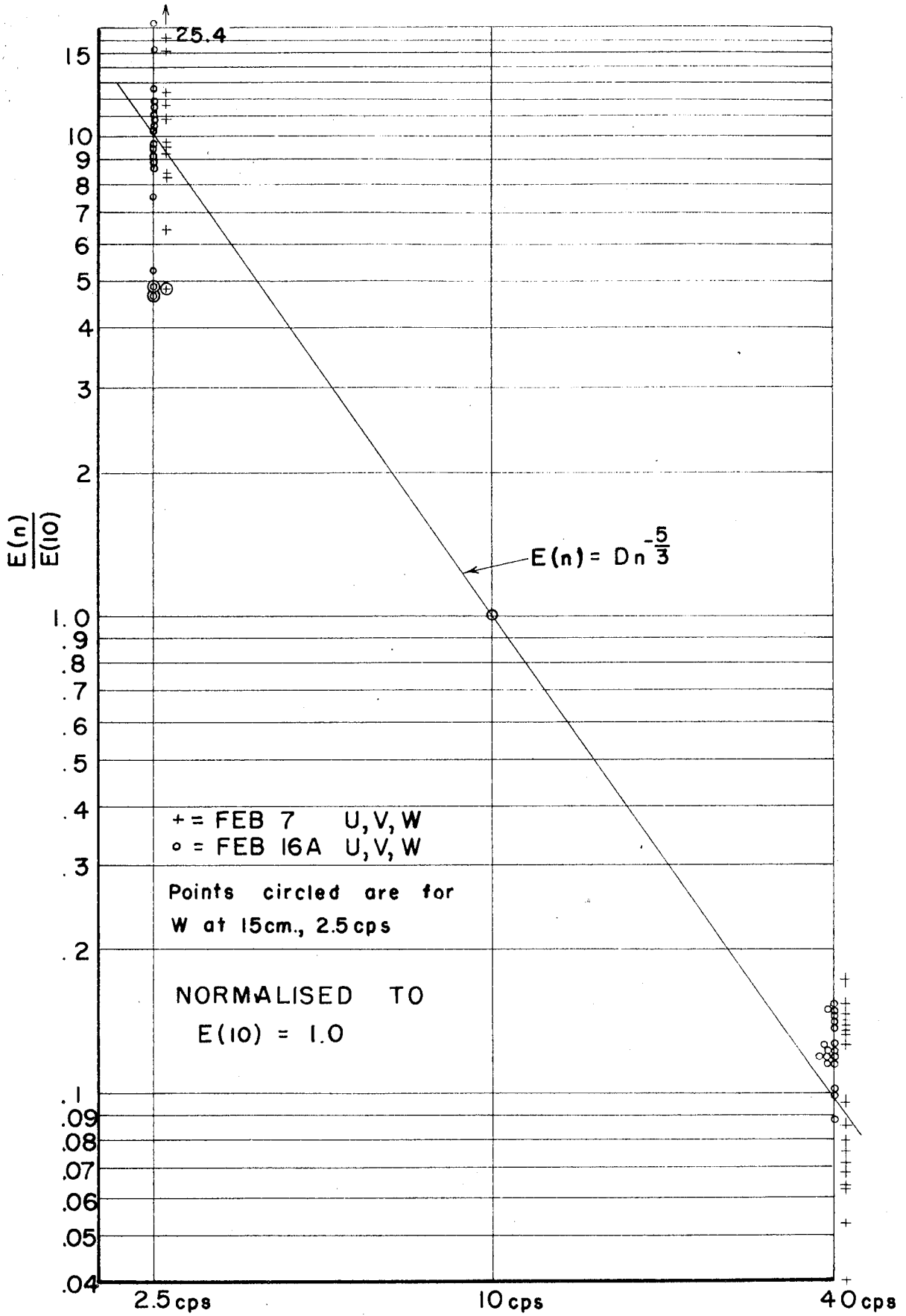

FIG. 41 ENERGY SPECTRUM

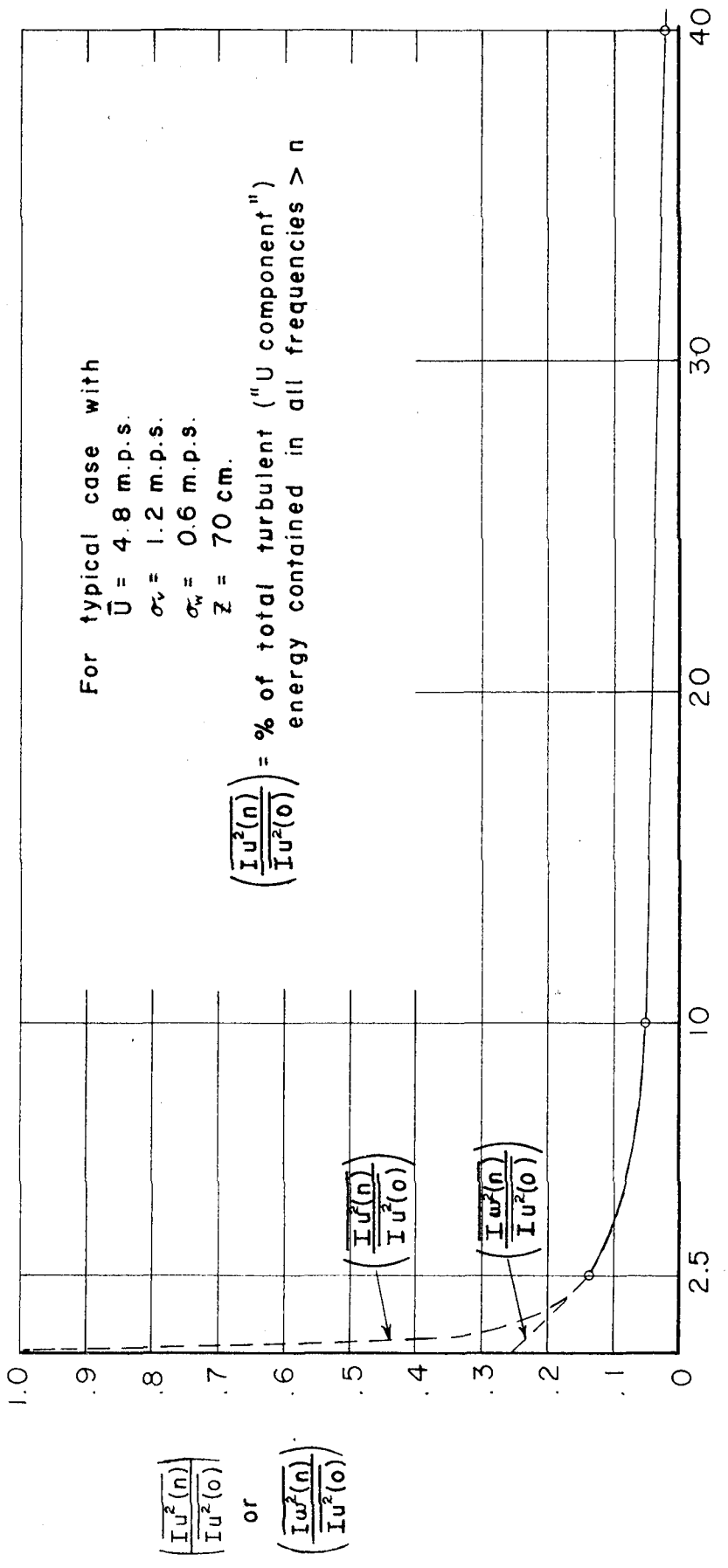

FIG. 42 INTEGRATED ENERGY SPECTRUM

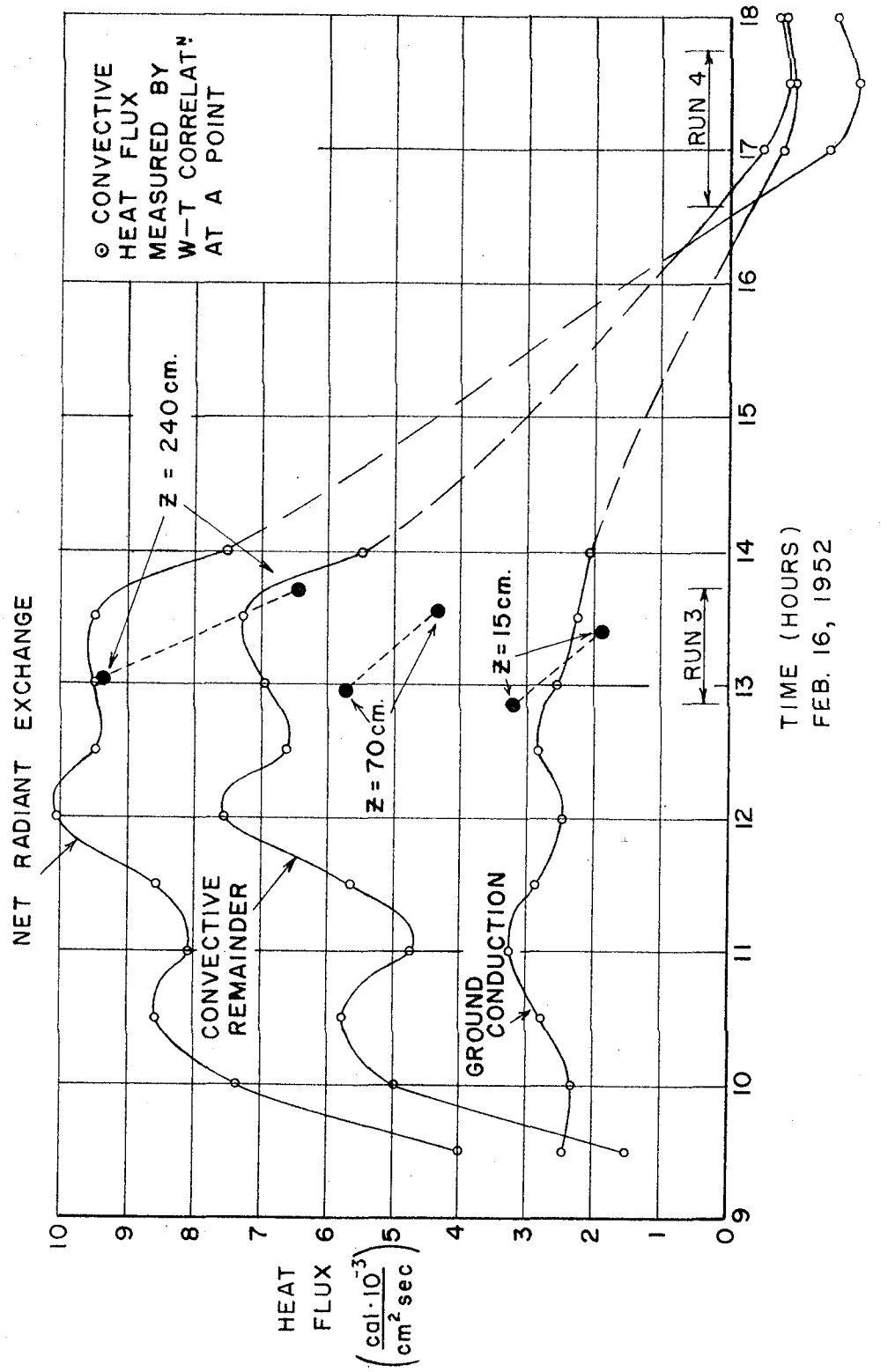

FIG. 43 HEAT FLUX

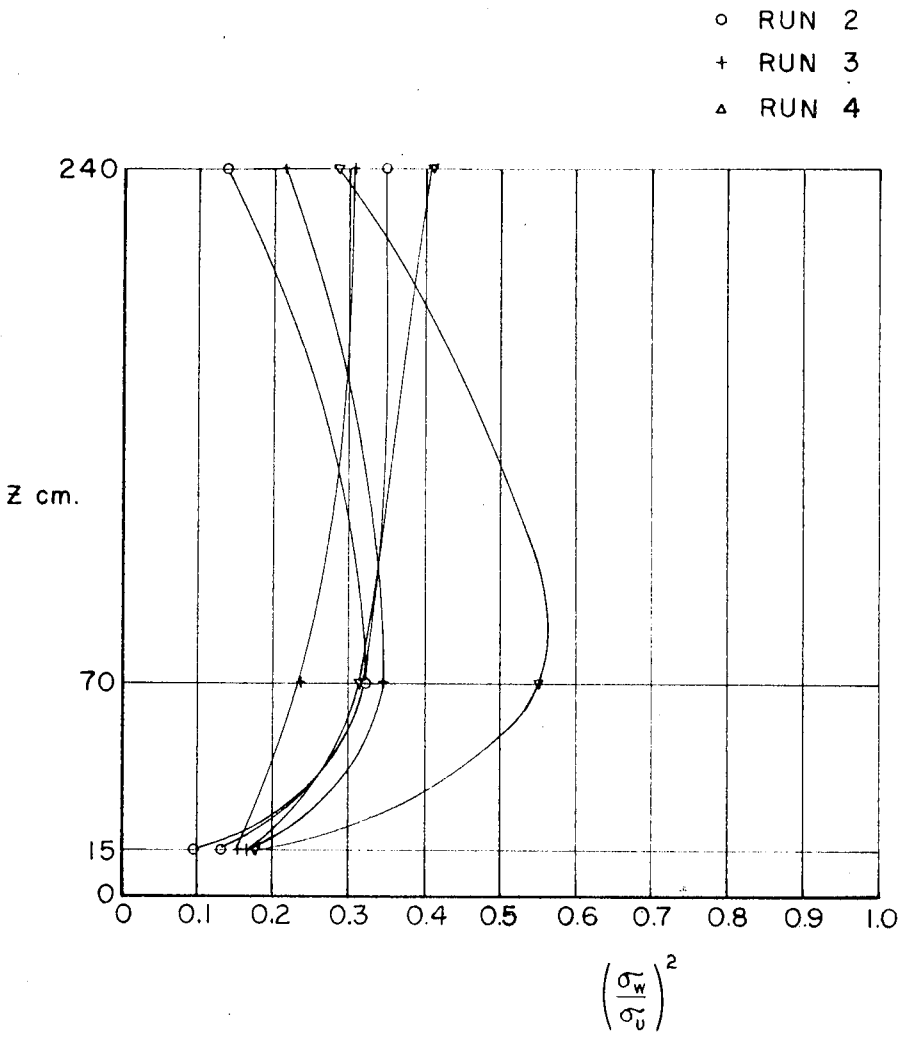

FIG. 44 TOTAL ISOTROPY

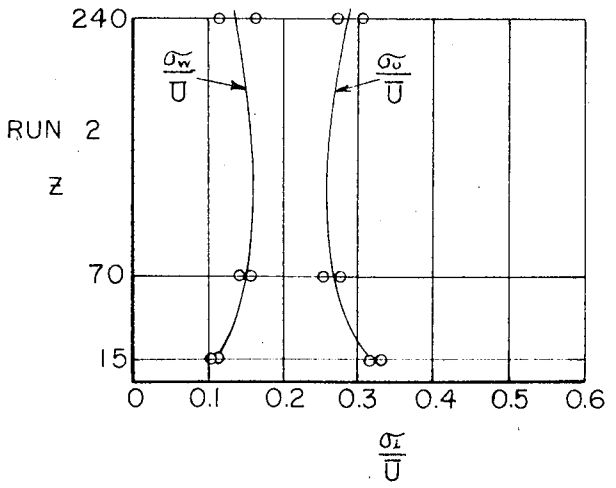

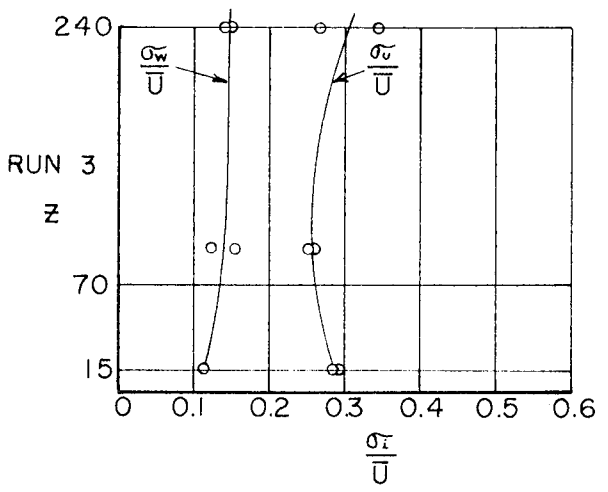

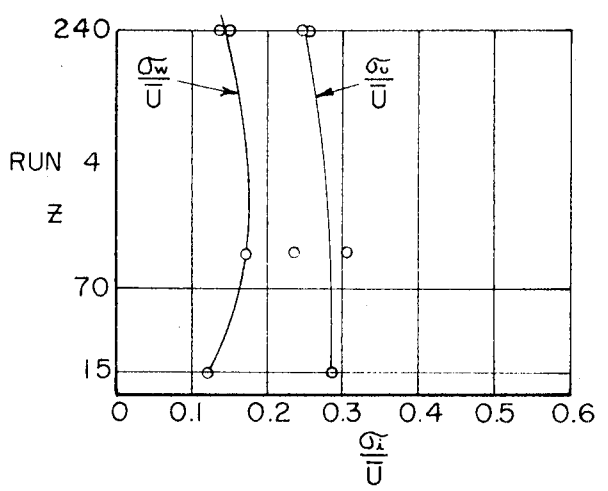

FIG. 45 TURBULENT COMPONENT CURVES

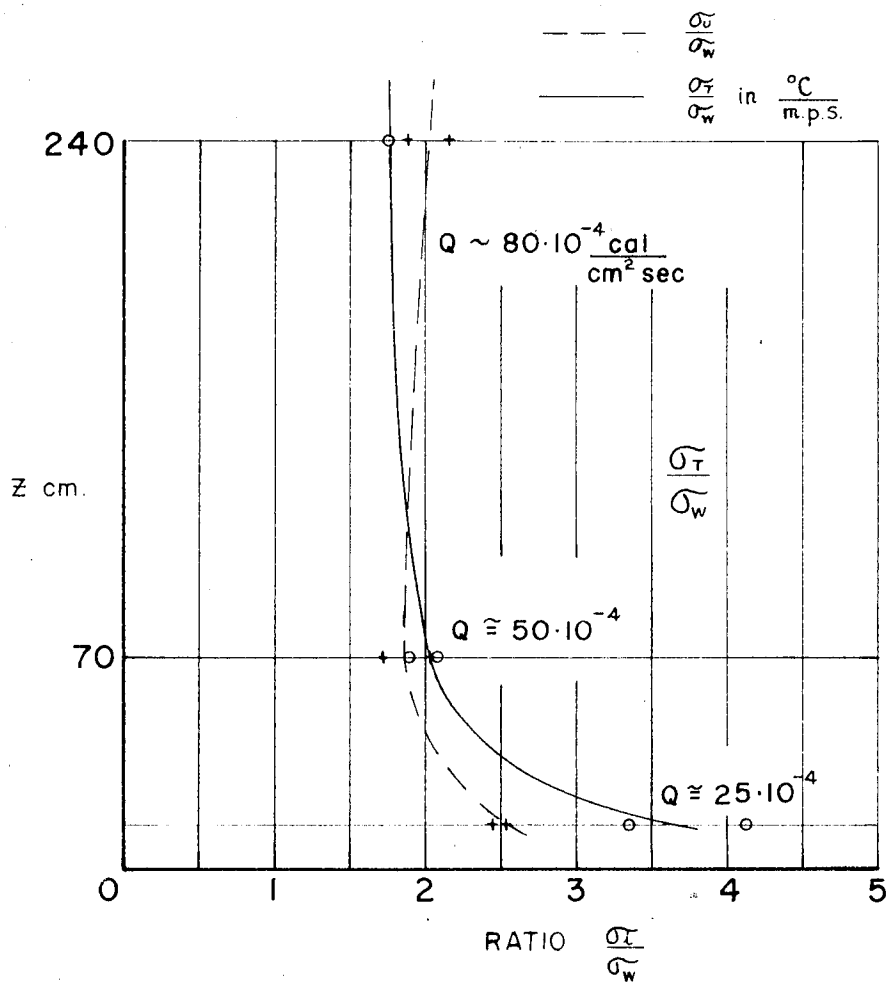

FIG. 46 T vs W CURVES